



University
of Glasgow

Veza, Marco (1986) Numerical methods for the design and unsteady analysis of aerofoils. PhD

<http://theses.gla.ac.uk/4885/>

Copyright and moral rights for this thesis are retained by the author

A copy can be downloaded for personal non-commercial research or study, without prior permission or charge

This thesis cannot be reproduced or quoted extensively from without first obtaining permission in writing from the Author

The content must not be changed in any way or sold commercially in any format or medium without the formal permission of the Author

When referring to this work, full bibliographic details including the author, title, awarding institution and date of the thesis must be given.

**NUMERICAL METHODS FOR THE DESIGN
AND UNSTEADY ANALYSIS OF AEROFOILS**

by

Marco Veza, B.Sc.

Thesis presented for the degree of Ph.D.
to the Faculty of Engineering,
The University of Glasgow.

Department of Aeronautics
and Fluid Mechanics

April, 1986.

BEST COPY

AVAILABLE

Variable print quality

ACKNOWLEDGEMENTS

I would like to thank Dr. R.A.McD. Galbraith for his support and guidance throughout the period of study. My thanks are also extended to the computing staff for their assistance, to Margaret for her many hours at the word processor, and especially to Irene, my wife, for her patience and understanding.

SUMMARY

A number of new numerical "panel" methods have been developed which form the basis of a design and analysis package that is particularly applicable to aerofoils undergoing unsteady motion in incompressible flow. One such application is to the retreating blade of a helicopter rotor and the often associated phenomenon of dynamic stall.

All of the methods are of the inviscid type, hence the flowfield is governed by the Laplace equation for the velocity potential and the pressure is obtained from the Bernoulli equation. This enables the use of singularity distributions, and in all cases the aerofoil is represented by a piecewise linear variation of vorticity which is continuous at the panel corners. Solutions are obtained by applying the appropriate boundary conditions at a specified number of control points and by implementing the relevant "Kutta" condition.

The presentation of the models is preceded by a survey of existing numerical methods which are applicable to the prediction of dynamic stall. The methods are split up into four categories, and a large number of factors have been considered when assessing the degree to which the models have successfully reproduced the physical phenomena. For ease of assimilation, the survey information is also presented in tabular form.

An inverse method was first developed for the design of an aerofoil with a specific pressure distribution. Originally two methods were proposed: the first was based on the hypothesis that the greater is the obstruction offered by a body in a uniform stream, the greater are the resulting suction over the surface of the body, and vice versa; the second used the governing flow equations when determining the modified profile ordinates. Both of these methods are iterative, but the latter exhibited superior stability, accuracy and efficiency.

The main research effort has been directed towards the development of methods for predicting unsteady flows about an aerofoil. A new method is presented for modelling unsteady, attached, potential flow. A solution is obtained at prescribed times from a linear system of equations, and circulation is shed from the trailing-edge in accordance with Kelvin's theorem. The vortex wake is represented by a system of discrete vortices which convect with the fluid particles to which they are attached. Results are presented which illustrate certain characteristics of unsteady, attached flow.

The inviscid formulation has been applied to the case of unsteady separation from the upper surface of an aerofoil. The appropriate "Kutta" relation is derived from the dynamical boundary conditions at the prescribed separation points, and the shear layers are represented by discrete vortices with finite cores. A solution is obtained at specified times from a linear system of equations, and results are presented first, for cases where the separation point is fixed, and second, with moving separation. These results highlight a number of interesting features associated with unsteady separation, in particular dynamic stall.

Finally, conclusions are drawn concerning the usefulness of the methods presented herein, with particular regard to the modelling of dynamic stall, and recommendations are made for a future program of work which would further enhance their predictive capability.

CONTENTS

	Page
Acknowledgements	(i)
Summary	(ii)
Contents	(iv)
Chapter 1 <u>Introductory</u>	
1.1 Introduction	1
1.2 Scope of present work	2
1.3 Symbol glossary	4
Chapter 2 <u>A survey of dynamic stall prediction</u> <u>methods</u>	
2.1 Introduction	7
2.2 Categorisation of the methods	9
2.3 Navier Stokes methods	11
2.4 Discrete vortex methods	13
2.5 Zonal methods	14
2.6 Predominantly empirical methods	16
2.7 Discussion	18
2.8 Conclusions	19

	Page
Chapter 3	
	<u>A comparison of two new inverse methods</u>
	<u>for the design of aerofoils with specific</u>
	<u>pressure distributions</u>
3.1	Introduction 21
3.2	Survey of past work 22
3.3	Method 1: profile modification based on pressure difference (ΔC_p method)
3.3.1	Development of the model 26
3.3.2	Results 26
3.4	Method 2: profile modification using an adapted analysis technique (A.A. method) 28
3.4.1	Development of the model 29
3.4.2	Results 31
3.5	Discussion and comparison of the methods 32
3.6	Conclusions 34
Chapter 4	
	<u>A new method for predicting unsteady</u>
	<u>potential flow about an aerofoil</u>
4.1	Introduction 35
4.2	Survey of past work 35
4.3	Development of the model 38
4.3.1	Theoretical description 38
4.3.2	Numerical implementation 40

	Page	
4.4	Results and discussion	41
4.4.1	Step change in incidence	41
4.4.2	Sinusoidal oscillations	42
4.4.3	Ramp motions	44
4.5	Conclusions	45
Chapter 5	<u>An inviscid model of unsteady, separated, aerofoil flow</u>	
5.1	Introduction	46
5.2	Theoretical description of the model	47
5.3	Numerical implementation	50
5.3.1	Model with fixed upper surface separation	50
5.3.2	Model with moving upper surface separation	54
5.3.3	Miscellaneous points	56
5.4	Results and discussion	56
5.4.1	Step change in incidence	56
5.4.2	Ramp motions	58
5.4.3	Sinusoidal oscillatons	59
5.5	Conclusions	61

	Page
Chapter 6	
<u>Conclusions and suggestions for</u>	
<u>future research</u>	62
6.1	
Introduction	62
6.2	
Summary of conclusions	63
6.2.1	
Dynamic stall prediction methods	63
6.2.2	
A comparison of two new inverse	
methods	63
6.2.3	
Modelling of unsteady potential	
flow about an aerofoil	63
6.2.4	
Modelling of unsteady, separated	
flow about an aerofoil	64
6.3	
Suggestions for future research	64
6.3.1	
Improvements in the aerofoil	
design model	64
6.3.2	
Mathematical study of the unstable	
nature of the unsteady flow model	
with separation	65
6.3.3	
Modifications to enhance the	
predictive capability of the	
unsteady flow models	65
6.4	
Concluding discussion	66

	Page
References	68
Appendix 1	
Vortex panel method - derivation of the influence coefficient at the i^{th} control point due to the j^{th} panel	78
2	
Matrix of coefficients	83
3	
Derivation of the iterative relations governing the shed vorticity	85

Table 1

Figures

CHAPTER 1

Introductory

1.1 Introduction

Aerodynamicists have studied unsteady aerofoils for most of the twentieth century, motivated by the desire to predict such effects as flutter, vibrations, buffeting, gust response and dynamic stall. A meaningful study incorporates the prediction of the magnitude and phase of the unsteady fluid dynamic loads experienced by the lifting surface based on an understanding of the mechanisms that produce such unsteady effects. Moreover, the knowledge gained from these studies is being utilised in a variety of fields, e.g. to improve the performance of turbomachinery, wind turbines and helicopter rotors.

Dynamic stall can occur, as explained more fully in chapter 2, when an aerofoil oscillates around an angle of incidence close to the static stall value. It is important to understand this phenomenon so that beneficial effects can be harnessed and undesirable effects avoided. To this end a dynamic stall facility was developed and commissioned at Glasgow University (Leishman, 1984), the main aim of experimentation being the consideration of detailed surface pressure measurements. Such a facility required that an aerofoil design package and a dynamic stall prediction code be developed for testing the suitability of any proposed hypothesis. In this way experimental research can be carried out more efficiently and effectively by the avoidance of any fruitless expenditure of both time and money. Suitable codes have been developed with the aim of fulfilling these requirements.

Although much of the knowledge about dynamic stall has resulted from experimental studies, a number of numerical methods exist for the prediction of its component features, and their merits are discussed in chapter 2. After due consideration was given to the existent models and having taken into account other factors, such as

the requirement to predict a number of aerofoil characteristics (e.g. C_L , C_M , C_p) and the limited computing power available, it was concluded that a useful way to proceed was to develop a discrete vortex method.

1.2 Scope

As mentioned in section 1.1 the intention when undertaking the program of research presented in this dissertation was to produce a design and analysis package to complement the experimental research into dynamic stall within the department. The first stage of this program was to conduct a literature survey of the current numerical methods that are applicable to the phenomenon of unsteady stall. This forms the subject matter of chapter 2. In particular, the state of the art in this field is summarised in table 1, which provides a readily accessible means of assessing the advantages and disadvantages of each method, as well as the future research needs.

The next stage was to develop the required numerical methods. All are of the inviscid type with no boundary layer corrections - this addition forms the basis of a current research program within the department. In some cases it is desirable to carry out unsteady tests on an aerofoil with a specific static pressure distribution over part or all of its surface, therefore a design method has been developed to produce such an aerofoil, the details of which are presented in chapter 3. This algorithm has already been used successfully within the department to design a modified NACA 23012 aerofoil, a model of which was subsequently constructed and tested (Niven and Galbraith, 1984).

Details of the analysis part of the package are presented in chapters 4 and 5. In chapter 4, the case of attached flow only is considered. A method in the same class as that of Basu and Hancock (1978b) has been developed, however, because of the manner of specifying the Kutta condition, the non-linearity in the system of simultaneous equations has been removed. The applicability of this method to a variety of cases is illustrated in the results presented.

Chapter 5 describes, in detail, the final stage of development of the analysis code, incorporating the presence of upper surface separation. Initially this separation point was fixed in position and a number of numerical constraints were implemented to improve both the stability of the model and the accuracy of the predictions. The results presented for the case of a step change in incidence illustrate that the time-dependent solution tends towards the correct steady-state condition. Further developments have enabled predictions to be made whereby the separation point is moving, e.g. when dynamic stall occurs. Few experimental comparisons can be made at this stage because the model does not incorporate sufficient details of the stalling mechanism, however qualitative agreement with the experimentally determined features of dynamic stall has been obtained.

Chapter 6 outlines the major conclusions of chapters 2 to 5 and offers suggestions as to the nature of future research. In the concluding discussion, the achievements of the work are concisely stated and it is considered that the numerical package is at a sufficient level of development to be used on a production basis.

1.3 Symbol Glossary

A	total influence coefficient of surface vorticity
B	part influence coefficient of γ_j
C	part influence coefficient of γ_{j+1}
C_L	lift coefficient
C_M	moment coefficient
C_N	normal lift coefficient
C_p	static pressure coefficient
CN	correction factor
c	aerofoil chord
D	part influence coefficient of γ_s
D_o, D_v	distance parameters associated with coalescence
e	velocity error
e_v	error estimate of coalescence
f	filtering factor
G	discrete vortex influence coefficient
$h, \Delta h$	total head
I_1, I_2, I_3, I_4	integrals associated with vortex panel method
$\underline{i}, \underline{j}$	unit vectors
k	reduced frequency of oscillation ($\Omega c / 2U_\infty$)
L	aerofoil panel length
M	Mach number
N	number of aerofoil panels
N_C	number of recently shed vortices not involved in coalescence
N_v	number of discrete vortices
\hat{n}	unit normal vector

p	static pressure
q	fluid velocity
q_s	velocity of separation point along aerofoil surface
R_1, R_2	regions with different total head
Re	Reynolds number
r	distance between two points
s, s'	arc length along aerofoil surface
$t, \Delta t$	time
U, U_∞	free stream velocity
V_r	velocity of point fixed to aerofoil
x, y	cartesian coordinates
z	complex number
α	angle of incidence
$\dot{\alpha}$	angular velocity
Γ	aerofoil circulation
γ	vorticity strength
Δ, λ	length of vortex wake panels
n	regulating function associated with vortex core
$\theta, \Delta\theta$	wake panel angles
Λ	length dimension
ρ	fluid density
σ	radius of vortex core
$\phi, \Delta\phi, \phi_c$	velocity potential
ψ	stream function
Ω	frequency of oscillation
ω	vorticity

Subscripts

a,a',b,b'	positions either side of vortex sheet
c	panel control point
i,j	index of aerofoil panels
m	time step counter
n	normal direction
p	index of wake panels
s	conditions at separation point
tp	trailing point
u,l	upper/lower surface
v	discrete vortex
w	vortex wake panel

Superscripts

a	actual value
d	iteration counter
r	required value

CHAPTER 2.

A survey of dynamic stall prediction methods.

2.1 Introduction

As mentioned in chapter 1, a program of experimental work has been initiated within the department (Leishman, 1984) to investigate the nature of the flow past aérofoils undergoing dynamic stall. This phenomenon occurs when the angle of attack of an aerofoil is changed at a finite rate, and should this motion be of an oscillatory nature, around a mean angle approximately equal to that of the static stall, large hystereses develop in the fluid dynamic loads, as indicated in fig. 2.1. The behaviour of lift, drag and pitching moment under dynamic conditions differ significantly from the static case, having greater maximum values, or overshoot. Such conditions are likely to be present in the case of the helicopter rotor in forward flight, where the retreating blade encounters lower velocities than those on the advancing blade (see fig. 2.2), and to maintain roll control the angle of attack of the retreating blade is increased. The fundamental motion for one complete revolution of a blade is therefore of an oscillatory nature. In optimising the rotor performance, the angle of attack of the retreating blade often exceeds the static stall angle but returns to a lower value before the stall has time to develop (Wilby, 1980). The increased lift coefficient for the dynamic case may therefore be utilized, but the assessment of how much has proven to be a most difficult task.

Virtually everything that is known today about dynamic stall has been acquired through experimentation (see, for example, McCroskey et al., 1976; McCroskey et al., 1981; McCroskey and Pucci, 1981). These investigations have shown that its occurrence is characterised by the shedding of a leading edge vortex which traverses the upper surface of the aerofoil at a speed somewhat less than $1/2 U_{\infty}$, resulting in the aforementioned hystereses in lift, pitching moment and drag (see fig. 2.1). There is also evidence

(McCroskey et al., 1976) to suggest that the initiation of this vortex is marked by a tongue of reverse flow reaching the leading edge from an initial downstream location, and other data (McCroskey et al., 1981) have also shown that dynamic stall events, once they are underway, are relatively independent of the aerofoil motion. One important physical consequence of these events, in addition to the load hystereses, is the presence of aerodynamic damping, i.e. the net cyclic work done on the fluid by the body due to its motion which, if negative, results in an increase in the pitch oscillations unless the body is restrained. If these oscillations coincide with a natural frequency of the system, stall flutter results.

The specification of light stall and deep stall regimes, illustrated in fig. 2.1, has been another major observation of the experimentors. The stall onset condition, where limited separation occurs, marks the maximum amount of lift that can be obtained without a high pitching moment penalty. Light stall occurs for a maximum angle slightly above that for stall onset, and shows some of the general features of classical static stall such as loss of lift and significant increase in drag and nose-down pitching moment compared with the theoretical inviscid values. The main distinguishing feature of this regime, however, is that the width scale of the viscous zone remains of the order of the aerofoil thickness, normally less than that for static stall. The general characteristics of light stall are known to be particularly sensitive to aerofoil geometry, reduced frequency, maximum incidence, Mach number and probably three-dimensional effects, whereas the detailed behaviour depends to a large extent on the type of boundary layer separation present, for example leading edge or trailing edge, and to changes in the nature of this separation with maximum angle, reduced frequency and Mach number. Figure 2.3a illustrates the extent of the viscous zone during light stall.

Deep stall occurs as a result of increasing the maximum angle of attack to values well in excess of the static stall value during large amplitude oscillations. Flow breakdown is signified by the formation of a strong vortex in the leading edge region which is

subsequently shed from the boundary layer over the upper surface of the aerofoil, producing a viscous zone, the width scale of which is of the order of the aerofoil chord, as illustrated in fig. 2.3b. The general characteristics of deep stall are fairly insensitive to aerofoil motion and geometry, Reynolds number and Mach number, providing this latter parameter is low enough to prevent leading edge shock waves from forming, whereas the detailed behaviour is dependent upon the angle of attack time history after the static stall angle has been exceeded.

To complement the experimental investigations much effort has gone into developing computational techniques for predicting dynamic stall in the hope of producing a sound numerical procedure for use in aerofoil design. The main problem encountered, however, has been one of correct theoretical modelling which has led to different approaches in the treatment of this phenomenon. All of the methods incorporate simplifying assumptions, but this does not detract from the advance which has been made, especially over the last fifteen years, as outlined in the following sections.

2.2 Categorisation of the methods

The various models to be considered have been grouped under similar headings to those used in other surveys (e.g. Philippe, 1977; Beddoes, 1980; McCroskey, 1981; Vezza and Galbraith, 1983a). However, in this case, a concise version of the survey is presented in tabular form (table 1) from which the strengths and weaknesses of the models can be seen more readily. The model categories are as follows :

- (a) Navier-Stokes methods
- (b) Discrete vortex methods
- (c) Zonal methods
- (d) Predominantly empirical methods

The Navier-Stokes methods attempt to solve the fundamental equations of fluid motion, by the use of numerical techniques, in

both laminar and turbulent flows. The discrete vortex approach was originally proposed as a means of directly modelling the regions of concentrated vorticity which are present during stall, e.g. when vortex shedding occurs.

The viscous nature of the flow is taken account of by the generation and subsequent transport of discrete vortices, which have been used both in purely inviscid formulations and also within a viscous framework. The zonal methods include the class of model where a predicted dividing boundary marks the border between the external potential flow and an inner separated or viscous region. In the numerical procedure these zones interact, normally in an iterative manner.

The last category, containing the predominantly empirical methods, considers models in which little, or no, direct account is taken of the equations of fluid motion. Reliance is placed on obtaining good quality empirical data from which correlations are made in order to estimate the unsteady airloads during dynamic stall. Due to the dependence of the stall on time and pitch rate, all of the methods incorporate these two parameters in non-dimensional form.

From table 1 it can be seen that various categories have also been employed for the assessment of the predictive capabilities of the methods. The headings cover most of the relevant features of dynamic stall (Young, 1981) and the main ones are five in number :

- (a) To stall onset
- (b) stall onset
- (c) post stall
- (d) motion
- (e) other factors

These headings have been further subdivided so that more detailed consideration could be given to such things as laminar-turbulent transition, wake modelling, etc. All of the

methods are capable of providing C_N and C_M predictions and so these parameters have been omitted from the table.

In order to assess the methods, the following symbols have been used to grade the appropriate feature :

- * good consideration
- + approximate
- o very approximate
- Δ being developed
- not modelled

The allocation of these symbols was based on the relevant published work and should not be considered as being an exact process. Nevertheless, it is thought that the tabular presentation provides an easily digestible means of assessing the present state of the art in numerical studies of dynamic stall, as well as the future research needs.

2.3 Navier-Stokes methods

The complex flowfield around an aerofoil experiencing dynamic stall could, theoretically, be accurately predicted by solving the full Navier-Stokes equations. However, problems are associated with this approach, and these are discussed in section 2.7. The two most notable works are considered, one being a purely laminar calculation and the other taking account of the turbulent flow.

In the first method, the Navier-Stokes equations were solved numerically by Mehta (1977) in terms of vorticity and stream function for laminar, unsteady, incompressible flow around an oscillating modified NACA 0012 aerofoil. This method used an extension of the approach of Mehta and Lavan (1975), who considered stationary aerofoils, to treat the unsteady problem. The theoretical formulation involved mapping the aerofoil on to a unit circle using the Joukowski transformation adapted to control the shape of the trailing edge. The governing equations were developed

for the rotating system with the appropriate boundary, and initial, conditions implemented, and the lift, drag and pitching moment were calculated from the computed pressure and vorticity values.

The computation was carried out using an implicit, factored algorithm for the vorticity equation and a direct solution procedure for the stream function equation. Also a higher order technique than the more usual second order schemes was developed to eradicate spurious results due to unresolved scales of fluid motion. Figure 2.4 illustrates some of the results obtained at a Reynolds number of 10,000 and a reduced frequency of 0.25, and shows a sequence of pictures of streamlines and equi-vorticity lines synchronised with the pressure distribution. The bubble and vortex formation are represented in great detail and correlate well with flow visualisation pictures obtained under dynamically similar conditions by Werlé at ONERA (1976). Also shown in fig. 2.4 are the C_L , C_M and C_D values for this case. Due to the fundamental nature of this approach it is thought that a good consideration has been given to appropriate factors in table 1, although the Reynolds number variation is assessed as approximate due to the laminar flow restriction.

A compressible, time-dependent, full Navier-Stokes calculation procedure which includes a model of the transition from laminar to turbulent flow was developed by Shamroth and Gibeling (1981), using the consistently split linearised block implicit method of Briley and McDonald (1977). To account for the three regimes of laminar, transitional and turbulent flow present in the flow field of an aerofoil, the proposed model was based on the turbulence energy equation with an algebraic length scale. A body coordinate system was used in which the aerofoil surface is a coordinate line and the grid point placement is specified by the user, a procedure described by Shamroth and Levy (1980) and originally developed by Gibeling et al. (1978). Figure 2.5 illustrates the pressure distributions obtained during a ramp of the NACA 0012 aerofoil from 6° to 19° which, although no lift or moment values were presented, are encouraging. Again it is felt that a good consideration has been

given to many of the features of dynamic stall in table 1 due to the fundamental nature of the model.

2.4 Discrete vortex methods

Only three of the methods in this section will be discussed and are attributable to Baudu et al. (1973), Spalart et al. (1983) and Lewis and Porthouse (1983). The usefulness of the other methods can be assessed from table 1 with further details available in the given references.

The method of Vezza and Galbraith is the subject of chapters four and five and so is omitted here.

Baudu et al. (1973) adapted the potential flow method of Giesing (1968) to the modelling of dynamic stall. The stall was accounted for by the shedding of discrete vortices from a leading edge separation point which was calculated by the laminar boundary layer method of Thwaites (1949), and the strength of the shed vorticity was determined by following a similar approach to that in the study of flows around circular cylinders (e.g. Sarpkaya, 1968). Figure 2.6 illustrates the results obtained when oscillating the NACA 0012 aerofoil about an angle of fifteen degrees and at a reduced frequency of 0.24. Also shown are comparisons with flow visualisation results and normal lift data obtained by Martin et al. (1973).

The method of Spalart et al. (1983) is well developed and attempts to model the Navier-Stokes equations in the viscous region around the aerofoil by the use of discrete vortices with finite cores. These vortices are positioned at a small distance from the surface and the no slip condition invoked. For the case of dynamic stall the separation point is specified by a quasi-steady integral boundary layer calculation, although the incorporation of a truly, unsteady, implicit finite difference boundary layer solver is in progress. Figure 2.7 illustrates the results obtained when the NACA 0012 aerofoil is oscillated in pitch about the quarter chord.

From fig. 2.7a the passage of a vortex over the aerofoil upper surface can be discerned along with the associated pressure disturbance, and the magnitude and axis of application of the force is represented by the arrow emanating from the aerofoil. Figure 2.7b shows a comparison between the calculated lift and moment and the experimental observations of McCroskey et al. (1982). The results are encouraging and should improve with further developments.

In a similar manner Lewis and Porthouse (1983) attempted to model directly the Navier-Stokes equations by an adaption of the surface vorticity method of Martensen (1959). Following the potential flow calculation the vortex elements are repositioned a small distance from the aerofoil surface, simulating the presence of the boundary layer. The method includes an interesting model of viscous diffusion which involves randomly displacing the vortices after they have been convected. Application to the case of the NACA 0012 aerofoil at a fixed incidence of 20° has been attempted and the results are shown in fig. 2.8. The characteristic features of massive separation have been reproduced although it is questionable whether the pure vortex method applied in this manner, as noted by Spalart et al. (1983), could model successfully the case of limited separation because of the chaotic motions of the vortices. The various features of all of the vortex methods are further illustrated in table 1.

2.5 Zonal methods

Attempts have been made to duplicate the complexity of developing separation by coupling the external flow to the inner viscous flow via regional boundaries whose locations are to be found, usually as a result of an iterative process. The quasi-steady method of Rao et al. (1978) represents the aerofoil surface by a distribution of constant strength doublet panels and a uniform source sheet, and the free shear layers by vortex sheets. The computational procedure consists of an outer loop for the viscous-inviscid flow and an inner loop to determine the wake shape, calculated at a modified angle of attack to account for the delay in

unsteady separation relative to the steady case. The outer loop takes the potential flow pressure distribution over to the boundary layer analysis where the separation points and source distribution are calculated using an integral method. This information is passed to the inner loop where the new wake shape is determined, iteratively, by ensuring that the free shear layers remain aligned with the local stream direction. The process is stopped when the change in lift coefficient falls below one percent, or when the iteration number limit has been reached. Results obtained for the lift and moment coefficients after the NACA 0012 aerofoil had undergone sinusoidal motion are presented in fig. 2.9. The recognisable features of dynamic stall, i.e. hysteresis loops and aerodynamic damping are illustrated, although the predictive accuracy of this method is limited by the omission of the laminar bubble bursting process, the dynamics of the separated wake and the unsteady boundary conditions on the aerofoil surface. These limitations have been tackled more recently by Maskew and Dvorak (1985), who have incorporated unsteady integral boundary layer calculations into their method as well as a dynamic wake model with vortex core amalgamation. They hope to extend the method to the modelling of three-dimensional flows; however, improvements to the two-dimensional case are continuing and preliminary results from a ramp test on the NACA 0012, illustrated in fig. 2.10, are encouraging.

The method of Crimi and Reeves (1972) incorporates a number of flow elements. The potential flow calculation invokes a thin aerofoil analysis with source and vortex singularities being distributed along, and the boundary conditions satisfied on, the x-axis. The method of finite differences is used in the analysis of both the laminar and turbulent boundary layers, incorporating the van Driest and Blumer (1963) transition model and the Smith-Cebeci (1967) eddy-viscosity model. The separated shear layer is split up into three regions, where applicable; the laminar mixing, the turbulent mixing and the reattachment regions, and these are analysed to determine the position of the shear layer and the pressure of the dead air. A leading-edge bubble criterion is also

included which determines whether or not the aerofoil is undergoing leading-edge stall. Both ramp and sinusoidal motions were considered for tests on the NACA 0012 aerofoil at a Reynolds number of two million. An example of the latter is illustrated in fig. 2.11, from which the gross features of dynamic stall can be discerned with the exception of the vortex induced lift.

The method of Scruggs et al. (1974) is not a pure dynamic stall method but rather an analysis of the effects of time dependence, in both the potential flow and boundary layer, on the delay in the forward movement of the flow reversal point at the surface of the aerofoil. The unsteady potential flow is calculated by the method of Giesing (1968) and the unsteady boundary layer by an adaption of the approach of Patel and Nash (1971). It was shown that this delay is not only affected by the alleviation of the gradients in the potential flow but also by the effects of unsteadiness in the boundary layer itself, a result which calls into question the accuracy of the quasi-steady methods. This work was an important contribution and the results have been used, for example, by Beddoes (1982). Further appreciation of the zonal methods can be gained from table 1.

2.6 Predominantly empirical methods

At present a host of empirical methods exist for estimating the unsteady airloads on oscillating aerofoils. All of the methods rely heavily on correlations with experimental data so that the effect of relevant parameters, such as the pitch rate, can be discerned.

The time delay method of Beddoes (1982) is based on the use of indicial functions for the modelling of various dynamic stall phenomena. The attached flow airloads are calculated via a generalised indicial lift function, incorporating compressibility effects, based on the Wagner function, with the angle of attack time history being represented by a superposition of step functions. The dynamic stall process is modelled via two time delays; one

between the onset of separation, obtained from a leading edge pressure criterion, and moment divergence, and one for the vortex passage, during which the lift is maintained at its attached level. Reattachment occurs when the angle of attack falls below the angle of static moment break. Shock wave interaction has also been taken into account via a correlation between the critical shock pressure rise and the pressure ahead of the shock, and a model of trailing edge separation has been included which uses correlations between Kirchhoff's theory and the numerical data of Scruggs et al. (1974). The accuracy of this approach can be appreciated from fig. 2.12.

The method of Gangwani (1984) is highly empirical and invokes curve fitting techniques, applied to experimental data, to determine the values of a number of parameters that are used in expressions to predict certain dynamic stall events. The three basic variables of the method are the instantaneous angle of attack, the non-dimensional pitch rate and a decay parameter that is based upon the Wagner function. A three stage procedure is followed whereby a data set is initially prepared for the required flow conditions, the empirical coefficients determined through least squares fitting and the original data reconstructed from the empirical relations for comparison purposes. The method calculates the angles at which dynamic moment stall is initiated, the vortex leaves the aerofoil trailing edge, and reattachment occurs, the three being used in the expressions for the loads. Whilst fig. 2.13 illustrates the high degree of accuracy of this approach, it is still limited, however, by the inability to predict results significantly outwith the range of the original test data.

A system of differential equations is employed in the method of Tran and Petot (1980) to simulate the time delay effects of the flow. The identification of the coefficients of the model's equations requires experimental tests to be carried out on aerofoils in static conditions and in small amplitude harmonic oscillations or random vibrations. The dynamic loads are calculated by first splitting them up into two parts, one part governed by a first order

linear equation and the other by a second order non-linear equation. Below the angle of static stall the non-linear part vanishes and the solution is similar to that given by classical linear theory. Above the static stall angle the coefficients of the non-linear equation must also be identified and the two parts added to give the required value of the loads. Although the equations were derived for small amplitude oscillations, the model's applicability to the larger oscillatory motions characteristic of helicopter rotors can be seen from fig. 2.14. This model has recently been used by McAlister et al. (1984) who indicated, however, that its accuracy is diminished when both the reduced frequency and amplitude of oscillation are large. Further details of the predominantly empirical methods can be obtained from table 1 and the references supplied therein.

2.7 Discussion

When consideration is given to table 1 it should be noted that the models have been assessed by their ability to reproduce the various flow phenomena relevant to dynamic stall rather than just by the accuracy with which they predict the resultant loads. It is not surprising, then, that the Navier-Stokes methods seem to provide the most comprehensive details of the flow field, as they utilise the fundamental equations of fluid motion. This approach, therefore, would initially appear to have the brightest future, although the computational expenditure required may prove prohibitive for many researchers. The main problem to be overcome, however, is that of turbulence modelling, the quality of the solution being dependent on the chosen hypothesis. Nevertheless, the excellent analysis of Mehta (1977), although restricted to laminar flow, is an illustration of the accuracy which may be achieved in future studies.

In contrast to the above approach, the predominantly empirical methods take very little direct account of the physical flow field but, rather, rely heavily on correlations with experimental data. As a result their standing in table 1 does not appear to be very

high, although they are almost exclusively used in the helicopter industry because of their ability to accurately predict rotor loads. In theory, as noted for example by Gangwani (1984), the more comprehensive the correlation studies the more accurate should be the predictions, although this would require more good quality empirical data, the collection of which is expensive and time consuming.

It could be argued that both the discrete vortex and zonal methods provide a compromise between the above two approaches, the relevant models being based on more simplified theory than that used in the Navier-Stokes methods but incorporating much more of the flow physics than do the empirical methods. The discrete vortex methods are particularly useful at modelling regions of concentrated vorticity, for example the dynamic stall vortex, but tend to be lacking when it comes to the boundary layer, although the method of Spalart et al. (1983) may change this. Alternatively, the zonal methods can predict the viscous effects adequately but are still generally poor at modeling the unsteady wake dynamics, although the recent work of Maskew and Dvorak (1985) is encouraging in this area. Recalling that dynamic stall is characterised by the shedding and subsequent transport of a vortex over the upper surface of an aerofoil, the discrete vortex approach should provide a useful method for incorporation into a design and analysis package. Throughout the table there are areas which correspond to phenomena not modelled and it is hoped that this will provide an indication of future research needs.

2.8 Conclusions

The purpose of this chapter has been to briefly describe the phenomenon of dynamic stall and to review the computational methods that are available for its prediction, with the aim of proposing a suitable field of research. The tabular form of presentation used in conjunction with the survey, table 1, provides an easily digestible means of assessing both the capabilities of the various methods and the future research needs. As developments appear, so

the table can be augmented accordingly.

In the long term the Navier-Stokes methods offer the most accurate analysis; however, at present both the computational expense required and the sensitivity of the results to the turbulence model used are prohibitive factors for many researchers to consider. The empirical methods, although being the main analytical tools within the helicopter industry, provide little detailed information about the flow field and require expensive data acquisition for correlation purposes.

A useful approach would be to develop a simplified model which incorporated the major features of dynamic stall, for example, the shed vortex and, for this purpose, a discrete vortex model is outlined in chapters 4 and 5.

CHAPTER 3.

A comparison of two new inverse methods for the design of aerofoils with specific pressure distributions.

3.1 Introduction

The need for an accurate, efficient method of designing aerofoils with specific pressure distributions has been mentioned in chapter 1. This is especially true today as sections are required that are optimised for their specific task, e.g. the improved performance of helicopter rotors during dynamic stall. The inverse problem, stated simply, is: to find the geometry of an aerofoil which produces a required velocity (or pressure) distribution. Care must be exercised, however, when defining a velocity distribution so that a corresponding geometry is obtainable, a problem not encountered during the reverse ("forward") process.

Two major categories of inverse method exist at present: exact transformation methods and surface singularity methods. Although some work has been done on the former, e.g. James (1977), these methods tend to be cumbersome and hence uneconomic in terms of computer time. The increase in the use of singularity methods to predict the pressure distribution over an aerofoil has been due to the rapid solutions of large systems of equations, characteristic of these methods, made possible by the use of modern computers.

Generally, the singularity distribution consists of sources and sinks (e.g. Hess and Smith, 1967), vortices (e.g. Martensen, 1959; Kennedy and Marsden, 1976) or a combination of both (e.g. Bhatelty and Bradley, 1972). However, when inverting the equations to use in an iterative-direct manner, the methods employing sources and sinks must be excluded, as the required surface velocities cannot be converted to required singularity strengths. This is not the case for methods employing a distribution of surface vorticity which are, therefore, more widely used.

The remainder of this chapter describes the development and application of two vortex design methods, following a brief survey of other work in this field. From the results presented comparisons are made between the respective approaches, and conclusions drawn regarding their relative stability, accuracy and efficiency. For further details, see Vezza and Galbraith (1983b).

3.2 Survey of past work

Goldstein and Jerison (1947) were pioneers in the use of a surface vortex design method for both isolated aerofoils and aerofoils in cascade. Their method sought to locate vortices of known strength, such that the resultant shape was a streamline of the flow. In the modification process, however, the pressure surface vortices were altered so that only the suction surface velocities could be specified. The characteristics of the designed section were determined by the use of a conformal transformation method, as surface singularity techniques were not available then.

A later method developed by Wilkinson (1967) employed a direct vortex singularity method to calculate the aerofoil surface velocities. A camber line vorticity distribution, which removed the difference between these velocities and the desired velocities, was then determined and the camber line adjusted so that it again became a streamline of the combined flow. The original thickness distribution was imposed on the modified camber line and a check for convergence made after each iteration by computing the new velocities on the aerofoil surface. Two major limitations of this method were that only the upper surface velocities could be specified, and the required thickness distribution had to be known in advance.

An improvement in the accuracy of aerofoil design would be expected by employing the method of Kennedy and Marsden (1978). This method was similar to those developed by Chen (1971) and Mavriplis (1974), but utilised a more accurate forward algorithm

(Kennedy and Marsden, 1976), the governing equations of which were rearranged and used directly in the design process. The particular potential flow analysis that was employed had been developed by Oellers (1962) and required that the stream function produced by the superposition of a uniform stream and a vortex sheet of varying strength on the aerofoil surface, be constant on the surface. The resulting Fredholm integral equation of the first kind was :

$$\psi = U_{\infty}y(s) \cos\alpha - U_{\infty}x(s)\sin\alpha - \frac{1}{2\pi} \int_{s'} \gamma(s') \ln r(s,s') ds' \quad 3.1$$

where s and s' represent two points on the aerofoil surface (see fig. 3.1).

A numerical representation of equation 3.1 was obtained by replacing the aerofoil surface with an inscribed polygon having N panels and implementing the constant stream function condition at the mid-point of each panel. The discrete analogue of equation 3.1 was then as follows :

$$\psi = U_{\infty}y_{ci} \cos\alpha - U_{\infty}x_{ci} \sin\alpha - \sum_{j=1}^N A_{ij} \gamma_j, \quad i = 1, 2, \dots, N \quad 3.2$$

where the vorticity was constant across each panel.

The relation 3.2 represented a linear system of N equations in $N+1$ unknowns, therefore another equation was required and this was obtained from the Kutta condition. The use of a trailing point Kutta condition by Kennedy and Marsden (1976) was a development over previous methods since it enabled accurate results to be obtained using a reduced number of panels. It involved the use of an extra control point which was located a short distance downstream from the trailing edge along the bisector of the trailing edge angle. The extra equation was, therefore :

$$\psi = U_{\infty}y_{tp} \cos\alpha - U_{\infty}x_{tp} \sin\alpha - \sum_{j=1}^N A_{tpj} \gamma_j$$

Equations 3.2, along with the above Kutta condition, were adapted to obtain, using an iterative procedure, the modified geometry of an aerofoil. Kennedy and Marsden (1978) inserted the required values of ψ and γ_j while retaining the A_{ij} from the previous iteration so that the iterative equations were as follows :

$$y_{ci}^d = \frac{1}{U_\infty \cos \alpha} [U_\infty x_{ci} \sin \alpha + \psi^r + \sum_{j=1}^N A_{ij}^{d-1} \gamma_j^r], \quad i = 1, 2, \dots, N$$

$$\text{and } y_{tp}^d = \frac{1}{U_\infty \cos \alpha} [U_\infty x_{tp} \sin \alpha + \psi^r + \sum_{j=1}^N A_{tpj}^{d-1} \gamma_j^r] \quad 3.3$$

Adjustments to the profile shape were made along lines $x_{ci} =$ constant, but could have been made along any other direction except one parallel to the uniform stream. The choice of ψ^r was arbitrary as this only determined the position of the aerofoil in the coordinate plane, but for the multi-component design process $\Delta\psi$, the volume flow rate through the slot, had to be specified to maintain the correct slot width. After each iteration the corner points had to be obtained from the control points and this was achieved by the so called 'shooting' or 'smoothing' methods, both of which are described in more detail in section 5 of this chapter. Figure 3.2 is a flow-chart of the design procedure with optional steps indicated.

Application of the above method to incorporate viscous effects was attempted by Dutt and Srekanth (1980), who took account of the laminar flow near the leading edge, the transition region, the turbulent flow and the turbulent wake. The design process consisted of constructing an intermediate aerofoil by adding the displacement thicknesses computed in successive iterations to an initial aerofoil until a suitable convergence criterion was satisfied. The required viscous velocity distribution was then used to calculate a new set of control points from which the modified aerofoil coordinates were obtained by subtracting the previous displacement thicknesses. This procedure required repetition until an optimum design was achieved. The method was limited in the angle of attack at which a design could be produced

by the requirement for attached flow, and the Kutta condition used by Kennedy and Marsden (1978) was replaced by the specification of zero net circulation on the first and last panels (i.e. at the trailing edge).

The inverse methods presented in the following sections have been developed from the forward algorithm of Leishman and Galbraith (1981a), who also made use of a distribution of vorticity around the aerofoil surface. In this case, however, the Neumann boundary condition of zero net flow normal to the surface was used, resulting in the following Fredholm integral equation of the first kind :

$$\vec{U}_\infty \cdot \hat{n} + \frac{1}{2\pi} \int \frac{\gamma(s')}{r(s, s')} \hat{r}_n \cdot \hat{n} \, ds' = 0 \quad 3.4$$

The discrete analogue of equation 3.4 was obtained by, first, using a polygonal representation of the aerofoil surface and, second, implementing the boundary conditions at the panel mid-points, to get:

$$\vec{U}_\infty \cdot \hat{n}_i + \sum_{j=1}^{N+1} A_{ij} \gamma_j = 0, \quad i = 1, 2, \dots, N \quad 3.5$$

where the vorticity varied linearly across each panel and was continuous at the panel corners. The mathematics associated with equations 3.5 are presented in Appendix 1.

System 3.5 also yielded N linear equations in N+1 unknowns and, as previously, a solution was obtained by implementing an appropriate Kutta condition at the trailing edge, namely

$$\gamma_1 + \gamma_{N+1} = 0$$

The properties of this algorithm are discussed elsewhere (Leishman and Galbraith, 1981a and 1981b), but its adaption to the inverse problem is presented in the following sections of this chapter.

3.3 Method 1: profile modification based on pressure difference
(ΔC_p method).

3.3.1. Development of the model

This method is based on the hypothesis that the greater is the obstruction offered by a body in a uniform, inviscid, incompressible stream, the greater are the resulting suction over the surface of the body, and vice versa. Applying this to the inverse problem of aerofoil design, the following modification at each corner point, along lines $x_j = \text{constant}$, has been proposed :

$$y_j^d = y_j^{d-1} \mp CN_j^{d-1} \Lambda, \quad j = 1, 2, \dots, N+1 \quad 3.7$$

The correction, CN_j is obtained from the difference between the required and actual pressure coefficients at the j^{th} corner point. Initially a divisor equal to the maximum required pressure coefficient was incorporated into this parameter, however this was latterly removed due to ineffective modifications at high angles of attack.

Λ represents some length dimension and three ways of specifying this were considered :

- (i) a standard value such as the aerofoil chord
- (ii) the absolute value of y_j^{d-1}
- (iii) the absolute value of the initial aerofoil coordinate at point j .

(i) was rejected from the outset as this would lead to massive modifications at the leading and trailing edges. (ii) was implemented during a number of tests but it was realised that this specification of Λ would result in an asymptotical approach to the x-axis by all points whenever $CN < 1$. As this would always be the case, no point could ever pass across the x-axis, if required.

These problems are surmountable by applying (iii), providing that the initial ordinates do not approach zero anywhere other than at the leading or trailing edges. As most standard aerofoil sections possess this characteristic, this is the specification that has been finally implemented.

The plus and minus signs in equation 3.6 refer to the lower and upper surfaces respectively, the change occurring at the required stagnation point. Initially the change of sign was to occur at the origin, but this was altered to achieve more accurate modifications in the leading edge region.

An iterative inverse procedure has been formulated by incorporating equation 3.6 into the forward algorithm mentioned in the last section (Leishman and Galbraith 1981a). This involves calculating the latest pressure distribution around the aerofoil, from which an array of corrections can be obtained and thus a modified profile derived. The stability of this approach had always been in question from the start due to the arbitrariness in the correction, CN, therefore it was decided that a limiting value would have to be imposed on this parameter. All the tests mentioned below, used to develop the model, relate to the design of the NACA 23012 aerofoil from the NACA 0012 aerofoil, using fifty panels unless otherwise stated.

Figure 3.3 is a plot of C_p^r and C_p^a versus x/c after the sixth iteration at $\alpha = 5^\circ$ and CN limited to 0.1. This is a clear illustration of an inherent instability, the origin of which can be more fully understood by referring to fig. 3.4. Unstable modifications to the profile would arise in this situation because point b has previously passed across the required pressure curve whereas points a and c have not, thereby setting up corrections of opposite sign. The corresponding profile modifications would result in points x, y and z taking up new positions at x' , y' and z' , and the formation of a sharp 'dip' which would give rise to a more unstable pressure distribution, and so on.

Attempts to control the instability by smoothing the profile after each iteration did not produce acceptable results (Veza and Galbraith, 1983b), however a process whereby the array of pressure corrections are smoothed, or filtered, provided a means of controlling this undesirable phenomenon. Figure 3.5 illustrates the effect of this filtering process, and the cause of previous problems is apparent if one examines the sample of initial corrections. The underlying trend is represented by the filtered values, and the filtering used was similar to that used for profile smoothing (Veza and Galbraith, 1983b).

A series of tests were carried out to obtain an optimum combination of correction limit and number of filterings. It was found that by successively and jointly reducing both of these in a step fashion, after a number of iterations, a reduction in the amplitude and wavelength of the oscillating pressure distribution on the modified profile could be achieved. With the above scheme implemented, limited results were obtainable and these are presented below.

3.3.2 Results

Figures 3.6 to 3.9 display the results obtained from a test carried out at $\alpha = 5^\circ$ with two step reductions in the correction limit and filtering factor. The effect on the modified pressure distribution mentioned at the end of the last section is illustrated in figs. 3.6 to 3.8, the final distribution being almost non-oscillatory and reasonably close to the required one. Figure 3.9 is a plot of the average velocity error versus iteration number, and from this the points at which the parameters changed can be identified. The velocity error at a point is defined thus :

$$e = \left| \frac{q^r - q^a}{U_\infty} \right|$$

The largest errors occurred around the leading edge where the pressure distribution was highly sensitive to the change in the local geometry. The designed aerofoil shape is illustrated in fig. 3.8 and represents a reasonably accurate solution when compared with the profile which produced the required pressure distribution.

Unfortunately, the applicability of this method to the design of non-standard aerofoils and to aerofoils at large angles of attack is severely limited, as the simple assumptions on which the method is based tend to break down. Various difficult designs were attempted, but acceptable results could not be obtained in these cases.

3.4 Method 2: profile modification using an adapted analysis technique (A.A. method)

3.4.1. Development of the model

This method was developed in an attempt to provide an efficient, stable and accurate means of designing arbitrary aerofoils in incompressible, potential flow. It was hoped that this could be achieved by incorporating an adapted form of the forward method of Leishman and Galbraith (1981a) directly into the design phase of the iterative procedure. Recalling the first term in equation 3.5, we have :

$$\begin{aligned} \vec{U}_\infty \cdot \hat{n}_i &= (\underline{i}U_\infty \cos\alpha + \underline{j}U_\infty \sin\alpha) \frac{[(y_i - y_{i+1})\underline{i} + (x_{i+1} - x_i)\underline{j}]}{L_i} \\ &= \frac{[(y_i - y_{i+1}) \cos\alpha + (x_{i+1} - x_i) \sin\alpha]}{L_i} \end{aligned}$$

where $L_i = i^{\text{th}}$ panel length.

Equation 3.5 can then be rearranged as follows :

$$\Delta y_{i \rightarrow i+1} = \frac{\Delta x_{i \rightarrow i+1} \tan \alpha}{U_\infty} + \frac{L_i \sum_{j=1}^{N+1} A_{ij} \gamma_j}{2\pi U_\infty \cos \alpha} \quad i = 1, 2, \dots, N \quad 3.7$$

From this equation it can be seen that if the arrays of Δx 's, influence coefficients, vorticity values and panel lengths can be specified at a particular angle of attack, then the Δy values can be calculated which, along with the Δx values, would define the aerofoil shape. Such a solution in one step is not possible as both the influence coefficients and panel lengths require the y components for their evaluation. Progress can be made, however, by examining the term in equation 3.7 which is causing the problem. The values of the L_i and A_{ij} are, in general, small, each taking values in the range of orders from 10^{-3} to 10^{-1} , therefore a change in the γ_j values by an order of 1 would only alter this term by a small amount.

An iterative scheme is set up whereby the γ_j 's are replaced by their respective required values, these being identical to the desired velocity distribution, and the influence coefficients and panel lengths are those of a starting aerofoil. The principle behind this procedure is that small changes in the Δy 's give rise to a different set of influence coefficients and panel lengths, these being closer to the designed values than their initial counterparts.

The iterative equation is then, as follows :

$$\Delta y_{i \rightarrow i+1}^d = \frac{\Delta x_{i \rightarrow i+1} \tan \alpha}{U_\infty} + \frac{L_i^{d+1} \sum_{j=1}^{N+1} A_{ij}^{d-1} \gamma_j^r}{2\pi U_\infty \cos \alpha} \quad i=1, 2, \dots, N \quad 3.8$$

with the Δx 's retaining their initial values.

Every time a modified array of Δy 's are obtained the panel corner points have to be located, and this is easily achieved by projecting back over the upper and lower surfaces from the leading to the trailing edge. The iterative process is stopped when a convergence criterion is satisfied, in this case when the change in average velocity error falls below one percent of the initial error. Figure 3.10 is a flowchart of the A.A. method.

A series of tests were carried out to determine the characteristics of this inverse routine and the results obtained are presented in the next section.

3.4.2. Results

Figures 3.11 and 3.12 illustrate the results obtained when the A.A. method was applied to the design of the NACA 23012 aerofoil from the initially supplied NACA 0012 aerofoil, at $\alpha = 5^\circ$ and using fifty panels. The accuracy of the final design is highlighted, in fig. 3.11, by the excellent agreement between the required and designed geometric profiles and pressure distributions. Figure 3.12 illustrates the nature of convergence, i.e. a large initial drop in error followed by increasingly more gradual reductions until, after eight iterations, the criterion was satisfied. This inherent stability is one of the major advantages of this method over the ΔC_p method.

To ensure that this method is applicable at higher angles of attack, a similar test to that described above was carried out at $\alpha = 10^\circ$. Figure 3.13 shows the designed profile along with the corresponding pressure distribution, and the close agreement with their required counterparts is evident. From fig. 3.14 it can be seen that convergence was achieved after only six iterations, fewer than was required at $\alpha = 5^\circ$; however, the slightly larger resultant error, along with the faster solution time, were representative of a trend when employing this method at higher angles of incidence.

The results from a relatively difficult test case are presented in figs. 3.15 and 3.16 and correspond to the design of the NASA GA(W)-1 aerofoil from the NACA 23015 aerofoil at 10° , using fifty panels. This was a difficult case because of the changes that were required in thickness and camber distributions around the trailing edge. The acceptable accuracy of the final design, however, is apparent from fig. 3.15. From fig. 3.16 it will be observed that the method converged to a solution after ten iterations with a resultant average velocity error of about one percent.

The most difficult test case that was considered was the design of the GU25-5(11)8 aerofoil, one of a series of low drag aerofoils developed by Nonweiler (1968) and investigated by Kelling (1968), from the NACA 0018 aerofoil at $\alpha = 10^\circ$ using fifty panels. The results are presented in figs. 3.17 and 3.18. The difficulty is represented by the parts of the required pressure distribution, in fig. 3.17, which are flat on the upper surface and deflected at the trailing edge but, despite this, the results show good agreement between the designed and desired characteristics. From fig. 3.18 it can be seen that the method converged after six iterations with a resultant error of about five percent, reducing from an initial value of over twenty-one percent.

In some cases, when this method was employed, acceptable designs could not be obtained, and this tended to occur when large changes in the thickness distribution of the initial profile were required. Although this limitation detracts from the arbitrariness of the method, difficult sections can still be designed, as the results show, if reasonable care is taken when choosing the initial aerofoil.

3.5 Discussion and comparison of the methods

When consideration is given to the two inverse methods described previously, stark contrasts can be made between their respective features. The superior stability of the A.A. method, apparent if

one compares fig. 3.11 with figs. 3.6 to 3.8, comes from the use of the analysis equations in the design process, whereas the ΔC_p method is based on an arbitrary multiplier and only takes into account the effect of the surrounding panels by filtering the corrections. The method of Kennedy and Marsden (1978) appears also to be very stable, but this is not surprising when one considers that they, again, approached the design problem by adapting an accurate analysis method.

An appreciation of the relative accuracy of the ΔC_p and A.A. methods can be gained by comparing fig. 3.9 with fig. 3.12, both of which refer to the same test, i.e., the design of the NACA 23012 from the NACA 0012 at $\alpha = 5^\circ$. These graphs clearly illustrate the greater accuracy, represented by the smaller resultant average velocity error, that was achieved by the A.A. method. The decisive factor, however, is the unsuitability of the ΔC_p method to the design of profiles which either have unusual geometries or are oriented at high angles of attack.

Kennedy and Marsden (1978) also seem to have achieved accurate results when applying their method to the design problem. The main advantage which their method appears to have over the A.A. method is that it is more applicable where relatively large changes in the thickness distribution are required between the initial and final aerofoils. One disadvantage, however, is that inaccuracies can arise when determining the panel corner points from the designed control points. They proposed two methods for locating these points (see fig. 3.19). The first consists of passing a cubic spline through the control points and interpolating. However, as shown in fig. 3.19a, large errors would occur in regions of high curvature and would have to be corrected by rotation about a fixed point, e.g. the trailing edge. The second locates the trailing edge at the trailing point (see section 3.2) so that the corner points can be found by projection through successive control points, as shown in fig. 3.19b. However, this could lead to the development of a saw-tooth surface shape, which again would have to be smoothed.

This problem in locating the corner points was further highlighted by Dutt and Sreekanth (1980), who found that the use of the projection method caused program shutdown due to rapid oscillations in the aerofoil coordinates. The A.A. method is considered less complex and more reliable in this matter in the sense that the corner points are directly obtainable from the array of computed Δy 's, and the starting point in itself does not introduce any errors.

In terms of efficiency, the A.A. method again has proved its superiority over the ΔC_p method. Comparing the graphs of error versus iteration number illustrated in figs. 3.9 to 3.12, both corresponding to the design of the NACA 23012 from the NACA 0012 at $\alpha = 5^\circ$, it can be seen that fifteen iterations were required for convergence using the ΔC_p method whereas only eight were required using the A.A. method.

3.6 Conclusions

Two new inverse methods have been presented in this chapter and comparisons have been made in order to ascertain the relevant characteristics of each one.

From the previous discussion it may be concluded that the A.A. method is superior to the ΔC_p method in the three categories of stability, accuracy and efficiency. This method compares favourably with that of Kennedy and Marsden (1978) but care must be taken when choosing an initial aerofoil, so that drastic changes in thickness distribution are avoided. Although this detracts from the generality of the method, fast, accurate results were obtained for difficult test cases and this has resulted in its application, within the department, to the design of an aerofoil section (see Niven and Galbraith, 1984) which has been tested as part of an experimental research programme concerned with certain phenomena associated with the dynamic stall of helicopter rotors.

CHAPTER 4.

A new method for predicting unsteady potential flow about an aerofoil.

4.1 Introduction

In the previous chapter the first part of the numerical package mentioned in chapter 1, a design model, was presented. In the following two chapters, i.e. chapters 4 and 5, a description is given of the unsteady analysis part of the package.

For some time aerodynamicists have recognised that unsteady flow over lifting bodies can produce beneficial effects, e.g. the phenomenon of stall delay (Carta, 1971), therefore it is important to have a method which is capable of predicting these effects. Presented in this chapter is a model for the calculation of the incompressible, inviscid flow around an aerofoil undergoing unsteady motion. Only attached flow is considered; however, the incorporation of upper surface separation is described in chapter 5. The model was developed from the steady flow algorithm of Leishman and Galbraith (1981a), in which the aerofoil surface was replaced by a linear distribution of panel vorticity. The procedure is in the same class as that of Basu and Hancock (1978b), but involves a simpler specification of the Kutta condition.

In the next section a survey of existing unsteady potential flow models is presented, followed by details of the new model. Results are presented and discussed for a number of cases which clearly illustrate relevant characteristics of unsteady flow, and conclusions drawn concerning the usefulness and applicability of the model. Information can also be obtained from Vezza and Galbraith (1984a and 1985a).

4.2 Survey of past work

Among the first unsteady potential theories were those developed

by von Karman and Sears (1938) and Theodorsen (1935), who considered a thin flat plate executing small amplitude, simple harmonic motions. Solutions for these linear problems were expressed in terms of combinations of standard Bessel functions with argument k (the reduced frequency of oscillation). Flat plate solutions for transient motions were developed by Wagner (1925) and Küssner (1940), but again second order effects were omitted. Thickness effects were considered for small amplitude oscillations by Küssner (1960), van de Vooren and van de Vel (1964) and Hewson-Browne (1963); however, these methods were based on conformal mapping techniques and thus were limited in application by the use of specific transformation equations.

In recent years, the availability of greater computational power has encouraged the development of numerical panel methods for the assessment of unsteady flows. The most fundamental was developed by Giesing (1968) from the steady model of Hess and Smith (1967). This general, non-linear potential flow method was applied step by step in time along the aerofoil flight path, starting from an initial position and orientation, and the distortion of the vortex wake evolved naturally in the solution. The Kutta condition implemented in this method was the specification of equal velocities on the upper and lower trailing edge panels. This implies that a pressure discontinuity existed across the shedding vortex sheet, which would call into question its 'free' nature.

Basu and Hancock (1978b) adapted and simplified Giesing's method and applied it to a number of different cases which illustrated the characteristics of unsteady flow. In their method the aerofoil contour is replaced by N panels, across which are placed a distribution of sources and vortices. The source strength has a unique constant value on each panel whereas the vorticity strength is the same on all panels (see fig. 4.1) and is directly related to the aerofoil circulation. The vortex sheet comprising the free wake is represented by discrete potential vortices; however, the nascent wake vorticity takes the form of a vortex panel of unknown strength, length and orientation such that $\Delta_m \gamma_{wm} = \Gamma_{m-1} - \Gamma_m$. The

Kutta condition, which ensures that there is no pressure discontinuity at the trailing edge, is :

$$q_{1m}^2 = q_{Nm}^2 + \frac{2(\Gamma_m - \Gamma_{m-1})}{(t_m - t_{m-1})} \quad 4.1$$

where the velocities are tangential to the surface.

The implementation of the Neumann boundary condition at each of the panel control points, along with equation 4.1, leads to a system of $N+1$ equations in the $N+3$ unknowns ($N+1$ singularity values, Δ_m and Θ_m) which are solved via an iterative scheme, as described below,

Initial values are ascribed to Δ_m and Θ_m ; however, a straightforward matrix solution is still unobtainable due to the non-linear quadratic equation 4.1. It is necessary to determine, from the N linear equations, the source strengths in terms of the one vorticity value γ_m , and substitute these relations into equation 4.1 which is then solved for γ_m . Once the singularity strengths have been evaluated, the velocity at the mid-point of the shedding panel is calculated and a new value for Δ_m obtained as follows :

$$\Delta_m = q\Delta t$$

A new value for Θ_m is found by ensuring that the panel is tangential to the local stream direction, and the complete process is repeated until satisfactory convergence has been achieved. The pressure distribution is obtained from the unsteady Bernoulli equation and the loads by subsequent integration.

The model presented in this chapter is based on the steady flow algorithm of Leishman and Galbraith (1981a) and is in the same class as the method of Basu and Hancock (1978b). However, because of the different approach taken, resulting in a simplification of the Kutta condition, only a set of linear simultaneous equations have to be solved, unlike the above method (Basu and Hancock, 1978b) which is complicated by the necessary solution of a quadratic. The theoretical details of the new model are presented in the next

section.

4.3 Development of the model

4.3.1 Theoretical description

The non-linear problem is one of finding the time-dependent wake and aerofoil vorticity distributions that result from applying the Neumann boundary condition on the aerofoil surface and Kelvin's theorem of constancy of total circulation. The governing integral equation is :

$$\begin{aligned} \vec{U}_\infty \cdot \hat{n}(s,t) + \frac{1}{2\pi} \int_s \frac{\gamma(s',t)}{r(s,s')} \hat{r}_n(s,s',t) \cdot \hat{n}(s,t) ds' \\ + \frac{1}{2\pi} \int_w \frac{\gamma_w(s_w,t)}{r_w(s,s_w)} \hat{r}_w(s,s_w,t) \hat{n}(s,t) ds_w = \vec{V}_r(s,t) \cdot \hat{n}(s,t) \end{aligned} \quad 4.2$$

with $\Gamma + \Gamma_w = \text{constant}$. (see fig. 4.2).

In order to obtain a solution to equation 4.2, the unsteady problem is solved at successive intervals of time starting with the steady solution at time $t = 0$. The aerofoil is represented by N panels, from upper to lower trailing edge, across which there is a linear distribution of vorticity, and the circulation around the surface, is :

$$\Gamma_m, \text{ where } \Gamma_m = \int_s \gamma(s) ds.$$

The vorticity shed at earlier times is represented by discrete vortices which convect downstream according to the induced velocity pertaining to each.

The shed vorticity at time t_m manifests itself as an extra panel attached to the trailing edge of length Δ_m , inclination θ_m and a constant strength which is specified by making use of Helmholtz's theorem of continuity of vorticity. This is related, via Kelvin's

theorem, to the change in aerofoil circulation as follows :

$$\Delta_m (\gamma_1 + \gamma_{N+1}) = \Gamma_{m-1} - \Gamma_m \quad 4.3$$

At time t_m the panels and shed vortices are as illustrated in fig. 4.3.

The discrete analogue of equation 4.2 provides N equations which satisfy the Neumann condition at the panel mid-points :

$$\vec{U}_\infty \cdot \hat{n}_i + \sum_{j=1}^{N+1} A_{ij} \gamma_j + \sum_{g=1}^{m-1} G_{ig} K_g + (\gamma_1 + \gamma_{N+1}) A_{wi} = \vec{V}_r \cdot \hat{n}_i, \quad i = 1, 2, \dots, N \quad 4.4$$

where the relevant components are due to the uniform stream, the bound vortex sheet, the wake vortices, the extra trailing edge panel and the moving boundary, respectively. The mathematical details associated with equations 4.3 and 4.4 are presented in Appendices 1 and 2.

There are, therefore, at time t_m , $N+3$ unknowns, i.e. $N+1$ values of vorticity, Θ_m and Δ_m , but only $N+1$ equations, 4.3 and 4.4, governing the flow. To obtain a solution Θ_m and Δ_m are obtained by iteration from an initial guess. The iterative scheme employed involves the application of the unsteady Bernoulli equation across the emanating wake vortex sheet, and the details of the derivation are given in Appendix 3.

Once Δ_m and Θ_m have been assumed, a solution is obtained by solving the $N+1$ linear simultaneous equations for the vorticity values $\gamma_1 \rightarrow \gamma_{N+1}$. A new value of Δ_m is obtained by ensuring that the condition of zero loading is satisfied (see Appendix 3):

$$\Delta_m = \frac{1}{2} (\gamma_{N+1} - \gamma_1) (t_m - t_{m-1})$$

and Θ_m is adjusted so that the wake panel lies along the local stream direction. The above procedure is repeated until Θ_m and Δ_m

converge.

The unsteady pressure coefficient, calculated with respect to the moving frame, follows from the unsteady Bernoulli equation (see Milne-Thomson, 1949):

$$C_p = 1 + \frac{V_r^2}{U_\infty^2} - \frac{\gamma^2}{U_\infty^2} - \frac{2}{U_\infty^2} \frac{\partial \phi}{\partial t}$$

The time derivative, $\frac{\partial \phi}{\partial t}$, is approximated by $(\phi_m - \phi_{m-1})/(t_m - t_{m-1})$, where the potential function is obtained by integrating the velocity field, as viewed in the moving frame, from upstream of the aerofoil to the leading edge, and then around the surface.

Once the calculation at time t_m has converged, the model is then set up for time t_{m+1} . The wake vortices and the extra trailing edge panel are convected to their new positions by determining the velocities at their centres and employing the first order Euler scheme :

$$\vec{r}_{vm+1} = \vec{r}_{vm} + \vec{q}_{vm} (t_{m+1} - t_m)$$

Normally the aerofoil would be rotated, if necessary, to its new position at time t_{m+1} ; however, in the present model the stream is rotated along with any wake vortices and upstream reference point, so that the influence coefficients due to the bound vortex sheet need only be calculated once at the start and thereafter remain unchanged.

4.3.2 Numerical implementation

The decision on the number of panels that should be used to represent an aerofoil was based on a compromise between accuracy on the one hand and time to perform the task on the other. In general the size of panel to be used is inversely proportional to the

surface curvature which means, for the aerofoils used here, concentration of panels around the leading edge. This was achieved by using the following analytic expression for the corner points:

$$x_i = 1 - \cos \theta_i, \theta_i = \frac{\pi}{N} (i-1), i = 1, 2, \dots, N/2+1, N \text{ even}$$

The y coordinates were then calculated from the available analytic functions for the respective NACA profiles. It has been shown (Leishman and Galbraith, 1981a) that when less than thirty panels are employed, the results obtained start to become significantly dependent on the number of panels used. Therefore, bearing in mind that the time taken to solve the matrix of coefficients is proportional to N^3 , a thirty panel representation was used for the tests presented in this chapter.

The reference potential point is initially located three chord lengths upstream from the leading edge and the change in potential calculated across each of thirty equal length panels up to this edge. The choice of what time step value, $\Delta t U_\infty / c$, to employ was made by balancing the computational time incurred with the accuracy of the results. Larger time steps were used in the lower frequency tests, where the induced velocities were not as great as occurred at higher frequencies.

Only four wake iterations were carried out per time step as thereafter both the length and orientation of the extra trailing edge panel showed little change. Figure 4.4 is a flowchart of the numerical procedure. Note that the details of the coding of the equivalent Basu and Hancock model are presented elsewhere (Veza and Galbraith, 1983c).

4.4 Results and discussion

4.4.1 Step change in incidence

The method described in section 4.3 was applied to the case

of the NACA 0012 aerofoil undergoing a sudden change in incidence from 0° to 5° . This problem represents the particular case of the time-dependent build up in lift as well as the phenomenon of the starting vortex.

The solution was obtained with short time intervals of 0.01 for $0 < tU_\infty/c \leq 0.3$, intervals of 0.05 for $0.3 < tU_\infty/c \leq 0.5$, 0.1 for $0.5 < tU_\infty/c \leq 2.0$ and finally intervals of 0.2 for $2.0 < tU_\infty/c < 20.0$. Figure 4.5a illustrates the results obtained for the build up in pressure. The evident approach to the steady state condition is further highlighted in fig. 4.5b, which illustrates the behaviour of the time dependent lift, i.e. very rapid increase over a short period followed by a more gradual increase towards the steady-state value. Figure 4.5c shows how the starting vortex comes off the trailing edge, convects downstream and rolls up in the characteristic way. Although this is not a true representation of that which actually happens, i.e. the vortex originating on the upper surface, its subsequent development is good.

4.4.2 Sinusoidal oscillations

Again using the NACA 0012 aerofoil, a solution was obtained for sinusoidal oscillations about the leading edge at a reduced frequency $k = 10$, a mean angle of 0° and amplitude 0.573° using a time step $\Delta t U_\infty/c \approx 0.04$, from zero to a time $tU_\infty/c \approx 1.9$.

Figure 4.6a illustrates the behaviour of the lift after the initial transients had faded and the response was repeatable. The very large values of this parameter were due to the high oscillation frequency, not unlike that encountered during aerofoil 'flutter'. However, not only is there a magnification of the load over the steady case, but a large lag exists of more than 180° as is shown by the initially decreasing lift values. This may be attributed to the large rates of change of the potential as well as to the magnitude of boundary velocity. The lift variations attributable to the Basu and Hancock model (1978b), to an earlier linearised model by the same authors (1978a), and to the standard linearised

solution, are also illustrated.

At high frequencies a very strong vortex sheet is shed from the trailing edge, as can be seen from the highly deformed wake pattern shown in fig. 4.6b. Also shown are the resulting wakes of similar tests carried out by both Basu and Hancock (1978b) and Giesing (1968), which further illustrate the highly non-linear nature of the problem.

Other sinusoidal tests of particular interest are low frequency, large mean angle and amplitude oscillations about the quarter chord, which are typical of helicopter rotor motions.

Figure 4.7a illustrates some results obtained from experiment (Galbraith and Leishman, 1983) and theory for a test carried out on a NACA 23012 aerofoil at a reduced frequency of 0.2, an amplitude of 6° and a mean angle of 10° . The Reynolds number and freestream Mach number of the test were 1.027×10^6 and 0.076 respectively, and the data were averaged over ten cycles. The theoretical computation was carried out using a time step $\Delta t U_\infty / c = 0.3141$ from zero to a time $t U_\infty / c = 31.41$, which corresponds to two complete cycles of oscillation, the second of which is shown. Although there appears to be poor agreement between the two results, this may be attributed to the relatively low Reynolds number at which the experiment was carried out. As may be seen from fig. 4.7b this particular aerofoil exhibits a marked variation of C_L with Reynolds number. Taking account of this variation, the results presented in fig. 4.7a are very encouraging in that the experimental lift loop has been reproduced theoretically, as has the relative orientation to the static line.

The above comparison illustrates how the unsteady potential model reproduces the characteristic lift behaviour when viscous effects are not of first order in magnitude. However, when the aerofoil motion induces the classic effects of dynamic stall then few recognisable features can be reproduced. Figure 4.8 illustrates this with results obtained from a test carried out,

again on the NACA 23012, at a reduced frequency of 0.2, amplitude of 10° and a mean angle of 13° . The experimental Reynolds number and freestream Mach number were 1.036×10^6 and 0.077 respectively, and the same time step and limit that were used in the sub-stall test were used in the theoretical model. It can be seen that the omission of unsteady separation from the model limits its applicability, although the lift variation during the upstroke has been reproduced fairly well (taking account of the Reynolds number effect).

4.4.3 Ramp motions

The ramp tests consisted of rotating an aerofoil, about the quarter chord position, at a constant angular velocity. The experimental tests incorporated angular acceleration up to the constant rate, whereas for the present calculation an 'ideal' ramp was used. Figure 4.9 illustrates the experimental (A.R.A, 1983) and theoretical results obtained from tests carried out on the NACA 0012 aerofoil at reduced ramp rates $\dot{\alpha}c/2U_\infty = 0.0016$ and 0.0065. The experimental Reynolds number and freestream Mach number were 2.6×10^6 and 0.3 respectively. This Mach number represents approximately the upper limit of applicability of incompressible theory without significant error being incurred. The theoretical tests were carried out using time steps $\Delta t U_\infty / c \approx 0.32$ for the test at $\dot{\alpha}c/2U_\infty = 0.0065$.

For ease of comparison the experimental results represent smoothed values of C_N and as can be seen the correlation with the predicted values is very good. Analogous to the sinusoidal tests mentioned in the previous section, the effect of increasing the reduced ramp rate is to modify the slopes of the lift curves, representing an increase in the lag of the response.

Also shown in fig. 4.9 are the predicted and experimental ($Re=3 \times 10^6$) static curves. The agreement in this case is much better than that obtained with the 23012 and may be attributed to the observed insensitivity of this profile to the Reynolds number

over the given range (Loftin and Smith, 1949).

4.5 Conclusions

A successful method for calculating the unsteady, incompressible potential flow around an arbitrary aerofoil has been developed. The method differs from that of Basu and Hancock (1978b) in three main ways :

- (i) the singularity distribution used, i.e. a linear distribution of panel vorticity on the aerofoil surface;
- (ii) the implementation of the Kutta condition, in particular the use of Helmholtz's theorem, to relate the shedding and net trailing edge vorticity values;
- (iii) the resultant system of equations which, because of their linearity, exclude any quadratic terms.

It is points (ii) and (iii) in particular which lead to this algorithm being simpler than that of Basu and Hancock (1978b).

It may be concluded also, from the preceding discussion in section 4.4., that the method predicts fully attached potential flow about an aerofoil, but is inappropriate where significant viscous effects, e.g. marked Reynolds number dependence and separation, or compressibility effects are present.

CHAPTER 5.

An inviscid model of unsteady, separated, aerofoil flow.

5.1 Introduction

In chapter 4 an attached potential flow model was described, forming the first part of the dynamic stall analysis code. Details of the second part are provided in this chapter, which describes the development of a new method for the prediction of unsteady, incompressible, separated flow over a two-dimensional aerofoil. The model makes use of an inviscid formulation for the flowfield and discrete vortices with finite cores are used to model the separating shear layers.

The discrete vortex method has been applied to unsteady aerofoil problems for some time (see chapter 2). Clements and Maull (1975) provided an early history of the method, and subsequently made use of it to model vortex shedding from a square based body. Other, more recent, uses of the method have been the asymptotically steady analyses of Sarpkaya (1975) and Katz (1981), who considered a flat plate and thin cambered aerofoil respectively. These efforts highlight the attempts that have been made to reproduce what are essentially viscous phenomena by the use of inviscid algorithms, i.e. they incorporate the assumption that the flow is irrotational over the entire region except at the body and its wake elements. In such schemes the magnitude of the vorticity shed from the body is usually determined from velocities sampled at the edge of the shear layer, an approach validated by the experiments of Fage and Johansen (1927) and by the analysis of boundary layer separation on aerofoils by Sears (1956 and 1976).

Recently the detailed mathematical and numerical techniques associated with discrete vortex methods were reviewed by Leonard (1980). Application of the point vortex, vortex blob and newer contour dynamics methods to two-dimensional vortical flows were discussed as well as developments in three-dimensional vortex

methods. Leonard subsequently was part of a team who incorporated the vortex core method into a new numerical scheme for the prediction of separated flows (Spalart et al.; see chapter 2).

In the following two sections, details of an unsteady, separated flow model are provided. The method is of the inviscid type and employs vortices with finite cores; however, reliance is not placed on the explicit evaluation of the shear velocities for the shed vorticity which is, rather, one of the variables in a 'Kutta' condition. The location of the separation point is a necessary input into the algorithm.

Results are presented and discussed for the cases of static and moving separation and conclusions drawn concerning the suitability and level of development of the method with regard to its applicability to the prediction of dynamic stall. Further details can be obtained from Vezza and Galbraith (1984b and 1985b).

5.2 Theoretical description of the model

The model at time t_m is set up as shown in fig. 5.1. The aerofoil is represented by N panels from upper to lower trailing-edge over which there is placed a vortex sheet of varying strength that is piecewise linear and continuous at the panel corner points. With upper surface separation present, the distribution of vorticity within the separated zone is constrained to take starting and finishing values of zero. The circulation around the aerofoil is :

$$\Gamma_m, \text{ where } \Gamma_m = \int \gamma ds,$$

and the vorticity shed at previous times is represented by discrete vortices except in the region close to the upper surface separation point, where it takes the form of $N_p - 1$ constant strength vortex panels. Two additional constant strength vortex panels appear at time t_m , one at each separation point, to account for the latest change in aerofoil circulation, in accordance with Kelvin's theorem

(Milne-Thomson, 1949). The strengths of the emanating sheets are determined by making use of Helmholtz's theorem of continuity of vorticity (Milne-Thomson, 1973) which, when applied with the former theorem, results in the following condition :

$$\Delta_1 \gamma_s + \lambda \gamma_{N+1} = \Gamma_{m-1} - \Gamma_m \quad 5.1$$

where Δ_1 and λ are the lengths of the respective panels.

In order to obtain a solution for the unknown bound vortex sheet strengths, the Neumann boundary condition specifying the flow normal to the surface is applied at the control points of the aerofoil panels, resulting in the following system of equations :

$$\begin{aligned} \vec{U}_\infty \cdot \hat{n}_i + \sum_{j=2}^N A_{ij} \gamma_j + A_{i1} \gamma_s + A_{iN+1} \gamma_{N+1} + \sum_{g=2}^{N_p} A_{ig} \gamma_{pg} + \sum_{g=1}^{N_v} G_{ig} K_g \\ = \vec{V}_r \cdot \hat{n}_i, \quad i = 1, 2, \dots, N \end{aligned} \quad 5.2$$

The second, third and fourth terms in equation 5.2 are the normal induced velocities at the i^{th} control point due to the bound vortex sheet and the two separating panels at time t_m , respectively. These terms contain the unknown vortex strengths, whereas the first, fifth, sixth and seventh terms can be completely evaluated and are the normal induced velocities at the i^{th} control point due to the free stream, the remaining wake panels, all wake vortices and the moving boundary respectively. The theoretical details associated with equations 5.1 and 5.2 are considered in Appendices 1 and 2.

The expressions 5.1 and 5.2 amount to a system of $N+1$ simultaneous equations that are linear in the $N+1$ unknown γ values. However, as Δ_1 and λ are also unknown, a solution can be obtained only by iteration from initial values assigned to both of these variables. It follows that the iterative scheme must incorporate some means of assigning new values to Δ_1 and λ , and this is achieved by considering the Bernoulli equation as it applies to vortex sheets.

If we assume that a separated wake, as illustrated in fig. 5.2, gives rise to two isolated regions R_1 and R_2 with total heads h_1 and h_2 respectively, then the Bernoulli equation can be applied across each separation point (see Appendix 3). The resultant iterative scheme for Δ_1 and λ is:

$$\Delta_1 = \left| \frac{\gamma_s}{2} - q_s \right| \Delta t$$

$$\lambda = \left| \frac{\gamma_{N+1}}{2} \right| \Delta t$$

Within the iterative cycle, the trailing edge panel is aligned with the local stream direction but, for numerical reasons which will be discussed later, this is not the case for the upper surface panels.

Once a converged solution has been obtained, the unsteady pressure coefficient is determined from Bernoulli's equation in the moving frame. In region R_1 (see fig. 5.2) this is

$$C_p = 1 + \frac{V_r^2}{U_\infty^2} - \frac{\gamma^2}{U_\infty^2} - \frac{2}{U_\infty^2} \frac{\partial \phi}{\partial t}$$

In region R_2 the equation becomes

$$C_p = 1 + \frac{V_r^2}{U_\infty^2} - \frac{\gamma^2}{U_\infty^2} - \frac{2}{U_\infty^2} \frac{\partial \phi}{\partial t} - \frac{2}{U_\infty^2} \Delta h$$

$$= 1 + \frac{V_r^2}{U_\infty^2} - \frac{\gamma^2}{U_\infty^2} - \frac{2}{U_\infty^2} \left[\frac{\partial \phi_a}{\partial t} + \frac{\partial \Delta \phi_a}{\partial t} + \frac{\partial}{\partial t} (\phi - \phi_a') + \Delta h \right]$$

$$= 1 + \frac{V_r^2}{U_\infty^2} - \frac{\gamma^2}{U_\infty^2} - \frac{2}{U_\infty^2} \frac{\partial \phi_c}{\partial t} - \frac{\gamma_s^2}{U_\infty^2} + \frac{2\gamma_s q_s}{U_\infty^2}$$

i.e.
$$C_p = 1 + \frac{V_r^2}{U_\infty^2} - \frac{(\gamma^2 + \gamma_s^2)}{U_\infty^2} + \frac{2\gamma_s q_s}{U_\infty^2} - \frac{2}{U_\infty^2} \frac{\partial \phi_c}{\partial t}$$

where ϕ_c = continuous potential in region R_2 .

The potential function is approximated by integrating the velocity field, as viewed in the moving frame, from upstream of the

aerofoil to the leading edge and then around the surface, proceeding through the upper surface separation point in a continuous manner. The term $\partial\phi/\partial t$ is taken as $(\phi_m - \phi_{m-1})/\Delta t$, and the loads are determined by integrating the pressure distribution.

Once a complete solution has been obtained at time t_m , the model is then set up for time t_{m+1} . Existing vortices are convected to their new positions by calculating the velocities of their centres and using the first order Euler scheme :

$$\vec{r}_{vm+1} = \vec{r}_{vm} + \vec{q}_{vm} (t_{m+1} - t_m)$$

The vortices are then rotated, along with the upstream reference point, through the appropriate angular increment for the time step.

The same scheme as above is used to convect the extra trailing edge panel to its new position as a discrete vortex. The upper surface panels, however, are treated differently, as detailed in section 5.3.

5.3 Numerical implementation

5.3.1 Model with fixed upper surface separation

(i) Upper surface separation

As illustrated in fig. 5.1, the separation point is located on one of the aerofoil panels between two corner points, as this positioning is essential if a solution is to be obtained.

Restrictions which follow from this are :

- (i) the separation point must be kept away from the corner points, otherwise there is one less unknown and a solution cannot be obtained.

(ii) the separation point must be kept away from the control points, otherwise infinite velocity components arise and the solution is meaningless.

Positioning the separation point at a distance of one quarter of the panel length to the right of the control point has yielded the most stable results. If separation occurs on the first panel a fully attached potential flow solution is obtained via an existing model (Veza and Galbraith, 1984a).

At the end of each time step, the vorticity emanating from the upper surface does not immediately take the form of a discrete vortex but remains as a sheet for a number of time steps. The reason for this is illustrated in fig. 5.3, where the velocity components of a constant strength vortex panel and an equivalent point vortex, placed at the centre of the panel are plotted at various stations. From this figure it may be seen that the discrete vortex approximation to a vortex sheet is very poor close to the sheet which leads, in this case, to an erroneous solution in the wake immediately downstream of the separation point. In arriving at a method of convecting this vorticity, various schemes were tried; however, greatest stability was achieved with a scheme which convects panels as a whole, i.e. $\Delta_{\text{new}} = \Delta_{\text{old}}$, $\gamma_{\text{new}} = \gamma_{\text{old}}$. This is due to the fact that any fluctuations in γ_s only propagate one panel at a time, thereby avoiding massive instantaneous changes in the local velocity field.

Unlike the trailing edge panel, geometric restrictions have been introduced to control the separated upper surface panels. The angle between the first panel and the local surface tangent, θ_p , is fixed and the angular deflection of each subsequent panel has an upper limit of $\Delta\theta_p$.

Once the panels have been convected as described above, the outermost panel becomes a discrete vortex, except at the start when the wake contains fewer than N_p panels.

(ii) Discrete vortex modelling

Initially point vortices were used to represent the shear layers. However, it was soon realised that stable solutions would not be obtained, owing to the singular nature of the flow in the vicinity of such vortices along with their proximity to the aerofoil surface. To overcome this problem, and obtain acceptable solutions, vortices with finite cores have been used. The resulting vorticity field can be written as follows :

$$\omega(\vec{r}) = \frac{1}{2\pi} \sum_{g=1}^{N_v} K_g \gamma_v (|\vec{r} - \vec{r}_g|) \quad 5.3$$

where the function γ_v describes the distribution of vorticity within the core and satisfies the normalising condition,

$$\int_0^\infty \gamma_v r dr = 1.$$

The velocity field is obtained by inserting equation 5.3 into the Biot-Savart equation to obtain (see Spalart et al., 1983):

$$\vec{q}_v = \frac{1}{2\pi} \sum_{g=1}^{N_v} K_g n (|\vec{r} - \vec{r}_g|) \begin{bmatrix} y_g - y \\ x - x_g \end{bmatrix}$$

where n is a function which makes the velocity regular throughout the core and is defined by the equation :

$$\frac{d}{dr} (r^2 n) = r \gamma_v$$

All of the results presented herein have been obtained using a constant vorticity core,

i.e. $\gamma_v = \frac{2}{\sigma^2}$, $q_v = \frac{1}{2\pi} \sum_{g=1}^{N_v} \frac{K_g}{\sigma^2} \vec{r}_n$ inside the core.

Once the vortices have been released into the stream they convect according to the induced velocities at their centres. It has been found necessary, however, to impose restrictions whenever unacceptable motions occur. These motions are due to an

inappropriate time step for vortices close to the surface of the aerofoil which, if left unhindered, can cross over this surface. Initially such vortices were eliminated from the computation, but this produced unacceptable peaks in circulation and lift and so a different scheme was developed whereby they were reflected from the surface. This was an improvement but did not stop the problem of some vortices settling very near to the surface, and hence not convecting downstream. This problem has been resolved by further ensuring that all vortices are kept outwith a given distance from the surface. At present this distance has been taken to be equal to the core radius, σ , and any vortex found within this region is relocated at the limiting boundary along the normal to the surface. Figure 5.4 illustrates these restrictions. Vortices that are close to the upper surface separation point very often do not reach this boundary for a few time steps and in such cases the temporary limiting distance used is the maximum normal distance to the surface yet achieved.

The large amount of time expended when vortex methods are used in computations usually dictates that a limit be placed on the total number of vortices contained in the wake. This is achieved by suitable coalescence. In the model described herein, two methods of coalescing vortices were used, one for each of two regions :

- (i) within a distance D_0 of the aerofoil surface, vortices of opposite sign which come closer than a distance D_v are coalesced into a single equivalent vortex. The total circulation is conserved but not the first moment of vorticity as this could result in the combined vortex being far removed from the immediate vicinity. Instead the location is calculated as if both vortices were of the same sign, i.e.,

$z_3 = (|K_1|z_1 + |K_2|z_2) / (|K_1| + |K_2|)$ where z_3 is the new position and z_1 and z_2 are the respective positions of the original two vortices.

(ii) Outwith a distance D_0 of the aerofoil surface, any two vortices are coalesced if an error criterion is satisfied. The total circulation and the first moment of vorticity are conserved in the combination, which is carried out only if the error produced at the surface is less than a certain value, e_v . The expression used to calculate this error is similar to that used by Spalart et al. (1983) :

$$\left| \frac{K_1 K_2}{K_1 + K_2} \right| \frac{|z_1 - z_2|^2}{\Delta t \, d_1^{1.5} \, d_2^{1.5}} < e_v$$

It should be noted that the most recent N_c vortices to be shed are not involved in coalescence, so that the shear layer can initially remain relatively undisturbed.

5.3.2 Model with moving upper surface separation

The numerical details associated with the modelling of moving upper surface separation are essentially the same as those outlined in section 5.3.1; however, a few significant differences do exist and these are explained below.

(i) Separation panel geometry

When the separation point moves it is desirable that it does so in a smooth, continuous manner in order to eliminate large fluctuations in q_s . However, its movement along the separation panel, for the given geometry, would have to be restricted for the reasons mentioned in section 5.3.1. To accommodate both of the above conditions, the control point is repositioned, in the manner illustrated in fig. 5.5, to allow smooth passage of the separation point over the panel. The control point is located mid-way between the separation point and a corner point, the particular one dependent upon which side of the panel

mid-point the separation point lies. In addition, the separation point is not allowed to approach within a specified fraction of the panel length of either corner point.

(ii) Retardation of the separation point during reattachment

As a result of using empirical data for the location of the separation point there exists the possibility that reattachment, if it occurs, may proceed in an inappropriate manner, this being dependent upon the accuracy of the data used. The problem, illustrated in fig. 5.6, is associated with the speed at which reattachment occurs, which cannot be faster than the convection velocities of local wake vortices. In such cases the separation point is relocated so that the outermost wake panel does not encroach on these vortices, with the limiting condition that it cannot be positioned further upstream than the location of the previous separation point.

(iii) Additional modifications

In some instances, in particular when leading edge separation occurs, a strong vortex sheet is shed from the upper surface resulting in fairly large wake panels which can protrude for a significant distance into the near wake. Since this was not the purpose of introducing these panels, which was to provide a more regular velocity field in the neighbourhood of the separation point than was obtainable with discrete vortices, the number of wake panels is temporarily reduced until the remainder lie within a given limiting distance from the aerofoil surface. The discarded panels are replaced by equivalent discrete vortices and the limiting distance implemented to date has been the vortex core radius, σ .

As mentioned in section 5.2, an iterative procedure is invoked at each time step in order to obtain a converged solution for the unknown surface vorticity distribution. The error will normally be at a minimum after the final iteration; however, if this is not the case the results from the iteration which produced the minimum error are carried forward and used in subsequent calculations.

5.3.3 Miscellaneous points

All of the results presented in the next section were obtained using a thirty panel representation of the aerofoil, as this number has been found to be satisfactory (see Leishman and Galbraith, 1981a and 1981b). To calculate the velocity potential, a reference point is located three chord lengths upstream from the leading edge and the change in potential calculated across each of thirty equal length panels which form a line between both points. The choice of what time step to use is a balance between the cost of the computation, the flow resolution required and the desire to generate a relatively stable solution.

Four iterations are carried out per time step, as this number was found to be sufficient for acceptable convergence. The numerical parameters that were assigned the same value in all of the test cases were: $N_p=4$, $N_c=20$, $\theta_p=10^\circ$, $\sigma=0.05$, $D_v=0.1$, $e_v=5 \times 10^{-4}$. Others are mentioned in the next section. A flowchart of the numerical procedure for the model with moving separation is provided in fig. 5.7.

5.4 Results and discussion

5.4.1 Step change in incidence

Figure 5.8 illustrates the results obtained following a step change in incidence from 0° - 18.25° for the NASA GA(W)-1

aerofoil. For this test $\Delta t U_\infty / c = 0.05$, $\Delta \theta_p = 0^\circ$, $D_o = 1$ and $x_s / c = 0.575$. From fig. 5.8a it may be seen that the wake at $t U_\infty / c = 15$ consists of two well defined shear layers which come together a short distance downstream followed by a thin region which extends far downstream while gradually opening out. This representation compares well with other wake models (e.g. Maskew and Dvorak, 1977), and there is no need to make initial assumptions concerning the wake shape. Figures 5.8b and 5.8c show the time dependent behaviour of the normal force and quarter chord moment. Although the initial response will not be physically accurate, as the fixed separation point does not correctly model the true initial conditions, the approach to a steady value can be observed. The build up in pressure near the leading edge to the steady state is particularly evident in fig. 5.8d and the settled chordwise pressure distribution shown in fig. 5.8e compares very favourably with the experimental data of McGhee and Beasley (1973), ($Re = 6.3 \times 10^6$, $M = 0.15$). An isometric projection of the pressure-time history is presented in fig. 5.8f, and illustrates well the constant pressure region downstream of the separation point.

Figure 5.9 illustrates the results obtained from a test where separation occurs near to the leading edge after a step change in incidence from $0^\circ - 21.14^\circ$ was applied to the same aerofoil. In this case $\Delta t U_\infty / c = 0.05$, $\Delta \theta_p = 3^\circ$, $D_o = 1$ and $x_s / c = 0.125$. From fig. 5.9a it can be seen that the shear layer emanating from the upper surface starts to break up soon after it is shed and this is due to the more severe flow field perturbations which accompany increasing amounts of separation. The result of this is that the near wake is wide and the far wake is no longer thin, exhibiting a periodic structure composed of alternately signed vortex clusters. The initial response of the normal force and quarter chord moment in figs. 5.9b and 5.9c corresponds to the passage of the first vortex cluster, although the forward movement of the separation point has not been modelled. The moment exhibits more of the oscillatory nature of the flow whereas the normal force is not unduly perturbed in its approach to a steady value. Owing to massive upper surface separation the behaviour of the leading edge pressure, illustrated

in fig. 5.9d, is markedly different from the previous cases, and the computed pressure distribution compares very favourably, fig. 5.9e, with the measured data of McGhee and Beasley (1973). The wake pressure is not always constant, owing to the passage of vortices over the aerofoil; however, for comparison purposes, a computed pressure distribution has been chosen, near $tU_\infty/c=20$, that exhibits the closest approximation to a uniform wake pressure. The pressure-time history is shown in fig. 5.9f. which illustrates well the vortex shedding and subsequent passage over the aerofoil.

5.4.2 Ramp motions

A ramp test was carried out whereby the NACA 0012 aerofoil was rotated, at a constant angular velocity about the quarter chord position, through a change in incidence from $0^\circ - 36^\circ$. For this test the reduced ramp rate $\dot{\alpha}c/U_\infty=0.02$, $\Delta tU_\infty/c=0.0545$, $\Delta\theta_p=1^\circ$ and $D_0=(1-x_g/c)/0.875$. D_0 is evaluated in the above manner to take account of the varying size of the near wake as the location of the separation point changes. The prescribed values for the separation point were obtained from the data of Scruggs et al. (1974). The direct application of their results is not strictly correct, as they presented the history of the boundary layer flow reversal point, which leads the occurrence of flow separation under unsteady conditions. However, their data provides a useful means of examining the model's capability of reproducing various features of unsteady, separated flow with moving separation.

Figure 5.10 illustrates the vortex wake produced at increasing angles of attack, ranging from fully attached flow, as illustrated in fig. 5.10a, to fully separated flow, i.e. from the leading edge of the aerofoil, as illustrated in fig. 5.10d. The moving position of the separation point can be observed from figs. 5.10b and 5.10c, and results initially in the formation of a relatively thin separating sheet which merges into a narrow far wake. However, as the separation point approaches closer to the leading edge, fig. 5.10d, strong, oppositely signed vortex clusters form immediately downstream of the aerofoil, producing a broad and highly distorted

far wake.

Figure 5.11 provides further details of the above test. Figures 5.11a and 5.11b are spline-fitted graphs of normal lift coefficient and moment coefficient versus incidence; fig. 5.11c shows the variation of the separation point location with incidence, taken from Scruggs et al. (1974), and fig. 5.11d illustrates the behaviour of the upper surface pressure coefficient with time. The post-stall oscillatory behaviour of the normal lift and moment is characteristic of flow with massive separation past a body at high incidence, e.g. a bluff body; and is associated with strong, alternate vortex shedding. This oscillatory feature is further highlighted by the spline-fitted pressure-time history within the separated zone, fig. 5.11d.

5.4.3 Sinusoidal oscillations

A test was carried out on the NACA 0012 aerofoil to obtain a solution for the case of sinusoidal oscillations in pitch about the quarter chord position at a reduced frequency $k = 0.125$, a mean angle of 12° and amplitude of 12° . This low frequency, high amplitude and mean angle combination is typical of the conditions which induce aerofoil dynamic stall, and so is of particular interest. For this test $\Delta t U_\infty / c = 0.0503$, $\Delta \theta_p = 1^\circ$ and $D_0 = (1 - x_s / c) / 0.875$. The prescribed values for the separation point were obtained, again, from the data of Scruggs et al. (1974), although these were modified during reattachment as described in section 5.3.2. As mentioned in the previous section (i.e. 5.4.2) the application of this data is not strictly correct, in this case also because a ramp is not being performed; however, it enables a qualitative assessment of the model to be made.

Figure 5.12 illustrates the wake produced as the aerofoil executes its prescribed oscillation, the arrows indicating whether the instantaneous motion is pitch-up or pitch-down. The results are presented for the second oscillatory cycle, when the solution is virtually repeatable, and illustrate well the whole process of

moving separation and vortex shedding. Figures 5.12a to 5.12d show how the wake develops from fully attached flow, at the mean incidence of 12° , to fully separated flow, at the maximum incidence of 24° . The wake remains thin, as can be observed in figs 5.12b and 5.12c, during the phase when the separation point moves forward rapidly, after which significant vortex shedding begins to occur. Figures 5.12e to 5.12h illustrate the process of reattachment, from massively separated flow, at an incidence of 19.17° , to fully attached flow, at an incidence of 0° . The wake is highly distorted during this phase due to the presence of strong, oppositely signed vortex clusters. The process of vortex shedding and passage over the upper surface of the aerofoil is particularly well illustrated in figs. 5.12f and 5.12g.

More results for the above test are presented in fig. 5.13. The behaviour of the spline-fitted normal lift and quarter chord moment in figs. 5.13a and 5.13b are qualitatively in agreement with the loads produced during aerofoil dynamic stall under similar conditions. When moment stall begins at about 19° , the normal lift continues to increase due to the extra suction produced by the shed vortices, the peak near the maximum incidence being usually referred to as the 'vortex-induced lift'. The pitch-down moment increases during this period due to the movement aft of the centre of pressure; however, after the passage of the major vortex the lift collapses and the centre of pressure moves forward reducing the negative moment. Subsequent oscillations in the normal lift and moment are due to the passage of smaller, secondary vortices, e.g. as illustrated in figs. 5.12f and 5.12g.

Figure 5.13c shows the variation of the prescribed separation point location with incidence. The most important feature of this diagram is the extent to which the separation point is retarded, compared with the prescribed values, during reattachment. The corresponding maximum speed of reattachment is modified from a prescribed value of approximately three quarters of the free stream speed to under one half of the free stream speed. It is interesting to note that this latter figure agrees with the result

of experiments that have been carried out (McCroskey, 1981).

The characteristic pressure disturbances associated with vortex shedding are illustrated in fig. 5.13d, which shows the spline-fitted pressure-time history during the second cycle of oscillation.

5.5 Conclusions

A new method has been presented in this chapter for the prediction of unsteady, incompressible, separated flow with moving separation around an arbitrary aerofoil. An inviscid formulation is used for the flow field and the shear layers are represented by discrete vortices with finite cores.

Although a number of numerical restraints have been imposed on the model, the results presented in figs. 5.8 to 5.13 are most encouraging in that many of the significant features of unsteady, separated flow have been reproduced. In relation to the work being carried out within the department of Aeronautics and Fluid Mechanics, the most interesting results are those which illustrate the typical features of dynamic stall, i.e. the ramp and sinusoidal tests. The process of vortex shedding and transport has been reproduced, as has the behaviour of the lift and moment.

This algorithm is thus regarded as being very useful, despite the fact that the moving location of the separation point has to be prescribed in advance, and forms an integral part of the design and analysis package presented in this dissertation.

CHAPTER 6.

Conclusions and suggestions for future research.

6.1 Introduction

Presented in this chapter is a summary of the major conclusions of the work detailed in chapters 2 to 5. In addition, a number of areas requiring further study are highlighted so that future research may produce improvements. The dissertation is then completed in a closing discussion on the overall merit of the work.

It is worth reiterating the purpose of carrying out this body of work. As mentioned in chapter 1, the program of research was undertaken to develop an aerofoil design and analysis package which would complement the experimental work carried out at the Glasgow University dynamic stall facility.

The program can be written down in concise form as follows :

- (i) conduct and present a survey of unsteady numerical methods applicable to the prediction of aerofoil dynamic stall;
- (ii) develop a design method capable of producing an aerofoil with a desired pressure distribution around its surface;
- (iii) develop the first part of the dynamic stall prediction code, i.e. an unsteady, attached flow algorithm;
- (iv) complete the dynamic stall prediction code by developing part 2, i.e. an unsteady, separated flow algorithm.

The extent to which this program has been carried out successfully can be determined from the summarised conclusions of the next section.

6.2 Summary of conclusions

6.2.1 Dynamic stall prediction methods

The empirical methods are used extensively within the helicopter industry but provide little detailed information about the flow field and require expensive data acquisition for correlation purposes. In the longer term the Navier-Stokes methods offer the most accurate analysis; however, at present both the computational expense and the present state of turbulence modelling could be prohibitive. The simplified models which incorporate the major features of dynamic stall, e.g. the stall vortex, utilise a mix of empiricism and theory, and are an attractive alternative for many researchers to consider. The tabular form of presentation, table 1, provides a readily available means of assessing the various models.

6.2.2. A comparison of two new inverse methods

The adapted analysis method is superior to the ΔC_p method in the three categories of stability, accuracy and efficiency. This method also compares favourably with that of Kennedy and Marsden (1978), but drastic changes in the thickness distribution should be avoided. Despite this limitation, accurate designs were obtained for a number of test cases, and the method was used within the department to design a modified NACA 23012 aerofoil which has been tested on the dynamic stall rig.

6.2.3. Modelling of unsteady, potential flow about an aerofoil

A successful method for calculating the unsteady, incompressible, potential flow about an aerofoil has been developed. The method is in the same class as that of Basu and Hancock (1978b) but differs in the singularity distribution used, the implementation of the Kutta condition and the linearity of the system of equations solved. From the variety of test cases presented it can be concluded that the method predicts fully

attached potential flow but is inappropriate where significant viscous or compressibility effects are present.

6.2.4. Modelling of unsteady, separated flow about an aerofoil

An inviscid numerical method has been developed for the prediction of unsteady, incompressible flow with moving separation around an aerofoil. Due to the inherent instability of the model a number of numerical restraints have been imposed; however, the results presented provide encouragement in that many of the significant features of unsteady, separated flow have been reproduced. The dynamic stall tests are of particular interest, with the significant features of the vortex shedding and transport process, as well as the behaviour of the unsteady loads, being reproduced. Although the location of the moving separation point has to be specified in advance, the algorithm is considered suitable for use on a production basis.

6.3 Suggestions for future research

6.3.1 Improvements in the aerofoil design model

As mentioned in chapter 3, the A.A. design method produces accurate results as long as drastic changes in thickness distribution between the initial and final aerofoils are avoided. Removal of this restriction would increase the generality of application of the model and make the choice of initial aerofoil less important. This could be achieved, perhaps, by producing step by step designs, in such difficult cases, corresponding to a number of intermediate velocity (or pressure) distributions, thereby reducing the severity of the modifications during any particular step. Additional improvements would result from the inclusion of a boundary layer displacement thickness distribution around the aerofoil during the design calculations, as this would produce a design with the required pressure distribution in "real" flow.

6.3.2 Mathematical study of the unstable nature of the unsteady flow model with separation

A mathematical study should be carried out on the nature of the instability occurring in the model incorporating moving separation. Any improvements could mean loosening some of the numerical constraints, e.g. vortex core radius, restrictions around the upper surface separation point. When major separation occurs, the vorticity value at the separation point can fluctuate considerably, and since this has a significant effect on the wake pressure, its control would stabilise the behaviour of the unsteady loads. This value is linked to the value at the trailing edge via the Kutta condition, and it is interesting to note that the latter value is very stable. This stability is not automatically transferred to the separation value, however, as it is in the steady model where the two values are equal in magnitude (see Leishman and Galbraith, 1981a), therefore a more rigorous link between the two, if possible, would be desirable.

6.3.3 Modifications to enhance the predictive capability of the unsteady flow models

The areas in which the models described in chapters 4 and 5 could be improved can be determined from table 1. Up to stall onset both models would benefit from the incorporation of viscous effects, e.g. an unsteady boundary layer calculation coupled with a laminar to turbulent transition model to determine the displacement thickness distribution, and compressibility effects, i.e. velocity corrections for compressible subsonic flow.

For the separated flow model, the conditions at stall onset could be reproduced more accurately by invoking an unsteady boundary layer calculation for predicting the location of the separation point. Some aerofoils, however, e.g. the NACA 23012, can experience sudden separation from a point in the neighbourhood of the leading edge. It is thought that this occurrence is due to the formulation of a leading edge bubble which contracts as the angle of

attack is increased, and finally ruptures, releasing vorticity into the stream. A criterion which takes account of this phenomenon could also be developed.

The prediction of the post-stall process of reattachment would be enhanced by including viscous influences, and other important factors, such as the effects of sweep and blade vortex interaction, could be given consideration in the longer term.

6.4 Concluding discussion

In response to the aims of the body of work presented in this dissertation, and outlined in section 6.1, the following conclusions can be drawn:

- (i) a detailed survey of numerical methods applicable to the prediction of dynamic stall has been carried out, the informative nature being greatly enhanced by the tabular presentation;
- (ii) a method for the design of an aerofoil with a specific static pressure distribution has been developed and is generally applicable if drastic changes in thickness distribution between the initial and final geometries are avoided;
- (iii) an unsteady, incompressible, potential aerofoil flow model has been developed which predicts fully attached flow when significant viscous and compressibility effects are not present;
- (iv) an inviscid numerical method has been developed for the prediction of unsteady, incompressible, aerofoil flow with moving separation and is particularly applicable, when the location of the separation point can be prescribed, to the case of dynamic stall originating from the trailing edge.

The methods are at a sufficient level of development to be used as part of an integrated research program within the department, in fact the design method has already been of use (see Niven and Galbraith, 1984). However, further improvements, e.g. those suggested in section 6.3, would, no doubt, enhance the predictive capabilities of the methods and therefore some consideration should be given to this in the future.

REFERENCES

- | | | |
|---------------------------------------|-------|---|
| A.R.A. | 1983 | Private communication. |
| Basu, B.C.;
Hancock, G.J. | 1978a | Two dimensional aerofoils and control surfaces in simple harmonic motion in incompressible inviscid flow. ARC-CP-1392. |
| Basu, B.C.;
Hancock, G.J. | 1978b | The unsteady motion of a two-dimensional aerofoil in incompressible inviscid flow. Journal of Fluid Mechanics, Vol.87, Part 1, pp.159-178. |
| Baudu, N.; Sagner, M.;
Souquet, J. | 1973 | Modilisation du rechrochage dynamique d'un profil oscillant. AAAF 10th Colloque d'Aeronautique Appliqué, Lille, France. |
| Beddoes, T.S. | 1980 | Prediction methods for unsteady separated flows. Special Course on Unsteady Aerodynamics, AGARD Report No. 679. |
| Beddoes, T.S. | 1982 | Representation of airfoil behaviour. AGARD-CPP-334. |
| Bhately, I.C.;
Bradley, R.G. | 1972 | A simplified mathematical model for the analysis of multi-element airfoils near stall. AGARD-CP-102. |
| Briley, W.R.;
McDonald, H. | 1977 | Solution of the multi-dimensional compressible Navier-Stokes equations by a generalised implicit method. Journal of Computational Physics, Vol.24, No.4, p.372. |
| Carta, F.O. | 1971 | Effect of unsteady pressure gradient reduction on dynamic stall delay. Journal of Aircraft, Vol.8, No.10. |

Clements, R.R.; Maull, D.J.	1975	The representation of sheets of vorticity by discrete vortices. Progress in Aerospace Sciences, Vol.16, No. 2, pp.129-146.
Chen, A.W.	1971	The determination of geometries of multiple element airfoils optimised for maximum lift co-efficient. NASA-TM-X-67491.
Crimi, P.; Reeves, B.L.	1972	A method for analysing dynamic stall. AIAA 10th Aerospace meeting, AIAA Paper No.72-87.
Dutt, H.N.V.; Sreekanth, A.K.	1980	Design of aerofoils for prescribed pressure distribution in viscous incompressible flows. Aeronautical Quarterly, Feb., pp.42-55.
Ericsson, L.E.; Reding, J.P.	1972	Dynamic stall of helicopter blades. Journal of AHS, Vol.17, No.1.
Fage, A.; Johansen, F.C.	1927	On the flow of air behind an inclined flat plate of infinite span. Proc. of Royal Society, A, Vol.116, pp.170-197.
Galbraith, R.A.McD.; Leishman, J.G.	1983	Private communication.
Gangwani, S.T.	1984	Synthesized airfoil data method for prediction of dynamic stall and unsteady airloads. Vertica, Vol.8, No.2, pp.93-118.
Gibeling, H.J.; Shamroth, S.J.; Eiseman, P.R.	1978	Analysis of strong interaction dynamic stall for laminar flow on airfoils. NASA-CR-2969.
Giesing, J.P.	1968	Nonlinear two dimensional potential flow with lift. Journal of Aircraft, Vol.5, No.2, pp.135-143.
Goldstein, A.W.; Jerison, M.	1947	Isolated and cascade airfoils with prescribed velocity distribution. NACA Report No. 869.

Gormont, R.E.	1972	A mathematical model of unsteady aerodynamics and radial flow for application to helicopter rotors. US Army AMRDL-EUSTIS Directorate Report TR-72-51.
Ham, N.D.	1968	Aerodynamic loading on a two-dimensional airfoil during dynamic stall. AIAA Journal, Vol.6, No.10.
Hess, J.L.; Smith, A.M.O.	1967	Calculation of potential flow about arbitrary bodies. Progress in Aeronautical Sciences, Vol.8, Paper 1.
Hewson-Browne, R.C.	1963	The oscillation of a thick aerofoil in an incompressible flow. Mechanics and Applied Mathematics, Vol.16, Part 1.
James, R.M.	1977	Theory and design of two-aerofoil lifting systems. Computational Methods in Applied Mechanical Engineering, Vol.10, No.1.
Johnson, W.	1969	The effect of dynamic stall on the response and airloading of helicopter rotor blades. Journal of AHS, Vol.14, No.2, pp.68-79.
Katz, J.	1981	A discrete vortex method for the non-steady separated flow over an airfoil. Journal of Fluid Mechanics, Vol.102, pp.315-328.
Kelling, F.H.	1968	Experimental investigation of a high lift, low drag aerofoil. G.U. Aero. Report No. 6802.
Kennedy, J.L.; Marsden, D.J.	1976	Potential flow velocity distributions on multi-component airfoil sections. Canadian Aeronautics and Space Journal, Vol.22, pp.243-256.

- Kennedy, J.L.;
Marsden, D.J. 1978 A potential flow design method for multicomponent airfoil sections. *Journal of Aircraft*, Vol.15, No.1, pp.47-52.
- Küssner, H.G. 1940 Das zweidimensionale problem der beliebig bewegten tragfläche unter berücksichtigung von partial bewegungen der flüssigkeit. *Luftfahrtforschung*, Vol.17, p.355.
- Küssner, H.G. 1960 Nonstationary theory of airfoils of finite thickness in incompressible flow. *AGARD Manual on Aeroelasticity, Part II, Chapter 8, Neuilly-sur-Seine, France.*
- Leishman, J.G.;
Galbraith, R.A.McD. 1981a An algorithm for the calculation of the potential flow about an arbitrary two dimensional aerofoil. *G.U. Aero. Report No. 8102.*
- Leishman, J.G.;
Galbraith, R.A.McD. 1981b A user guide to the Glasgow University potential flow computer programs. *G.U. Aero. Report No. 8103.*
- Leishman, J.G.;
Hanna, J.;
Galbraith, R.A.McD. 1982 Modelling of trailing edge separation on arbitrary two-dimensional aerofoils in incompressible flow using an inviscid flow algorithm. *G.U. Aero. Report No. 8202.*
- Leishman, J.G. 1984 Contributions to the experimental investigation and analysis of aerofoil dynamic stall. *Ph.D. dissertation, Glasgow University.*
- Leonard, A. 1980 Vortex methods for flow simulation. *Journal of Computational Physics*, Vol.37, pp.289-335.

Lewis, R.I.; Porthouse, D.T.C.	1983	Recent advances in the theoretical simulation of real fluid flows. General Meeting of N.E. Coast Inst. of Engineers and Shipbuilders, U.K.
Loftin, L.K. Jr.; Smith, H.A.	1949	Aerodynamic characteristics of 15 NACA airfoil sections at seven Reynolds numbers from 0.7×10^6 to 9.0×10^6 . NACA-TN-1945.
McAlister, K.W.; Lambert, O.; Petot, D.	1984	Application of the ONERA model of dynamic stall. NASA-TP-2399.
McCroskey, W.J.; Carr, L.W.; McAlister, K.W.	1976	Dynamic stall experiments on oscillating airfoils. AIAA Journal, Vol.14, No.1, pp.57-63.
McCroskey, W.J.	1981	The phenomenon of dynamic stall. Lecture Series 1981-4 in Unsteady Airfoils and Aeroelastic Problems in Separated and Transonic Flow, von Karman Institute.
McCroskey, W.J.; McAlister, K.W.; Carr, L.W.; Pucci, S.L.; Lambert, O.; Indergand, R.F.	1981	Dynamic stall on advanced airfoil sections. Journal of AHS, Vol. 26, No. 3, pp.40-50.
McCroskey, W.J.; Pucci, S.C.	1981	Viscous-inviscid interaction on oscillating airfoils in subsonic flow. AIAA Paper 81-0051.
McCroskey, W.J.	1982	Unsteady airfoils. Annual Review of Fluid Mechanics, Vol.14, pp.285-311.
McGhee, R.J.; Beasley, W.D.	1973	Low speed aerodynamic characteristics of a 17 percent thick aerofoil section designed for general aviation applications. NASA-TN-D-7428.

- Martensen, E. 1959 Die Berechnung der Druckverteilung an dicken Gitterprofilen mit Hilfe von Fredholmschen Integraleichungen Zweiter Art. Archive for Rational Mechanics and Analysis, Vol.3, No.3, pp.235-270.
- Martin, J.M.; Empey, R.W.; McCroskey, W.J.; Cardonna, F.X. 1973 A detailed experimental analysis of dynamic stall on an unsteady two dimensional airfoil. Aeronautical Quarterly, Vol. 1, pp.245-280.
- Maskew, B.; Dvorak, F.A. 1977 The prediction of Cl_{max} using a separated flow model. Journal of AHS, Vol.23, No.2, pp.2-8.
- Maskew, B.; Dvorak, F.A. 1985 Prediction of dynamic separation characteristics using a time-stepping viscid/ inviscid approach. 3rd Symposium on Numerical and Physical Aspects of Aerodynamic Flows, California State University, Long Beach, C.A.
- Mavriplis, F. 1974 Aerodynamic prediction and design methods of aircraft high lift systems. Proc. of the Aerodynamics Seminar, National Research Council of Canada, May, pp.1-9.
- Mehta, U.B.; Lavan, Z. 1975 Starting vortex, separation bubbles and stall - a numerical study of laminar unsteady flow around an airfoil. Journal of Fluid Mechanics, Vol. 67, pp.227-256.
- Mehta, U.B. 1977 Dynamic stall of an oscillating airfoil. AGARD-CP-227.
- Milne-Thomson, L.M. 1949 Theoretical Hydrodynamics. MacMillan and Co. Ltd., London, 2nd Edition, p.77.

- Milne-Thomson, L.M. 1973 Theoretical Aerodynamics. Dover Publications Inc., New York, 4th Edition, pp.168-169.
- Niven, A.J. 1984 A design procedure to modify the trailing edge upper surface pressure gradient of a given aerofoil. G.U. Aero. Report No. 8408.
- Galbraith, R.A.McD. 1968 A new series of low drag aerofoils. G.U. Aero. Report No. 6801.
- Nonweiler, T. 1962 Die Inkompressible potential stromung in der ebenen gitterstufe. WGLR, e.v., pp.349-353.
- Oellers, H.J. 1962 Numerical analysis of dynamic stall phenomenon of an oscillating airfoil by the discrete vortex approximation. Paper No.8, 7th International Conference on Numerical Methods in Fluid Dynamics, Stanford.
- Ono, K.; Kuwahara, K.; Oshima, K. 1971 Some solutions of the unsteady turbulent boundary layer equations. Recent Research on Unsteady Boundary Layers, Proc. IUTAM Symposium, Quebec.
- Patel, V.C.; Nash, J.F. 1977 Dynamic stall: an example of strong interaction between viscous and inviscid flows. AGARD-CP-227.
- Phillipe, J.J. 1978 Theoretical prediction of dynamic stall on oscillating airfoils. Presented at the 34th annual forum of the AHS.
- Rao, B.M.; Maskew, B.; Dvorak, F.A. 1968 An analytic study of separated flow about circular cylinders. Journal of Basic Engineering, Trans. ASME, series D, Vol.90, No.4, pp.511-520.
- Sarpkaya, T.

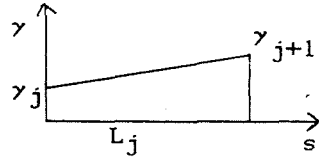
- Sarpkaya, T. 1975 An inviscid model of two dimensional vortex shedding for transient and asymptotically steady separated flow over an inclined plate. Journal of Fluid Mechanics, Vol.68, pp.109-128.
- Scruggs, R.M.; Nash, J.F.; Singleton, R.E. 1974 Analysis of flow reversal delay for a pitching foil. Paper No.74-83, 12th AIAA Aerospace Sciences Meeting, Washington, D.C.
- Sears, W.R. 1956 Some recent developments in airfoil theory. Journal of Aeronautical Sciences, Vol.23, No.5, pp.490-499.
- Sears, W.R. 1976 Unsteady motion of airfoils with boundary layer separation. AIAA Journal, Vol.14, No.2, pp.216-220.
- Shamroth, S.J.; Levy, R. 1980 Description of a constructive co-ordinate system generation computer code for isolated airfoils. Scientific Research Associates Report R80-1.
- Shamroth, S.J.; Gibeling, H.J. 1981 Analysis of turbulent flow about an oscillating airfoil using a time-dependent Navier-Stokes procedure. AGARD-CP-296.
- Smith, A.M.O.; Cebeci, T. 1967 Numerical solution to the turbulent boundary layer equations. McDonnell Douglas Report No. DAC 33735.
- Spalart, P.R.; Leonard, A.; Baganoff, D. 1983 Numerical simulation of separated flows. NASA-TM-84328.
- Theodorsen, T. 1935 General theory of aerodynamic instability and the mechanism of flutter. NACA Report No. 496.

Thwaites, B.	1949	Approximate calculation of the laminar boundary layer. Aeronautical Quarterly, Vol.1, Nov. 1949.
Tran, C.T.; Petot, D.	1980	Semi-empirical model for the dynamic stall of airfoils in view of the applications to the calculation of responses of a helicopter blade in forward flight. Paper No.48, 6th European Rotorcraft and Powered Lift Aircraft Forum, Bristol, England.
van de Vooren, A.I.; van de Vel, H.	1964	Unsteady profile theory in incompressible flow. Archiwum Mechaniki Stosowanej, Vol.3, No.16, pp.709-735.
van Driest, E.R.; Blumer, C.B.	1963	Boundary layer transition: freestream turbulence and pressure gradient effects. AIAA Journal, Vol.1, No.6, pp.1303-1306.
Veza, M.; Galbraith, R.A.McD.	1983a	A brief survey of dynamic stall prediction methods. G.U. Aero. Report No. 8301.
Veza, M. Galbraith, R.A.McD.	1983b	A comparison of two new methods for the design of aerofoils with specific pressure distributions. G.U. Aero. Report No. 8303.
Veza, M. Galbraith, R.A.McD.	1983c	An algorithm for the prediction of unsteady, potential flow about an arbitrary aerofoil. G.U. Aero. Report No. 8306.
Veza, M.; Galbraith, R.A.McD.	1984a	A method for predicting unsteady potential flow about an aerofoil. G.U. Aero. Report No. 8401.
Veza, M.; Galbraith, R.A.McD.	1984b	Modelling of unsteady, incompressible separation on an aerofoil using an inviscid flow algorithm. G.U. Aero. Report No. 8412.

- Veza, M.;
Galbraith, R.A.McD. 1985a A method for predicting unsteady potential flow about an aerofoil. International Journal for Numerical Methods in Fluids, Vol.5, No.4, pp.347-356.
- Veza, M.;
Galbraith, R.A.McD. 1985b An inviscid model of unsteady aerofoil flow with fixed upper surface separation. International Journal for Numerical Methods in Fluids, Vol.5, No.6, pp.577-592.
- von Karman, T.;
Sears, W.R. 1938 Airfoil theory for non-uniform motion. Journal of Aeronautical Sciences, Vol.5, pp.379-390.
- Wagner, H. 1925 Dynamischer auftrieb von tragflügeln. Zeitschrift Fuer Angewandte Mathematik und Mechanik, Vol.5, p.17.
- Werlé, H. 1976 ONERA film OAh No. 2506.
- Wilby, P.G. 1980 The aerodynamic characteristics of some new RAE blade sections and their potential influence on rotor performance. Vertica, Vol.4, pp.121-133.
- Wilkinson, D.H. 1967 A numerical solution of the analysis and design problems for the flow past one or more aerofoils or cascades. ARC R&M 3545.
- Young Jr., W.H. 1981 Fluid mechanics mechanisms in the stall process for helicopters. NASA-TM-81956

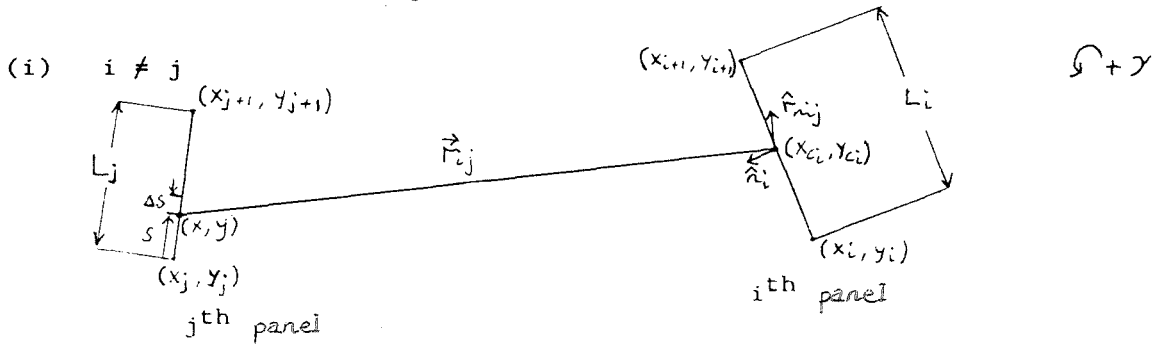
APPENDIX 1

Vortex panel method—derivation of the influence coefficient at the i^{th} control point due to the j^{th} panel.



The vorticity at any point along the panel is :

$$\gamma = \gamma_j + \frac{(\gamma_{j+1} - \gamma_j)}{L_j} s$$



velocity component normal to i^{th} panel induced by element of vorticity across Δs

$$|\Delta q_{nij}| = \frac{\gamma \Delta s}{2\pi |\vec{r}_{ij}|} (\hat{r}_{nij} \cdot \hat{n}_i)$$

\therefore total normal velocity component can be written:

$$|\vec{q}_{nij}| = \frac{1}{2\pi} \int_0^{L_j} \frac{\gamma (\hat{r}_{nij} \cdot \hat{n}_i)}{|\vec{r}_{ij}|^2} ds$$

$$\text{where } \hat{n}_i = \frac{(y_{i+1} - y_i)\underline{i} + (x_i - x_{i+1})\underline{j}}{L_i}$$

$$\vec{r}_{nij} = (y - y_{ci})\underline{i} + (x_{ci} - x)\underline{j}$$

$$\text{and } |\vec{r}_{ij}|^2 = s^2 + bs + c$$

$$\text{where } b = -\frac{2}{L_j} \left\{ (x_{ci} - x_j)(x_{j+1} - x_j) + (y_{ci} - y_j)(y_{j+1} - y_j) \right\}$$

$$c = (x_{ci} - x_j)^2 + (y_{ci} - y_j)^2$$

And so :

$$\begin{aligned} |\vec{q}_{nij}| &= \frac{1}{2\pi} \int_0^{L_j} \left[\frac{\left[\gamma_j + \frac{(\gamma_{j+1} - \gamma_j)s}{L_j} \right] \left\{ \left[\frac{y_j - y_{ci} + \frac{(y_{j+1} - y_j)s}{L_j} \right] \underline{i} \right. \right.}{s^2 + bs + c} \\ &\quad \left. \left. + \left[\frac{x_{ci} - x_j - \frac{(x_{j+1} - x_j)s}{L_j} \right] \underline{j} \right\} \cdot \hat{n}_i \right] ds \\ &= \frac{1}{2\pi L_j} [(I_1 \gamma_j + I_2 \gamma_{j+1})\underline{i} + (I_3 \gamma_j + I_4 \gamma_{j+1})\underline{j}] \cdot \hat{n}_i \quad (A1.1) \end{aligned}$$

where

$$I_1 = \int_0^{L_j} \frac{[L_j(y_j - y_{ci}) + (y_{j+1} - 2y_j + y_{ci})s - \frac{(y_{j+1} - y_j)s^2}{L_j}]}{s^2 + bs + c} ds$$

$$I_2 = \int_0^{L_j} \frac{[(y_j - y_{ci})s + \frac{(y_{j+1} - y_j)s^2}{L_j}]}{s^2 + bs + c} ds$$

$$I_3 = \int_0^{L_j} \frac{[(x_{ci} - x_j)L_j - (x_{j+1} - 2x_j + x_{ci})s + \frac{(x_{j+1} - x_j)s^2}{L_j}]}{s^2 + bs + c} ds$$

$$I_4 = \int_0^{L_j} \frac{[(x_{ci} - x_j)s - \frac{(x_{j+1} - x_j)s^2}{L_j}]}{s^2 + bs + c} ds$$

The evaluation of the integrals I_1 - I_4 is given in Leishman and Galbraith (1981a)

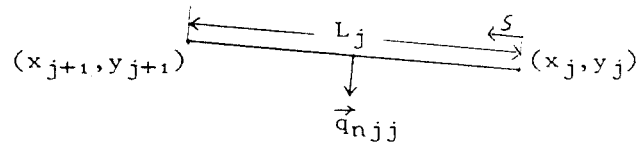
From equation A1 we can obtain the coefficients of γ_j and γ_{j+1}

$$|\vec{q}_{nij}| = B_{ij}\gamma_j + C_{ij}\gamma_{j+1}$$

where $B_{ij} = \frac{1}{2\pi L_j} (I_{1i} + I_{3j}) \cdot \hat{n}_i$

$$C_{ij} = \frac{1}{2\pi L_j} (I_{2i} + I_{4j}) \cdot \hat{n}_i$$

(ii) $i = j$



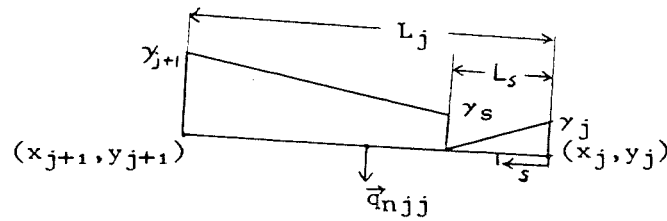
$$|\vec{q}_{njj}| = \int_0^{L_j} \frac{\gamma ds}{2\pi \left[\frac{L_j}{2} - s \right]}$$

$$= \frac{1}{2\pi} \int_0^{L_j} \frac{[\gamma_j + \frac{(\gamma_{j+1} - \gamma_j)s}{L_j}]}{\frac{L_j}{2} - s} ds$$

$$\begin{aligned}
&= \frac{1}{2\pi} \left\{ \left[-\gamma_j \ln \left| \frac{L_j}{2} - s \right| \right]_0^{L_j} - (\gamma_{j+1} - \gamma_j) \int_0^{L_j} \left[\frac{1}{L_j} - \frac{1}{L_j - 2s} \right] ds \right\} \\
&= \frac{1}{2\pi} (\gamma_j - \gamma_{j+1}) \\
&= B_{jj}\gamma_j + C_{jj}\gamma_{j+1}
\end{aligned}$$

where $B_{jj} = \frac{1}{2\pi}$, $C_{jj} = -\frac{1}{2\pi}$

(iii) $i = j$ and separation occurs on panel



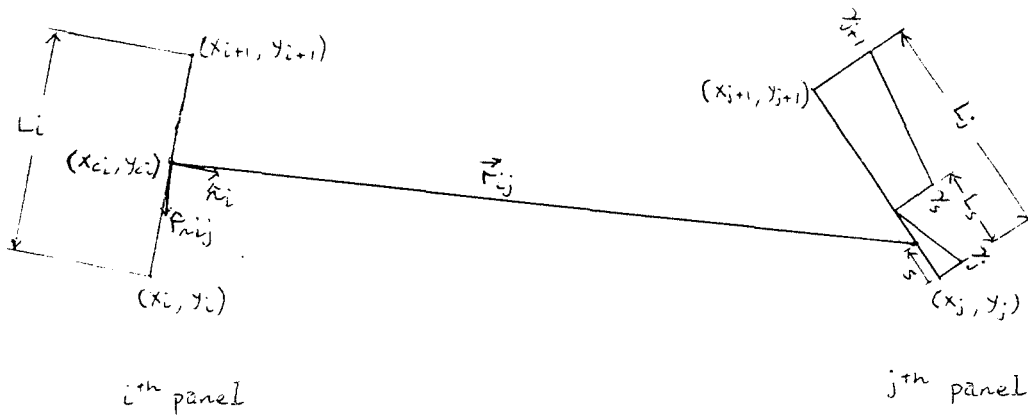
$$\begin{aligned}
|\vec{q}_{njj}| &= \int_0^{L_s} \frac{\gamma ds}{2\pi \left[\frac{L_j}{2} - s \right]} + \int_{L_s}^{L_j} \frac{\gamma ds}{2\pi \left[\frac{L_j}{2} - s \right]} \\
&= \frac{\gamma_j}{2\pi} \int_0^{L_s} \frac{\left[1 - \frac{s}{L_s} \right]}{\left[\frac{L_j}{2} - s \right]} ds + \frac{1}{2\pi} \int_{L_s}^{L_j} \frac{\left[\gamma_s + \frac{s-L_s}{L_j-L_s} (\gamma_{j+1} - \gamma_s) \right]}{\frac{L_j}{2} - s} ds \\
&= \frac{1}{2\pi} \left\{ \gamma_j \left[1 + \frac{L_j}{2L_s} - 1 \right] \ln \left| \frac{L_j - 2L_s}{L_j} \right| \right\} - \gamma_s \ln \left| \frac{L_j}{L_j - 2L_s} \right| \\
&\quad - \left[\frac{\gamma_{j+1} - \gamma_s}{L_j - L_s} \right] \left[L_j - L_s + \left[\frac{L_j}{2} - L_s \right] \ln \left| \frac{L_j}{L_j - 2L_s} \right| \right] \left\} \\
&= B_{jj}\gamma_j + C_{jj}\gamma_{j+1} + D_{jj}\gamma_s
\end{aligned}$$

where
$$B_{jj} = 1 + \left[\frac{L_j}{2L_s} - 1 \right] \ln \left| 1 - \frac{2L_s}{L_j} \right|$$

$$C_{jj} = - \left[1 + \frac{\left[\frac{L_j}{2} - L_s \right]}{\left[L_j - L_s \right]} \ln \left| \frac{L_j}{L_j - 2L_s} \right| \right]$$

$$D_{jj} = 1 - \left[\frac{\frac{L_j}{2}}{L_j - L_s} \right] \ln \left| \frac{L_j}{L_j - 2L_s} \right|$$

(iv) $i \neq j$ and separation occurs on panel j



This case involves the same integrals derived in (i) (see Leishman et al. 1982)

$$|\vec{q}_{n_{ij}}| = B_{ij}\gamma_j + C_{ij}\gamma_{j+1} + D_{ij}\gamma_s$$

The value of the coefficient A_{ij} in Appendix 2 for cases (i)-(iv) is given by :

$$A_{ij} = B_{ij} + C_{ij-1}$$

APPENDIX 2.

Matrix of coefficients

After the boundary conditions have been applied at each of the control points there are N equations in N + 1 unknowns :

$$\begin{array}{l}
 A_{11}\gamma_1 + A_{12}\gamma_2 + A_{13}\gamma_3 + \dots + A_{1N-1}\gamma_{N-1} + A_{1N}\gamma_N + A_{1N+1}\gamma_{N+1} = a_1 \\
 \cdot \\
 \cdot \\
 \cdot \\
 \cdot \\
 \cdot \\
 A_{N1}\gamma_1 + A_{N2}\gamma_2 + A_{N3}\gamma_3 + \dots + A_{NN-1}\gamma_{N-1} + A_{NN}\gamma_N + A_{NN+1}\gamma_{N+1} = a_N
 \end{array}$$

The necessary extra equation comes from specifying the shed circulation

(i) attached flow :

$$\begin{aligned}
 \Delta(\gamma_1 + \gamma_{N+1}) &= \Gamma_{m-1} - \Gamma_m \\
 \Rightarrow \Delta(\gamma_1 + \gamma_{N+1}) + \frac{1}{2} \sum_{j=1}^N (\gamma_j + \gamma_{j+1}) L_j &= \Gamma_{m-1} \\
 \Rightarrow \left(\Delta + \frac{L_1}{2}\right)\gamma_1 + \frac{(L_1 + L_2)}{2}\gamma_2 + \dots + \frac{(L_{N-1} + L_N)}{2}\gamma_N + \left[\frac{L_N}{2} + \Delta\right]\gamma_{N+1} &= \Gamma_{m-1}
 \end{aligned}$$

(ii) separated flow : ($\gamma_1=0$, replaced by γ_s in column 1)

$$\begin{aligned}
 \Delta_1\gamma_s + \lambda\gamma_{N+1} &= \Gamma_{m-1} - \Gamma_m \\
 \Rightarrow \Delta_1\gamma_s + \lambda_1\gamma_{N+1} + \frac{1}{2} \sum_{\substack{j=1 \\ j \neq N_s}}^N (\gamma_j + \gamma_{j+1}) L_j + \gamma_{N_s} \frac{L_s}{2} + \frac{[\gamma_s + \gamma_{N_s+1}]}{2} (L_{N_s} - L_s) &= \Gamma_{m-1}
 \end{aligned}$$

$$\begin{aligned}
=> \left[\Delta_1 + \frac{(L_{N_s} - L_s)}{2} \right] \gamma_s + \frac{(L_1 + L_2)}{2} \gamma_2 + \dots + \frac{(L_{N_s-1} + L_s)}{2} \gamma_{N_s} \\
& + \frac{(L_{N_s} - L_s + L_{N_s+1})}{2} \gamma_{N_s+1} + \dots + \frac{(L_{N-1} + L_N)}{2} \gamma_N + \left[\frac{L_N}{2} + \lambda \right] \gamma_{N+1} = \Gamma_{m-1}
\end{aligned}$$

APPENDIX 3.

Derivation of the iterative relations governing the shed vorticity.

(i) Attached flow

Bernoulli equation applied across the free vortex sheet emanating from the trailing edge yields :

$$\frac{P_1 - P_{N+1}}{\rho} = 0 = \frac{\gamma_{N+1}^2}{2} - \frac{\gamma_1^2}{2} + \frac{\partial(\Phi_{N+1} - \Phi_1)}{\partial t}$$

i.e.
$$\frac{\partial(\Phi_{N+1} - \Phi_1)}{\partial t} = \frac{1}{2} (\gamma_1^2 - \gamma_{N+1}^2) = \frac{\partial \Gamma_m}{\partial t}, \text{ as } \Gamma_m = \Phi_{N+1} - \Phi_1$$

However, $\Delta_m (\gamma_1 + \gamma_{N+1}) = \Gamma_{m-1} - \Gamma_m$

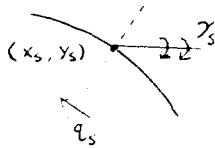
we must have :
$$\frac{1}{2} (\gamma_{N+1}^2 - \gamma_1^2) \Delta t = (\gamma_1 + \gamma_{N+1}) \Delta_m$$

and a new value of Δ_m is obtained from :

$$\Delta_m = \frac{1}{2} (\gamma_{N+1} - \gamma_1) \Delta t$$

(ii) Separated flow (see fig. 5.2)

Bernoulli equation applied across the free vortex sheet emanating from the upper surface yields :



$$\frac{P_a - P_a'}{\rho} = 0 = \Delta h + \left[\frac{\partial \Phi_a'}{\partial t} - \gamma_a' q_s \right] - \left[\frac{\partial \Phi_a}{\partial t} - \gamma_a q_s \right] + \frac{\gamma_a'^2}{2} - \frac{\gamma_a^2}{2}$$

$$\Rightarrow \frac{\gamma_s^2}{2} - \gamma_s q_s = \Delta h + \frac{\partial \Delta \phi_s}{\partial t} \quad (\text{A3.1})$$

Bernoulli equation applied across the free vortex sheet emanating from the trailing edge yields :

$$\frac{p_b - p_b'}{\rho} = 0 = \Delta h + \frac{\partial \phi_b'}{\partial t} - \frac{\partial \phi_b}{\partial t} + \frac{\gamma_b'^2}{2} - \frac{\gamma_b^2}{2}$$

$$\Rightarrow \frac{\gamma_{N+1}^2}{2} = \Delta h + \frac{\partial \Delta \phi_{N+1}}{\partial t} \quad (\text{A3.2})$$

Combining equations A3.1 and A3.2, we get :

$$\frac{\gamma_s^2}{2} - \gamma_s q_s - \frac{\gamma_{N+1}^2}{2} = \frac{\partial (\Delta \phi_s - \Delta \phi_{N+1})}{\partial t} \quad (\text{A3.3})$$

Simplifying the right hand side of equation A3.3, we get

$$\phi_a' - \phi_b' + \phi_b - \phi_a = \phi_a' - \phi_a - (\phi_b' - \phi_b)$$

$$\Rightarrow \Gamma_m = \Delta \phi_s - \Delta \phi_{N+1}$$

$$\frac{\gamma_s^2}{2} - \gamma_s q_s - \frac{\gamma_{N+1}^2}{2} = \frac{\partial \Gamma_m}{\partial t} = \frac{\Gamma_m - \Gamma_{m-1}}{\Delta t} \quad (\text{A3.4})$$

However, $\Delta_1 \gamma_s + \lambda \gamma_{N+1} = \Gamma_{m-1} - \Gamma_m$

and by examining equations A3.1, A3.2 and A3.4, it will become apparent that the relevant iterative scheme for Δ_1 and λ , consistent with continuity of vorticity at the separation points, is :

$$\Delta_1 = \left| \frac{\gamma_s}{2} - q_s \right| \Delta t$$

$$\lambda = \left| \frac{\gamma_{N+1}}{2} \right| \Delta t$$

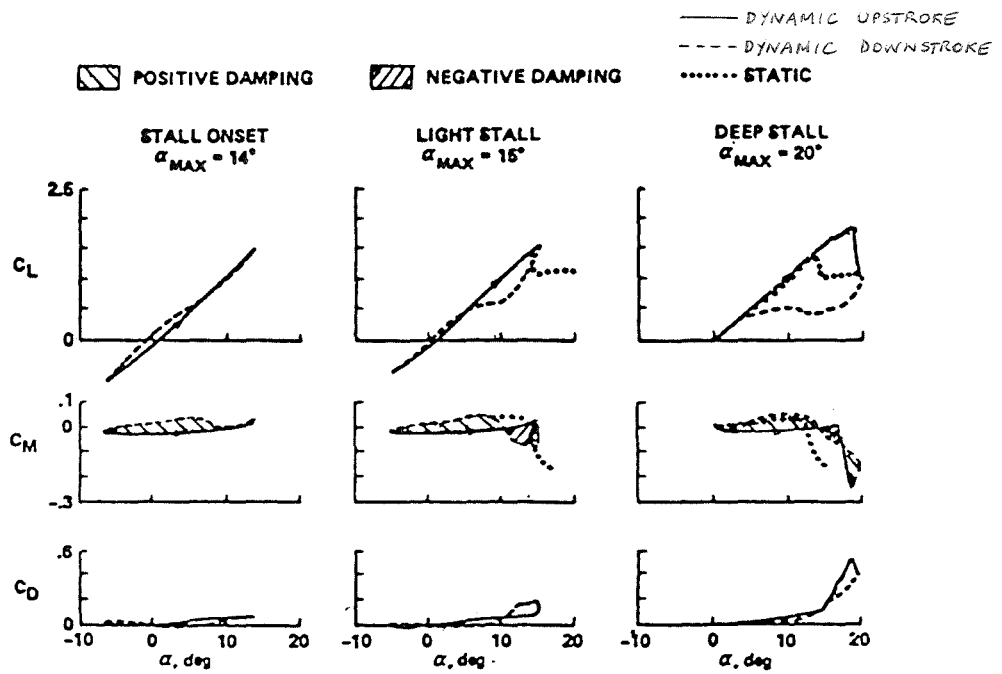


FIG 2.1 UNSTEADY LOADS IN THREE DYNAMIC STALL REGIMES:
 $M=0.3$, $\alpha = \alpha_0 + 10^\circ \cos(\Omega t)$, $k=0.1$
 (From McCROSKEY, 1982)

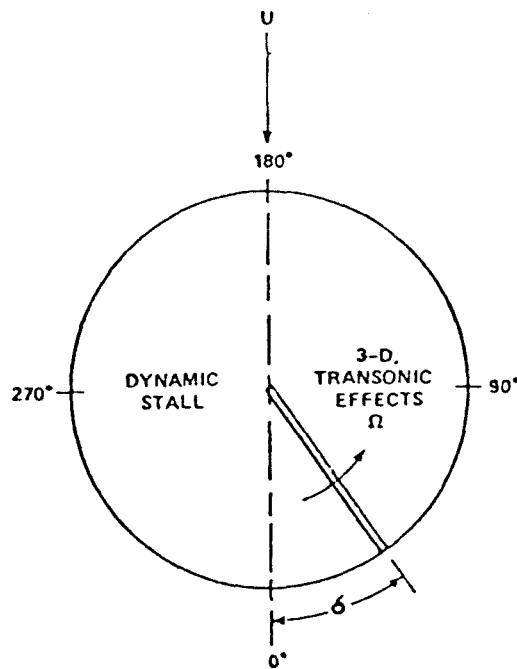
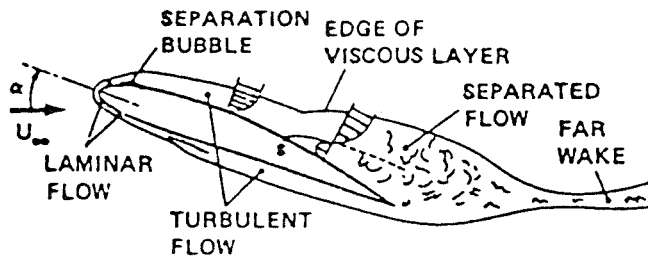


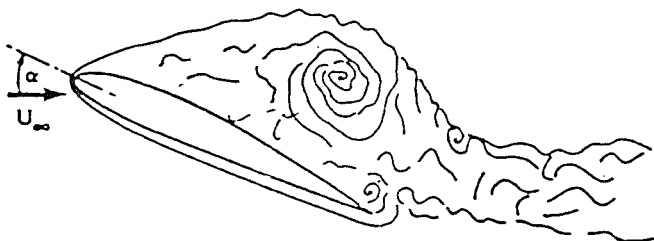
FIG 2.2 A ROTATING HELICOPTER BLADE IN UNIFORM FLOW
 (From MEHTA, 1977)

(a) LIGHT STALL
TRAILING-EDGE SEPARATION



- STRONG INTERACTION
- VISCOUS LAYER = $O(\text{AIRFOIL THICKNESS})$

(b) DEEP STALL



- VORTEX DOMINATED
- VISCOUS LAYER = $O(\text{AIRFOIL CHORD})$

FIG 2.3 FLOW FIELDS DURING DYNAMIC STALL
(From McCROSKEY, 1982)

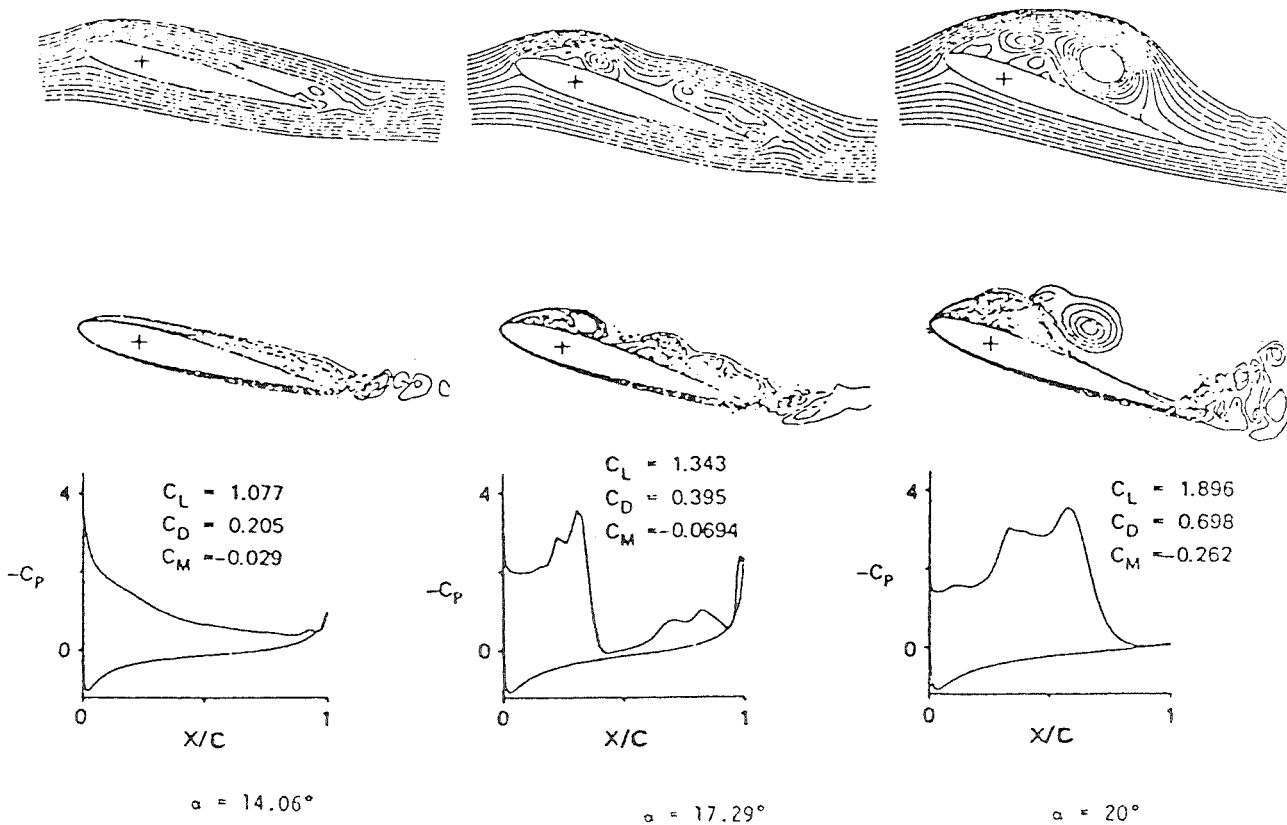


FIG 2.4 DYNAMIC STALL OF MODIFIED NACA 0012: $Re=10^4$,
 $\alpha=10^\circ(1-\cos(\Omega t))$, $k=0.25$
(from NEHTA, 1977)

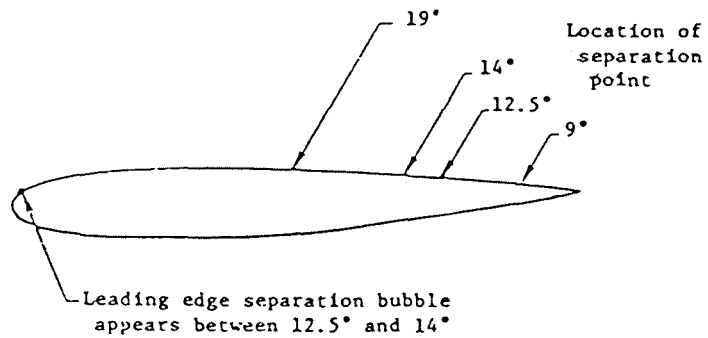
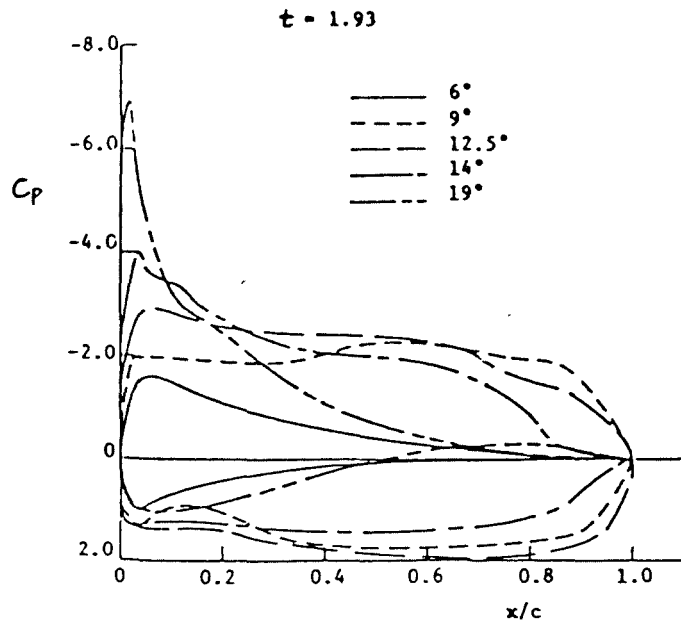
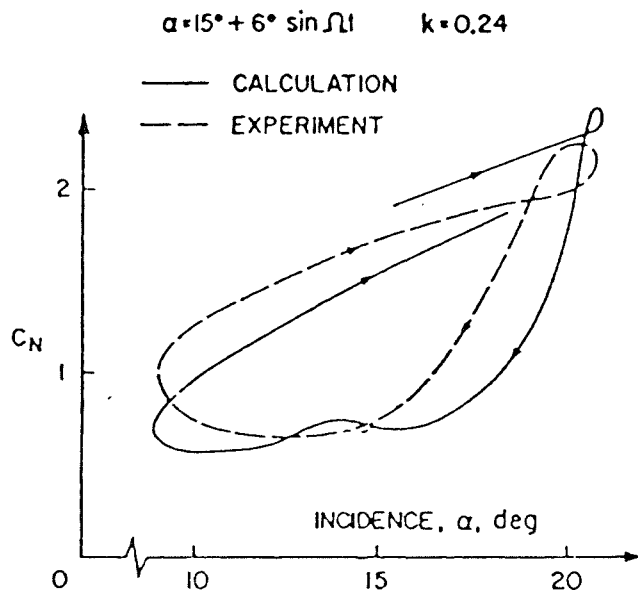
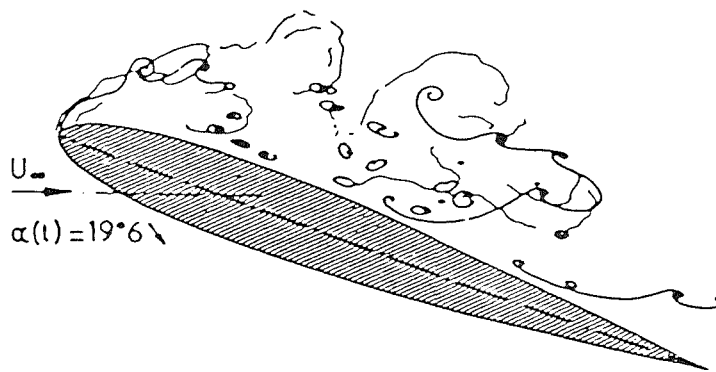


FIG 2.5 RESULTS FOR THE NACA 0012 IN RAMP MOTION:
 $M=0.147$, $\alpha = 6^\circ + 6.5^\circ(1 - \cos(\Omega t))$
 (From SHAMROTH and GIBELING, 1981)



NORMAL LIFT VARIATION

visualisation
 calculation



UNSTEADY VORTICAL WAKE

FIG 2.6 DYNAMIC STALL ON AN OSCILLATING NACA 0012
(From BAUDU et al., 1973)

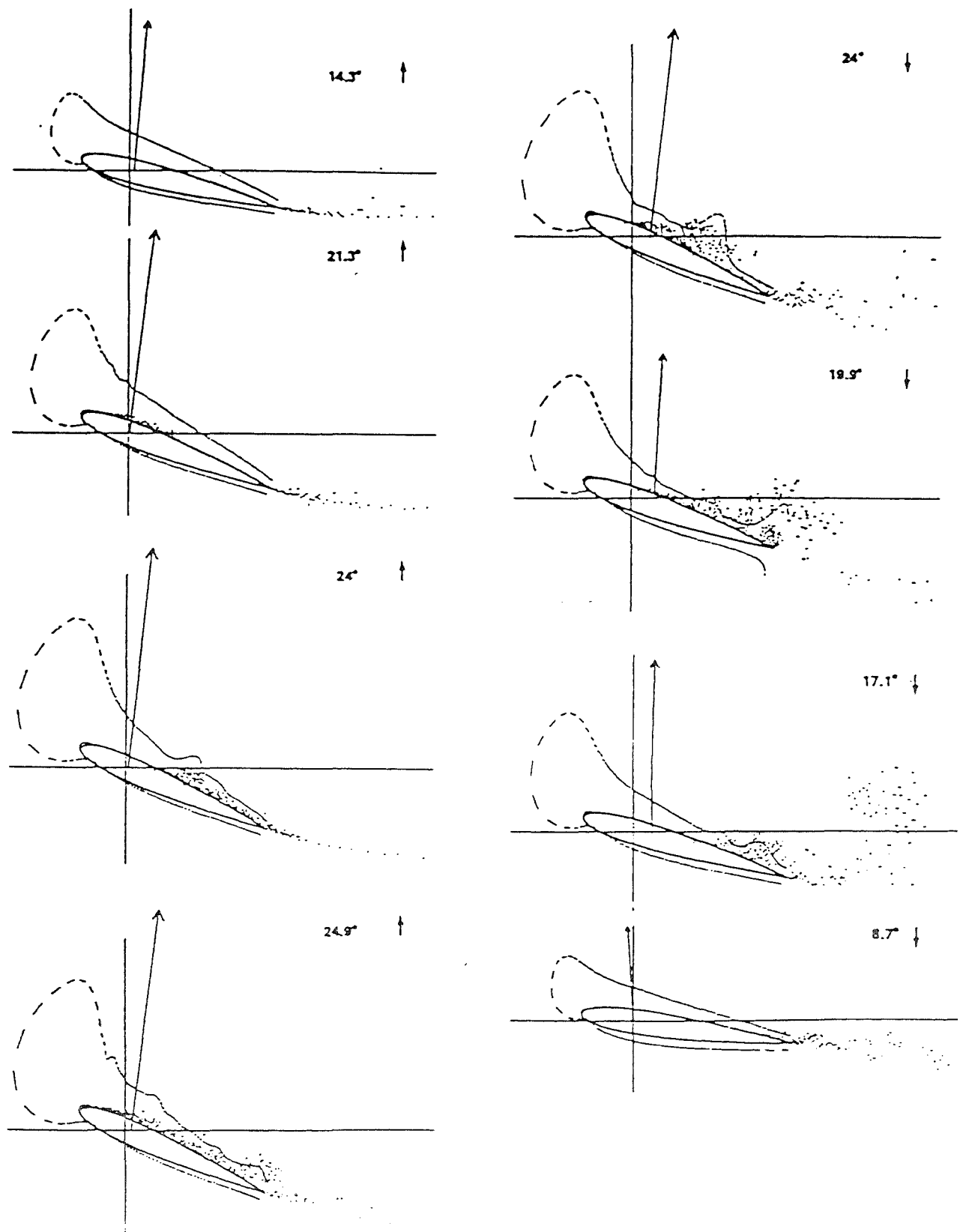


FIG 2.7(a) STILLS OF THE DYNAMIC STALL SIMULATION
 (From SPALART et al., 1983)

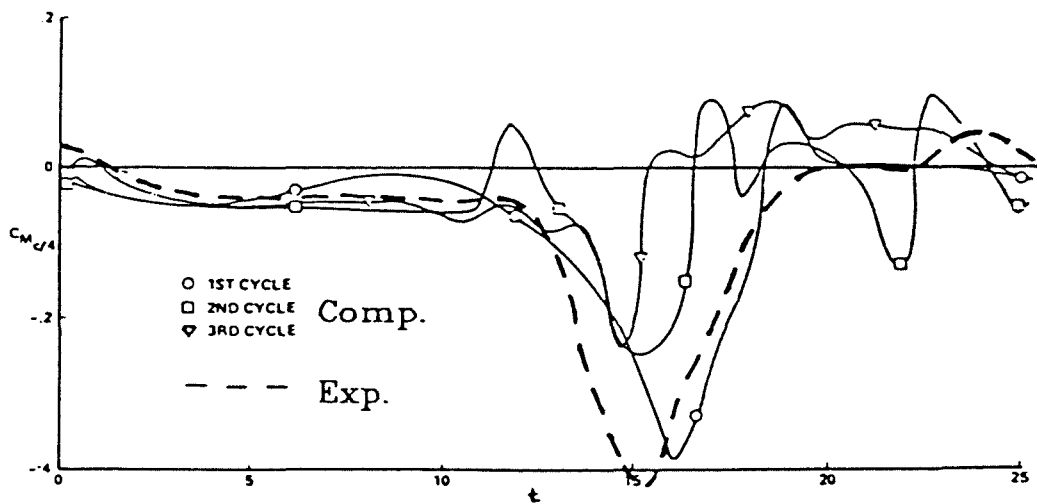
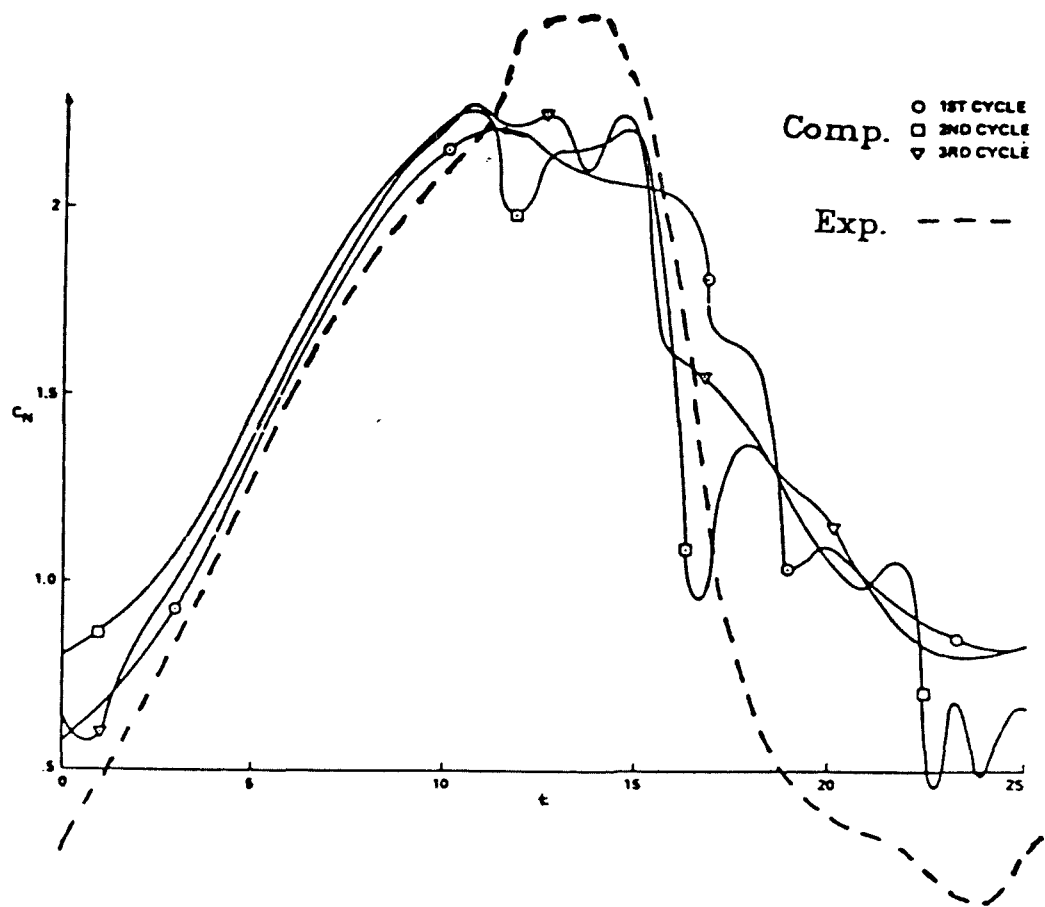
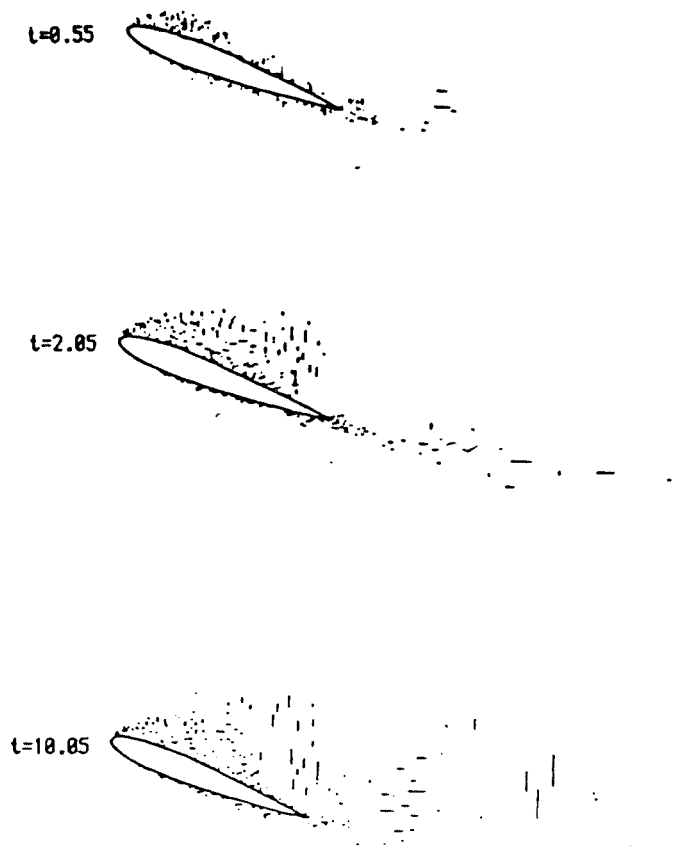
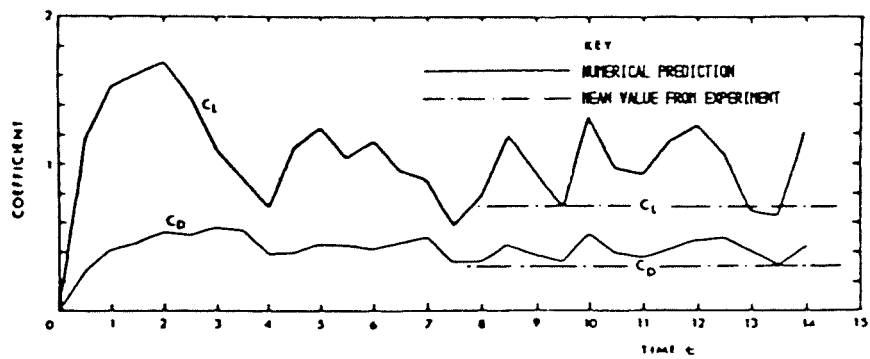


FIG 2.7(b) UNSTEADY LOADS DURING DYNAMIC STALL
 (From SPALART et al., 1983)

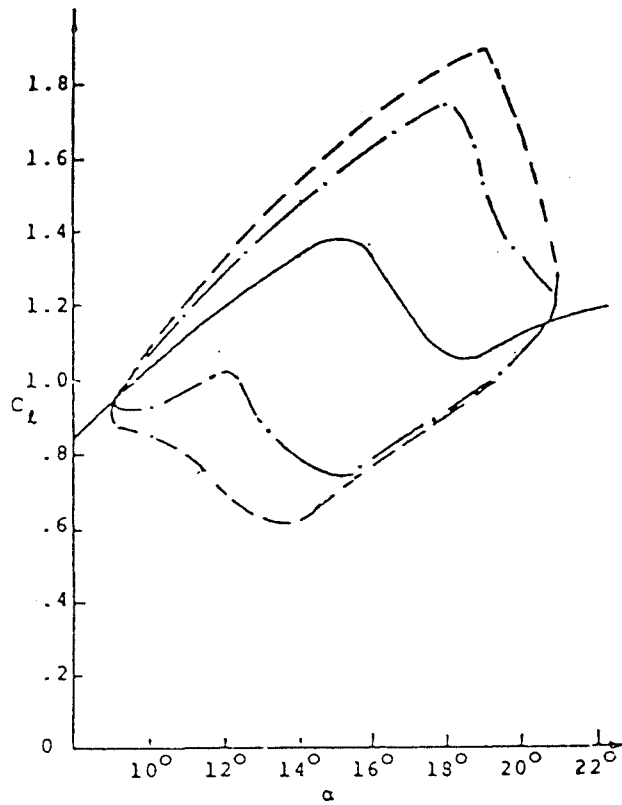


EVOLUTION OF UNSTEADY SEPARATION



TIME-DEPENDENT LIFT AND DRAG

FIG 2.8 STALLING OF THE NACA 0012 AT 20 DEGREES
(From LEWIS and PORTHOUSE, 1983)

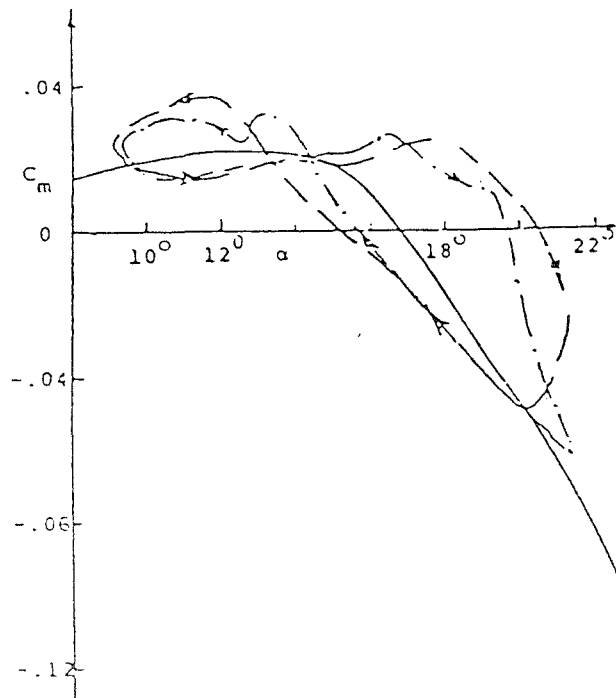


C_L Versus α .

$$\alpha = 15^\circ + 6^\circ \sin \Omega t$$

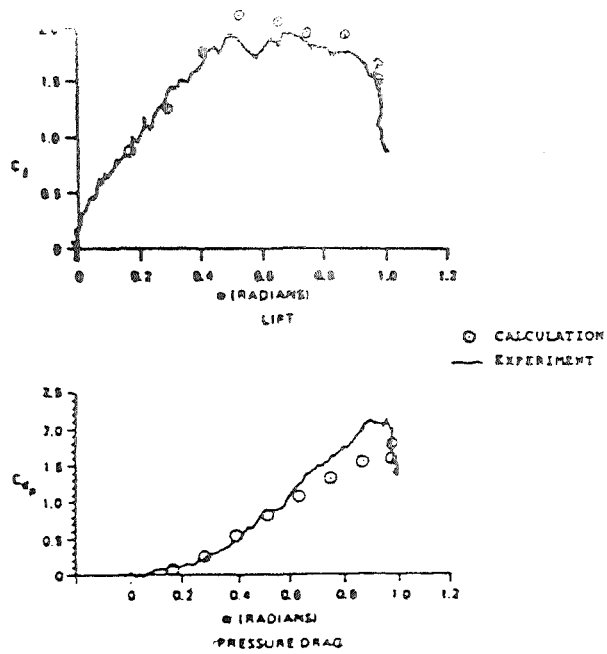
$$\alpha_{nop} = 15^\circ + 6^\circ \sin(\Omega t - \delta)$$

- $\delta = 0^\circ$
- · - $\delta = 30^\circ$ $k=0.0928$
- - - $\delta = 45^\circ$ $k=0.1392$



C_m Versus α .

FIG 2.9 RESULTS FOR THE NACA 0012 OSCILLATED IN PITCH
(From RAO et al., 1978)



$k = 0.089$, $\alpha_{max} = 56$ Degrees.

FIG 2.10 LIFT AND PRESSURE DRAG ON THE NACA 0012 DURING RAMP MOTION ABOUT $X/C=0.317$
 (From MASKEW and DVORAK, 1985)

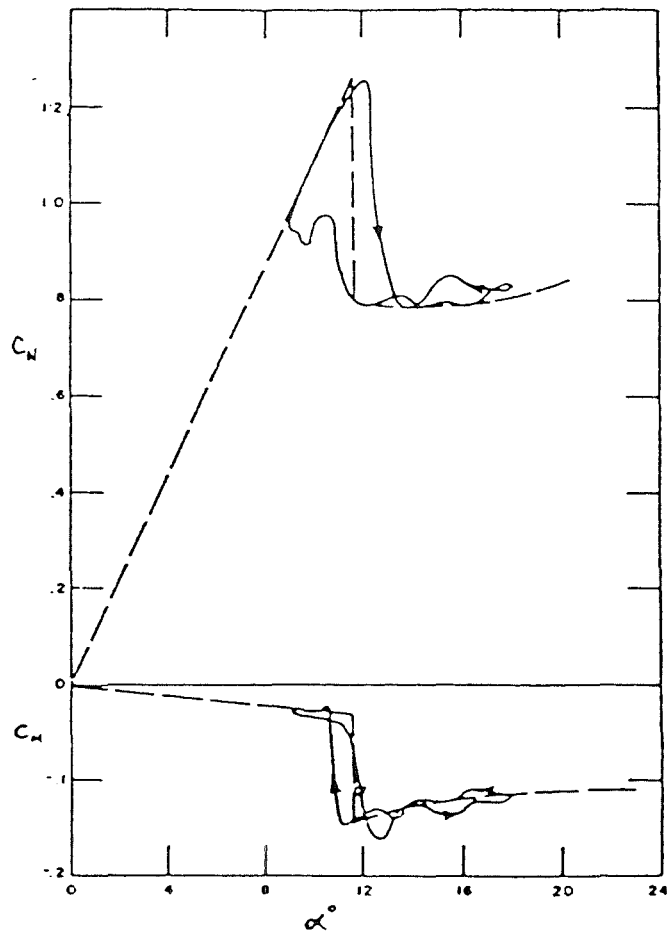


FIG 2.11 COMPUTED LOADING ON THE NACA 0012 FOR $k=0.13$, $\alpha_0=13.5$ DEGREES
 (From CRIMI and REEVES, 1972)

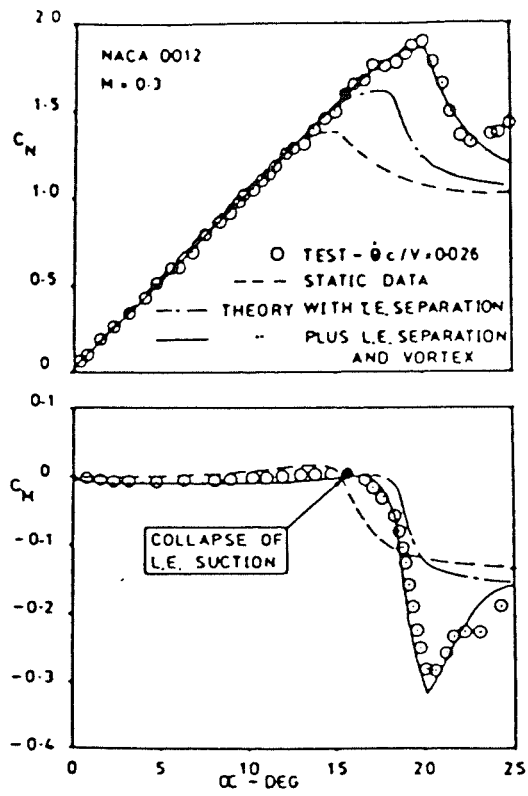


FIG 2.12 RESPONSE TO RAMP FORCING
(From BEDDOES, 1982)

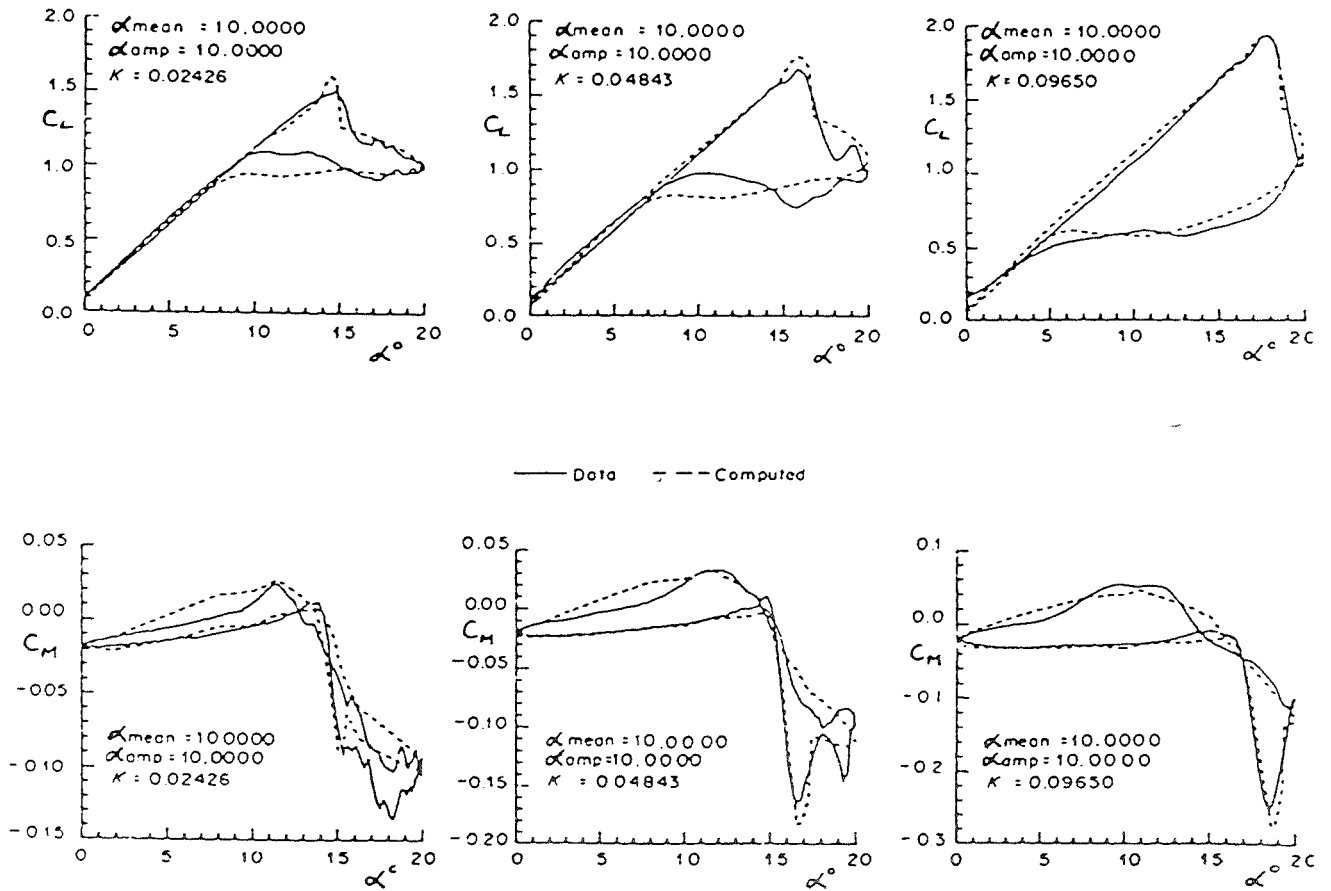
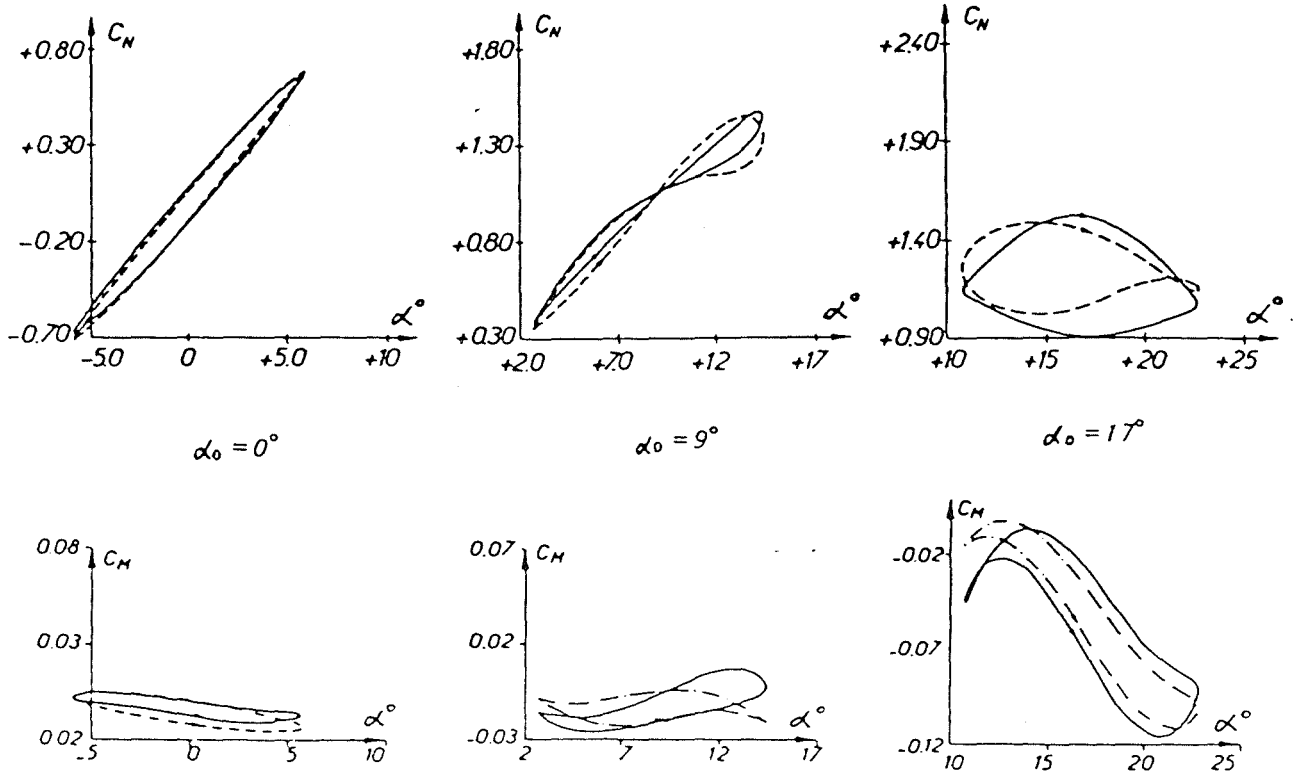


FIG 2.13 SYNTHESIZED LOADS FOR THE NLR-1 AEROFOIL:
M=0.3, $Re=3.8 \times 10^6$
(From GANGWANI, 1984)

— Experiment ; - - - model ; > sense of gyration.



Mach 0.3 ; reduced frequency : 0.05 ; oscillation amplitude : 6° .

FIG 2.14 LARGE AMPLITUDE HARMONIC OSCILLATIONS OF THE OA212 AEROFOIL (From TRAN and PETOT, 1980)

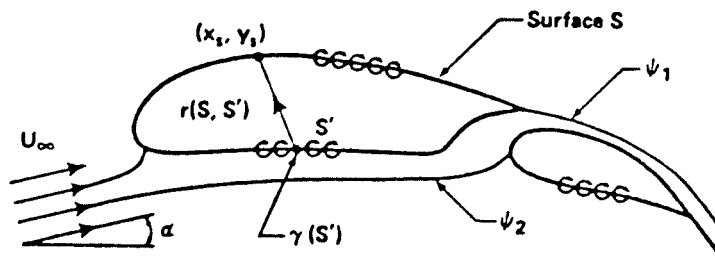


FIG 3.1 VORTEX REPRESENTATION OF AN AEROFOIL
(From KENNEDY and MARSDEN, 1978)

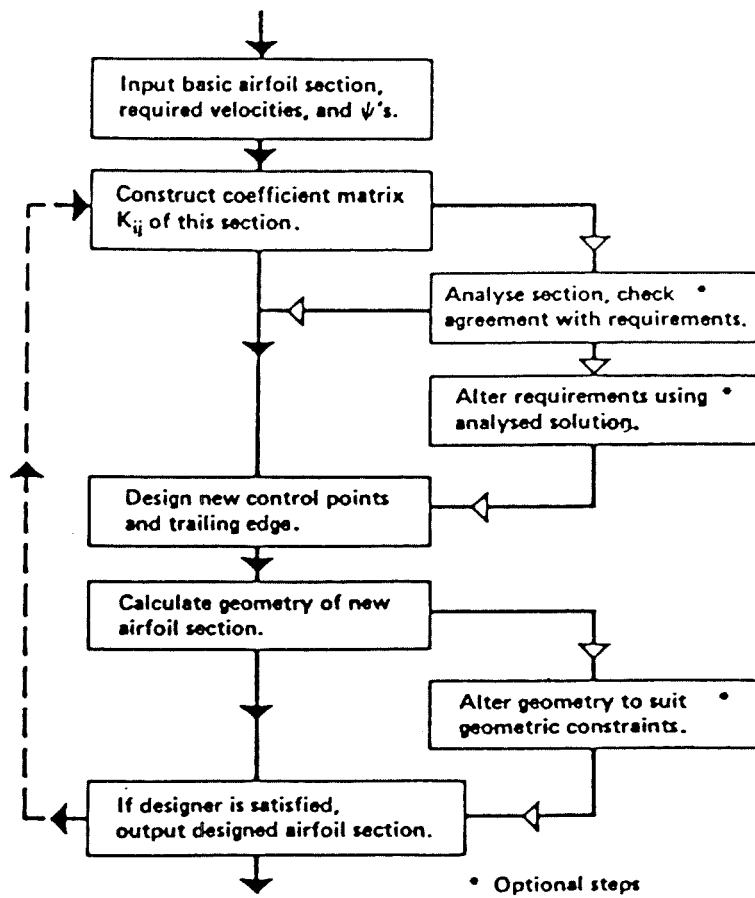


FIG 3.2 FLOW CHART OF DESIGN PROCEDURE
(From KENNEDY and MARSDEN, 1978)

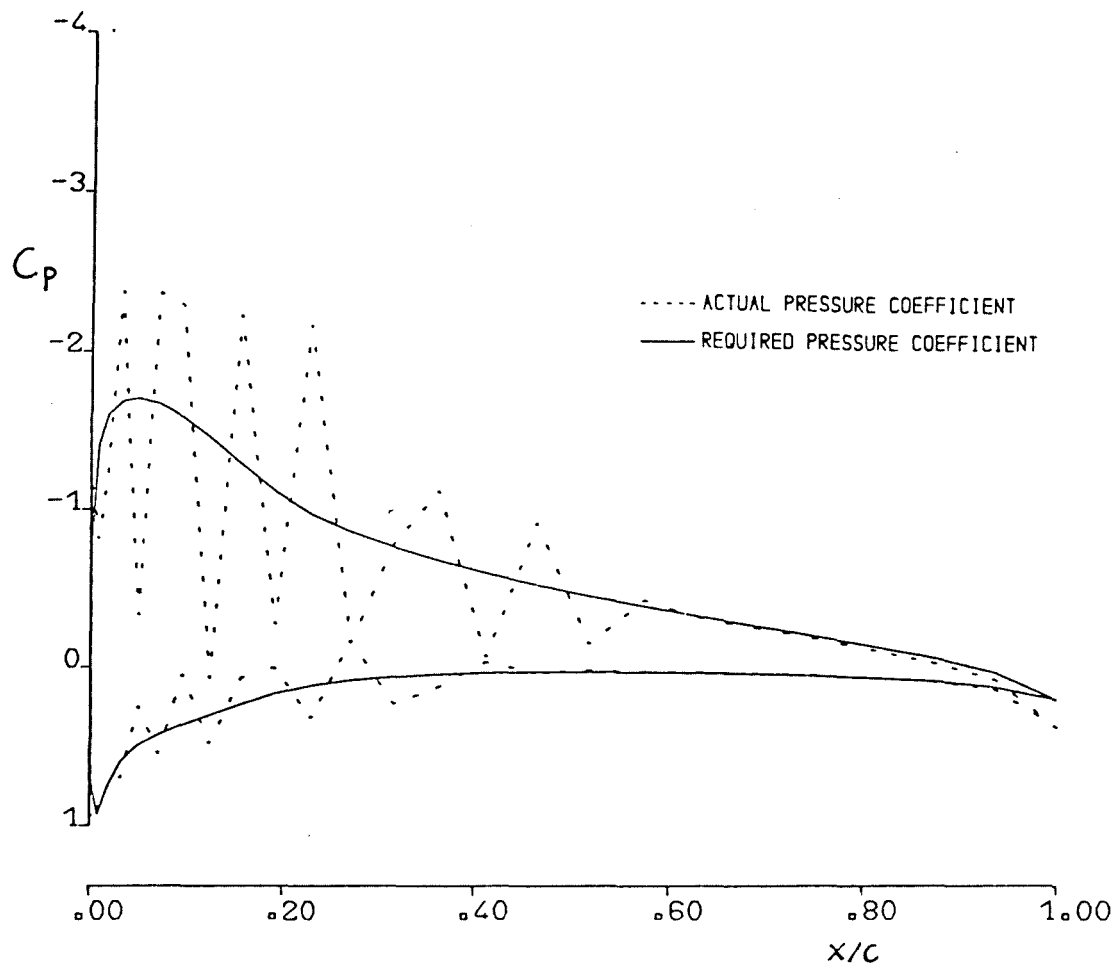


FIG 3.3 PRESSURE DISTRIBUTION AFTER 6TH ITERATION;
 $\alpha = 5^\circ$; $|CN| \ll 0.1$

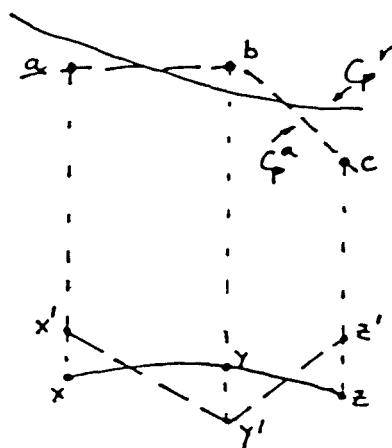


FIG 3.4 ORIGIN OF INSTABILITY (UPPER SURFACE)

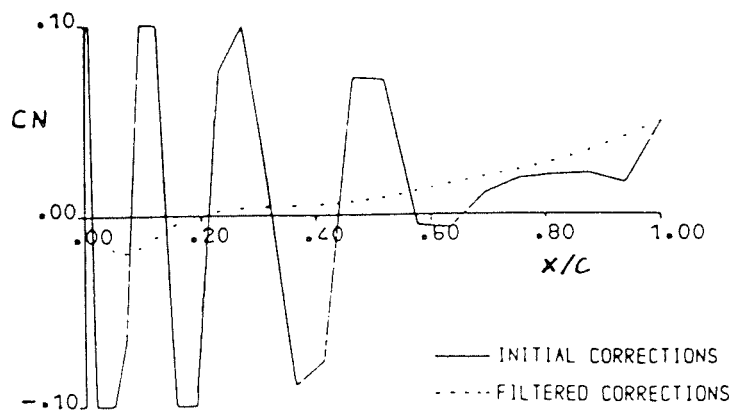


FIG 3.5 PRINCIPLE OF CORRECTION FILTERING

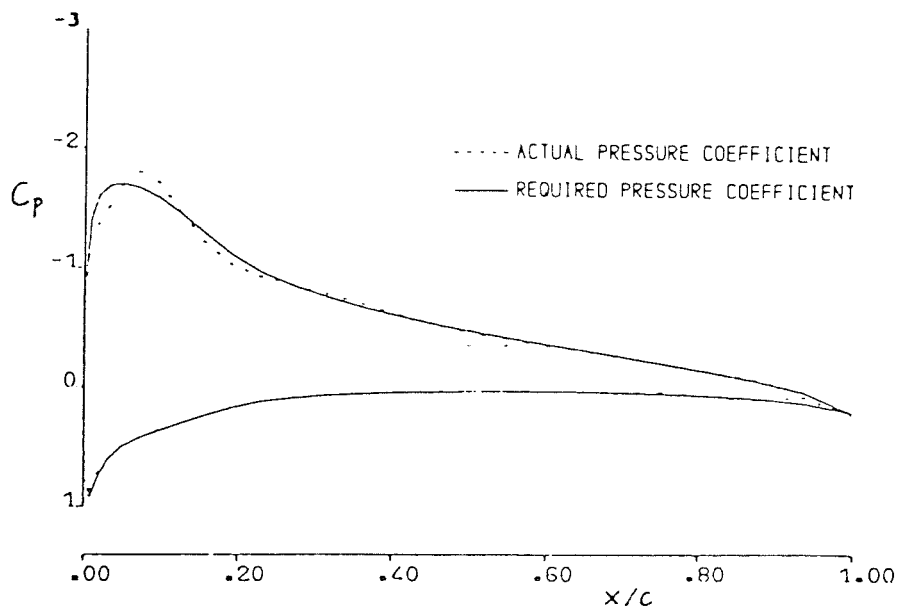


FIG 3.6 PRESSURE DISTRIBUTION AT END OF 1ST STAGE;
 $F_u = 10$, $F_c = 2$, $|CN| \ll 0.1$

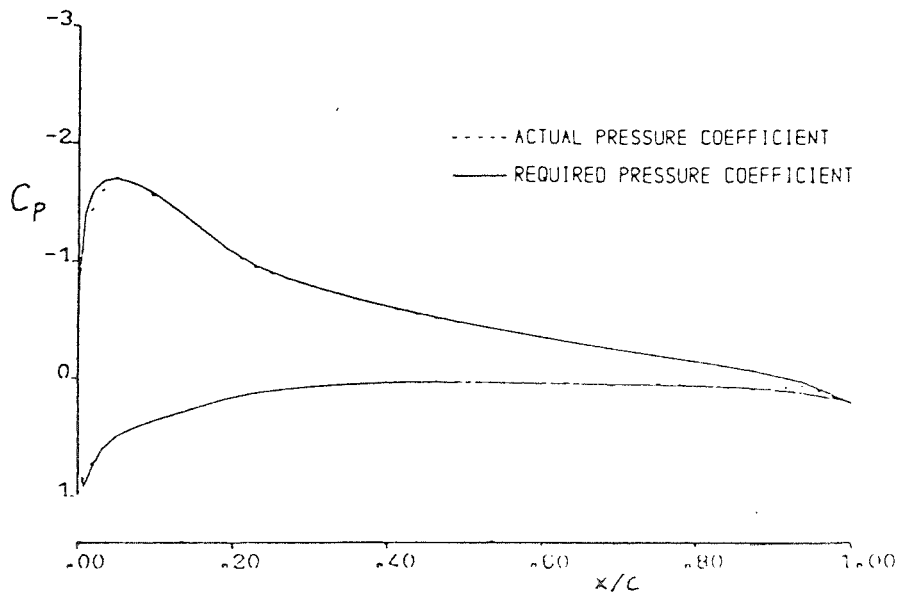


FIG 3.7 PRESSURE DISTRIBUTION AT END OF 2ND STAGE;
 $F_u = 2$, $F_c = 2$, $|CN| \ll 0.01$

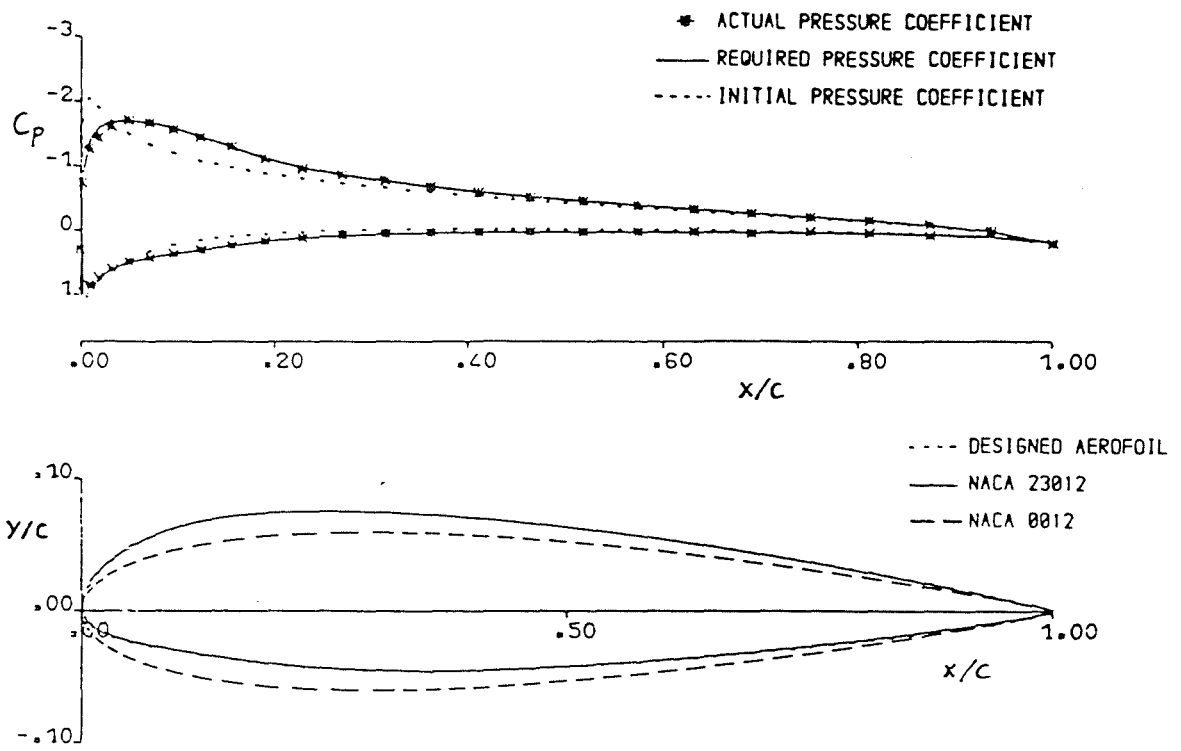


FIG 3.8 DESIGN OF THE NACA 23012 FROM THE NACA 0012 AT END OF 3RD STAGE; $\epsilon_u = \epsilon_l = 0$, $|CN| \ll 0.0005$, $\alpha = 5^\circ$

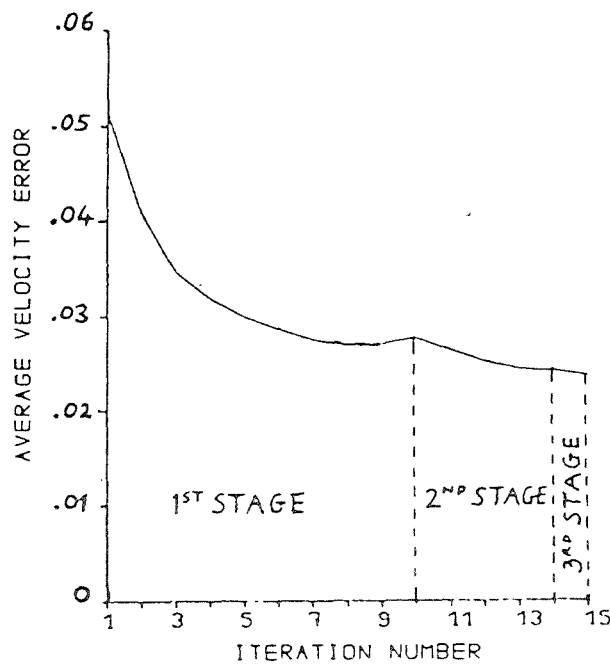


FIG 3.9 CONVERGENCE OF 3-STAGE DESIGN

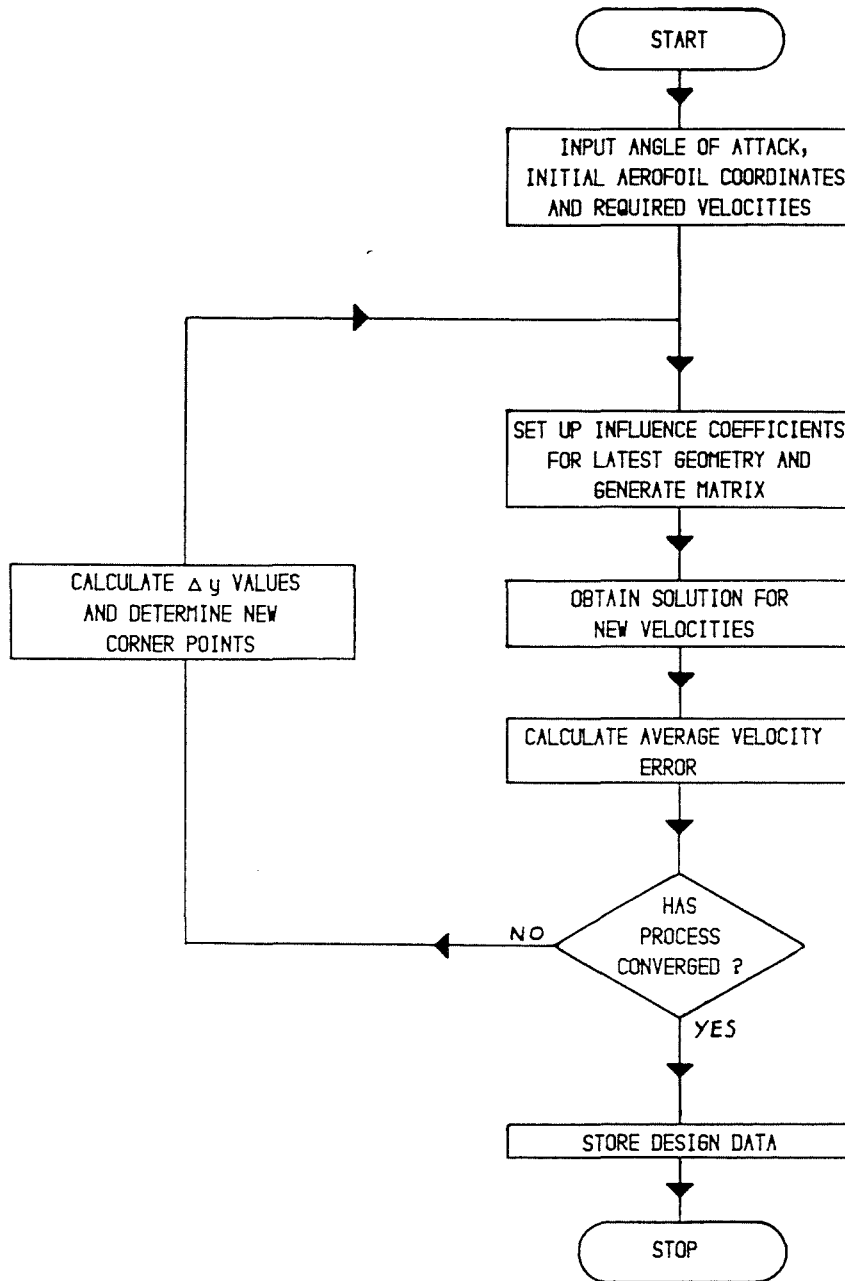


FIG 3.10 FLOW CHART OF A.A. METHOD

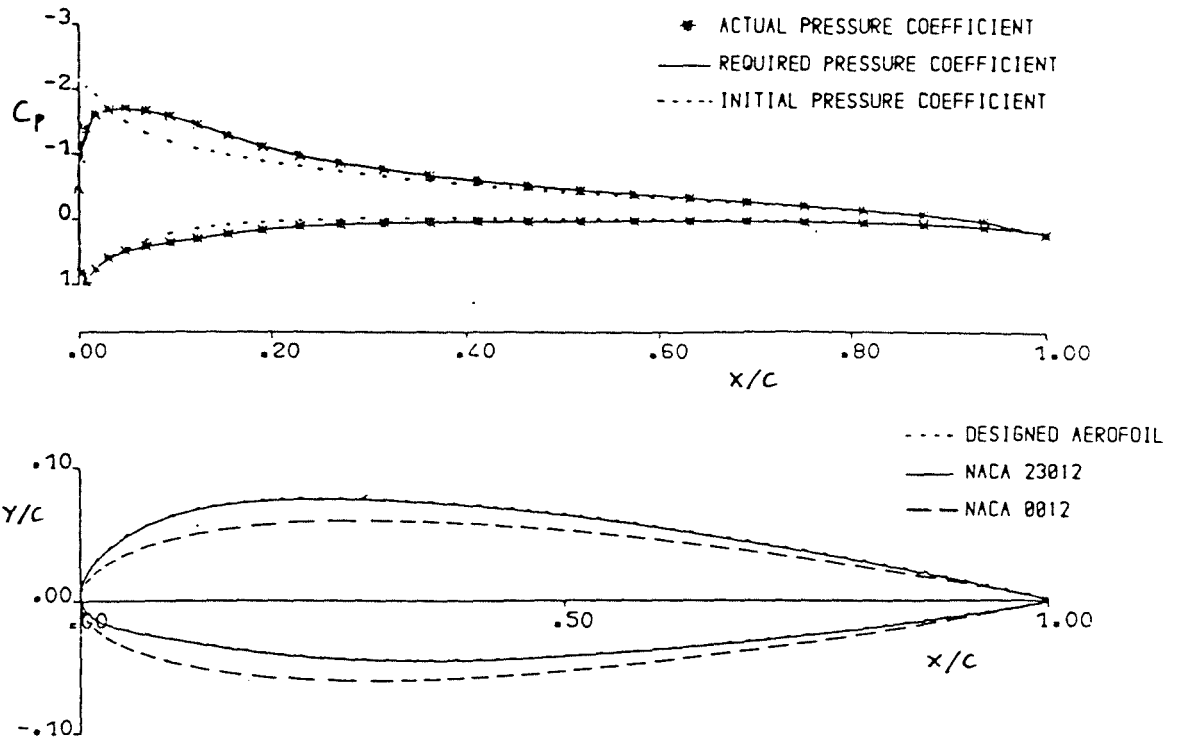


FIG 3.11 DESIGN OF THE NACA 23012 FROM THE NACA 0012; $\alpha = 5^\circ$

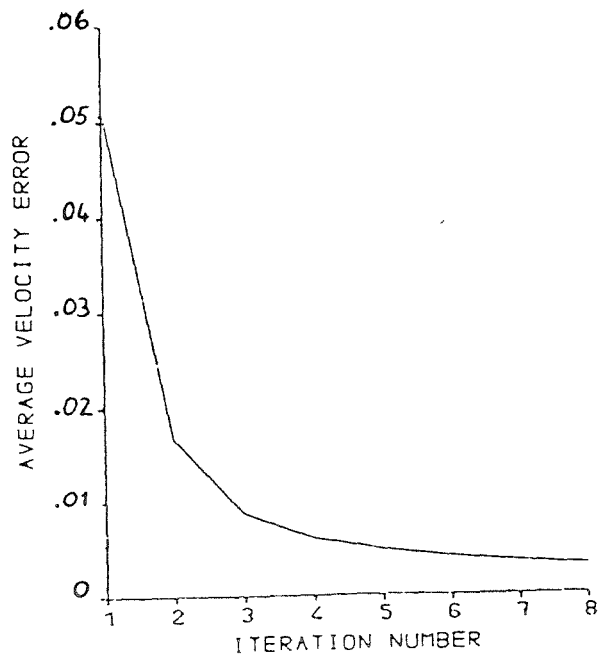


FIG 3.12 CONVERGENCE OF DESIGN PROCESS

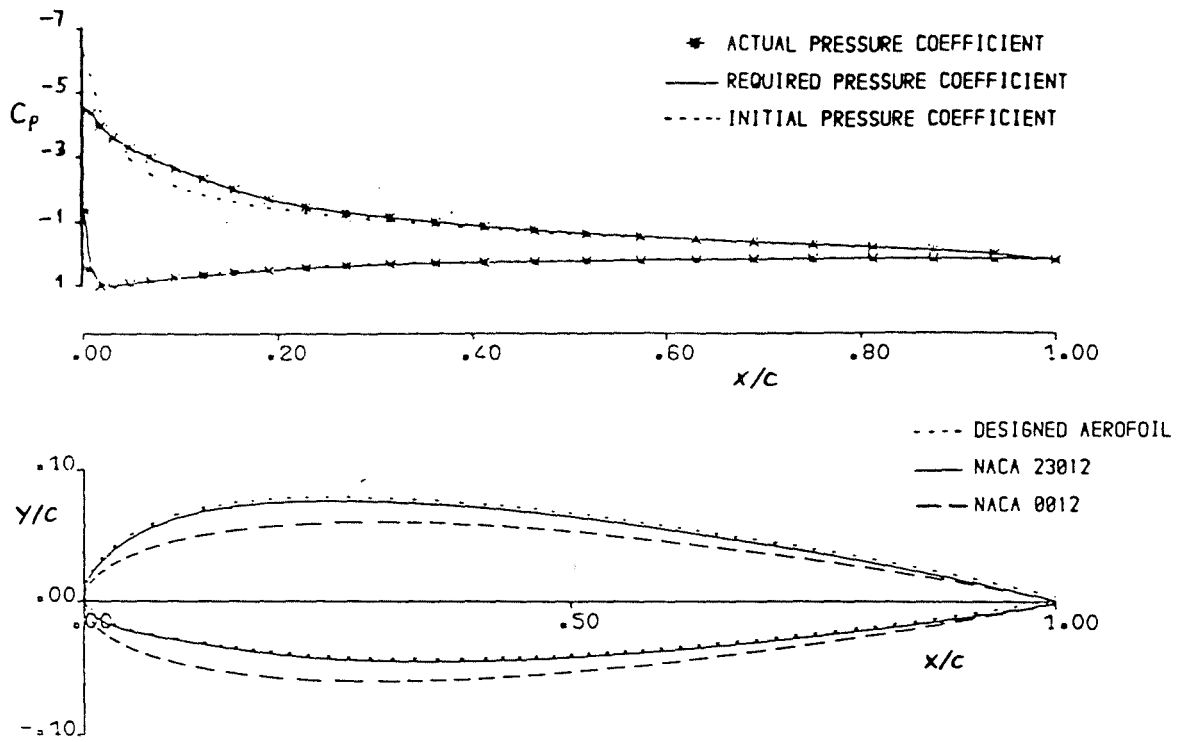


FIG 3.13 DESIGN OF THE NACA 23012 FROM THE NACA 0012; $\alpha = 10^\circ$

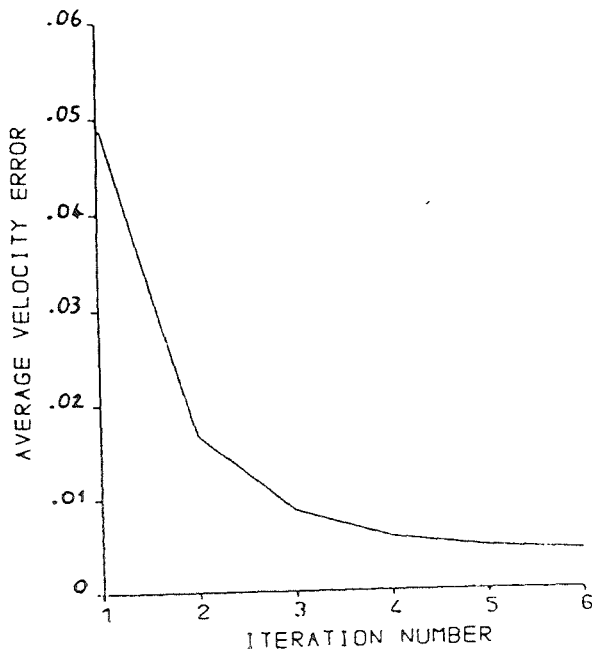


FIG 3.14 CONVERGENCE OF DESIGN PROCESS

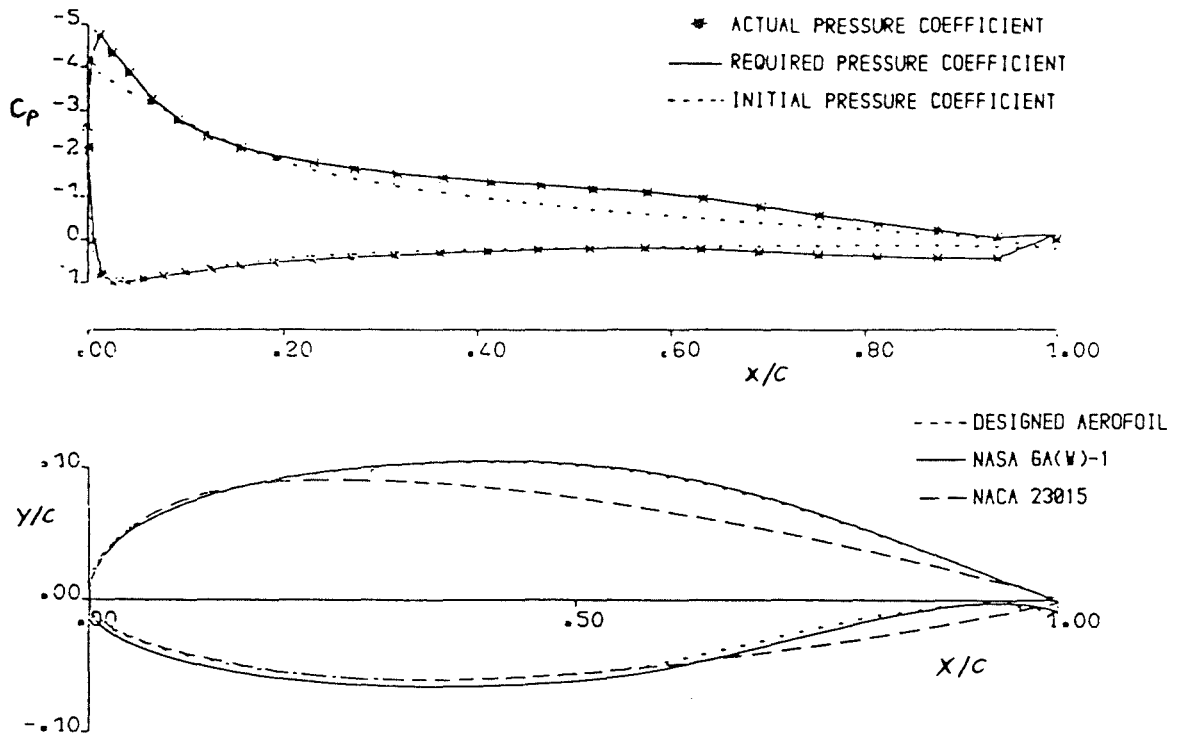


FIG 3.15 DESIGN OF THE NASA 6A(W)-1 FROM THE NACA 23015;
 $\alpha = 10^\circ$

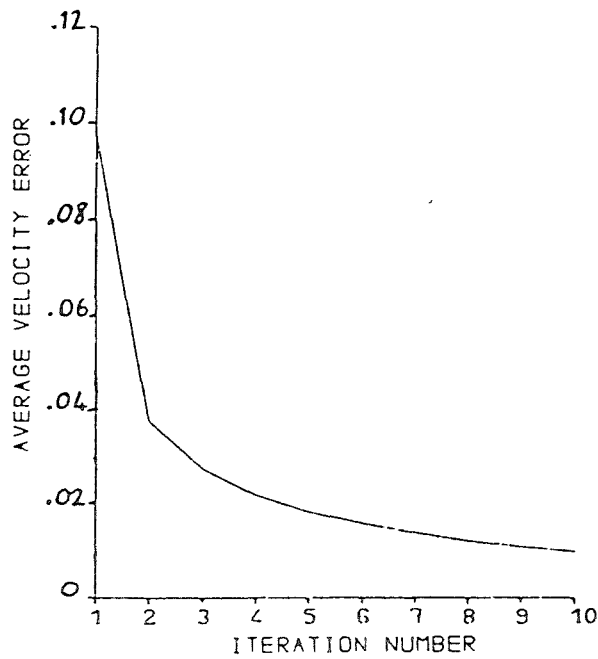


FIG 3.16 CONVERGENCE OF DESIGN PROCESS

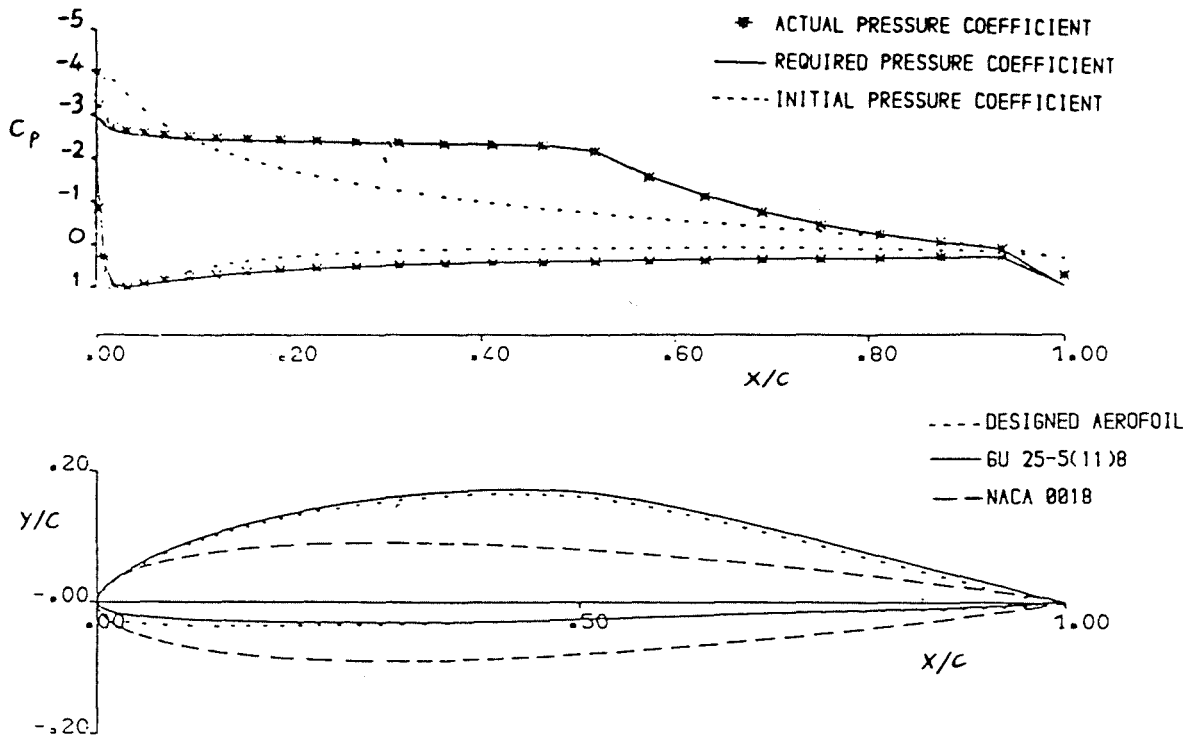


FIG 3.17 DESIGN OF THE GU 25-5(11)8 FROM THE NACA 0018;
 $\alpha = 10^\circ$

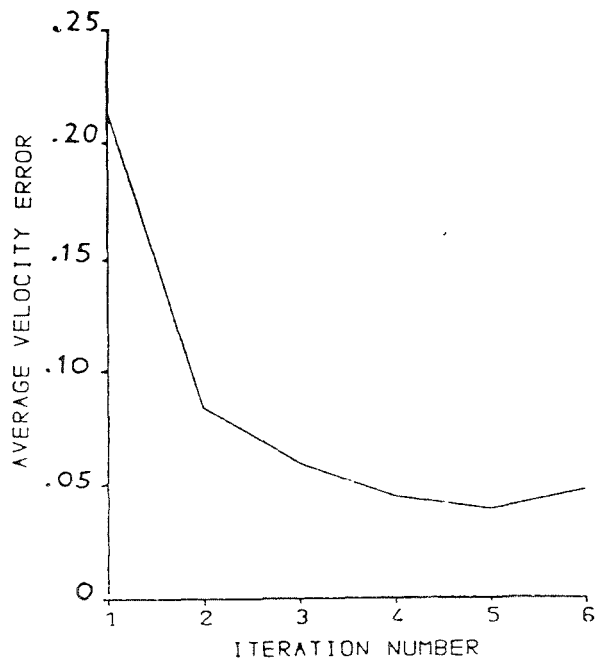


FIG 3.18 CONVERGENCE OF DESIGN PROCESS

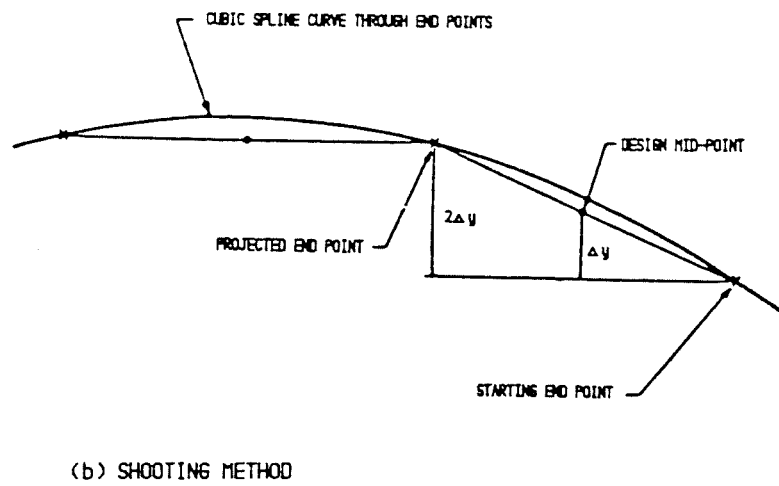
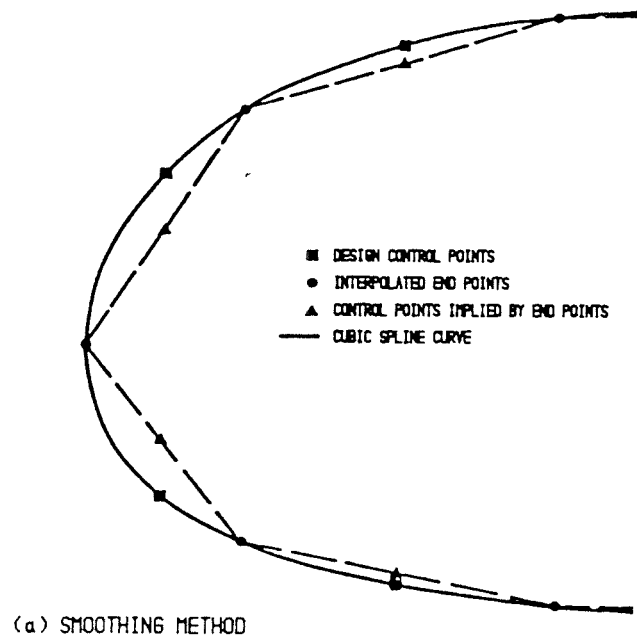


FIG 3.19 TWO METHODS OF DETERMINING AEROFOIL ORDINATES
 (From KENNEDY and MARS DEN, 1978)

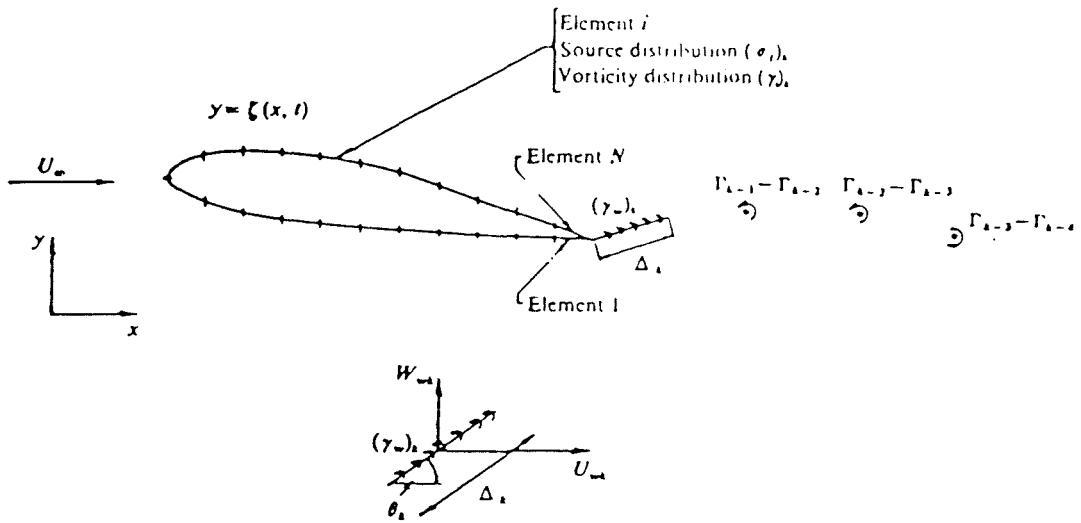


FIG 4.1 METHOD OF BASU AND HANCOCK(1978b)

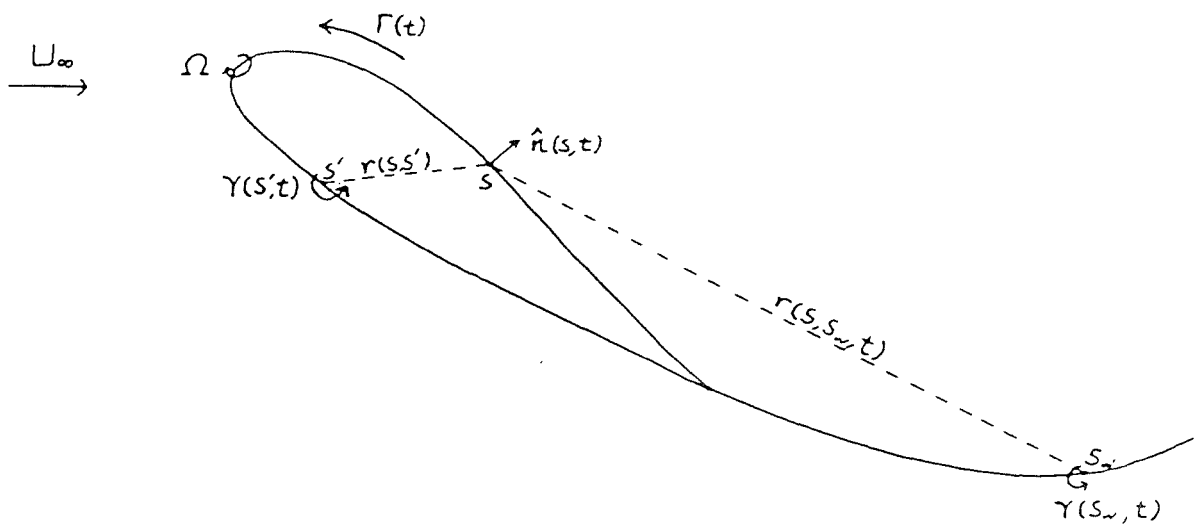


FIG 4.2 UNSTEADY POTENTIAL FLOW PROBLEM

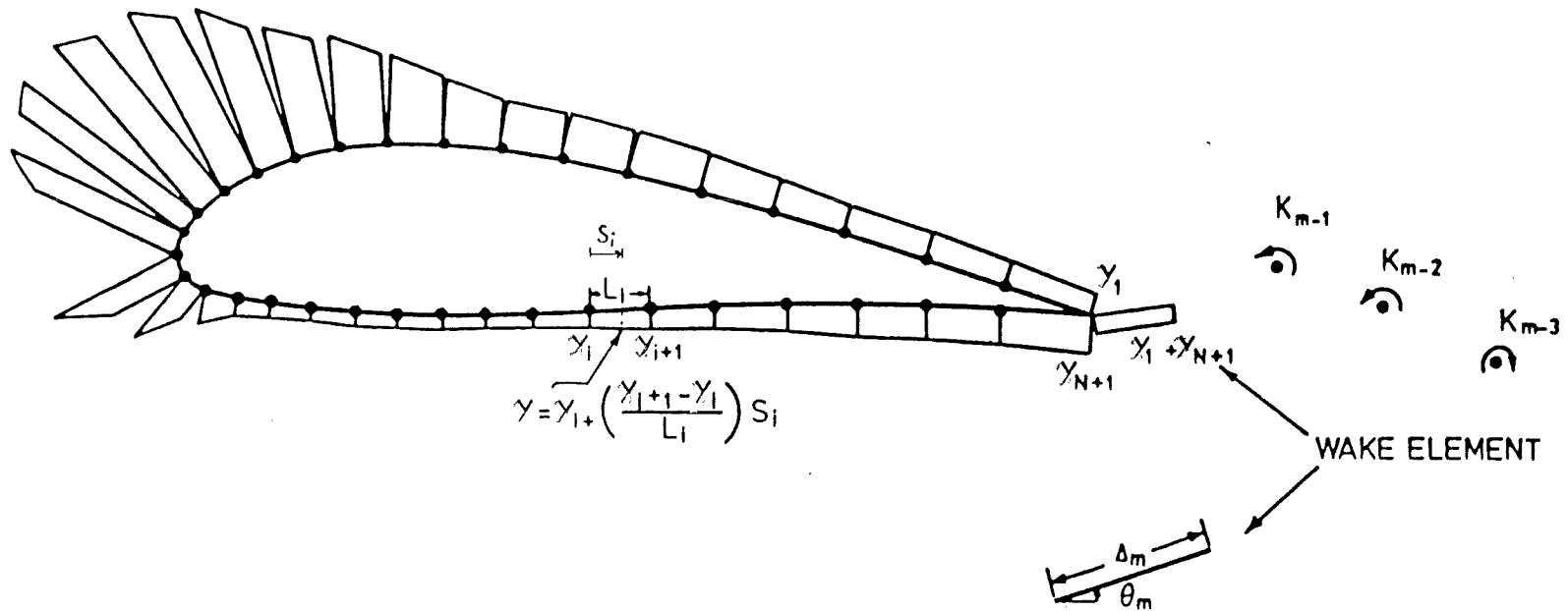


FIG 4.3 UNSTEADY MODEL AT TIME t_m

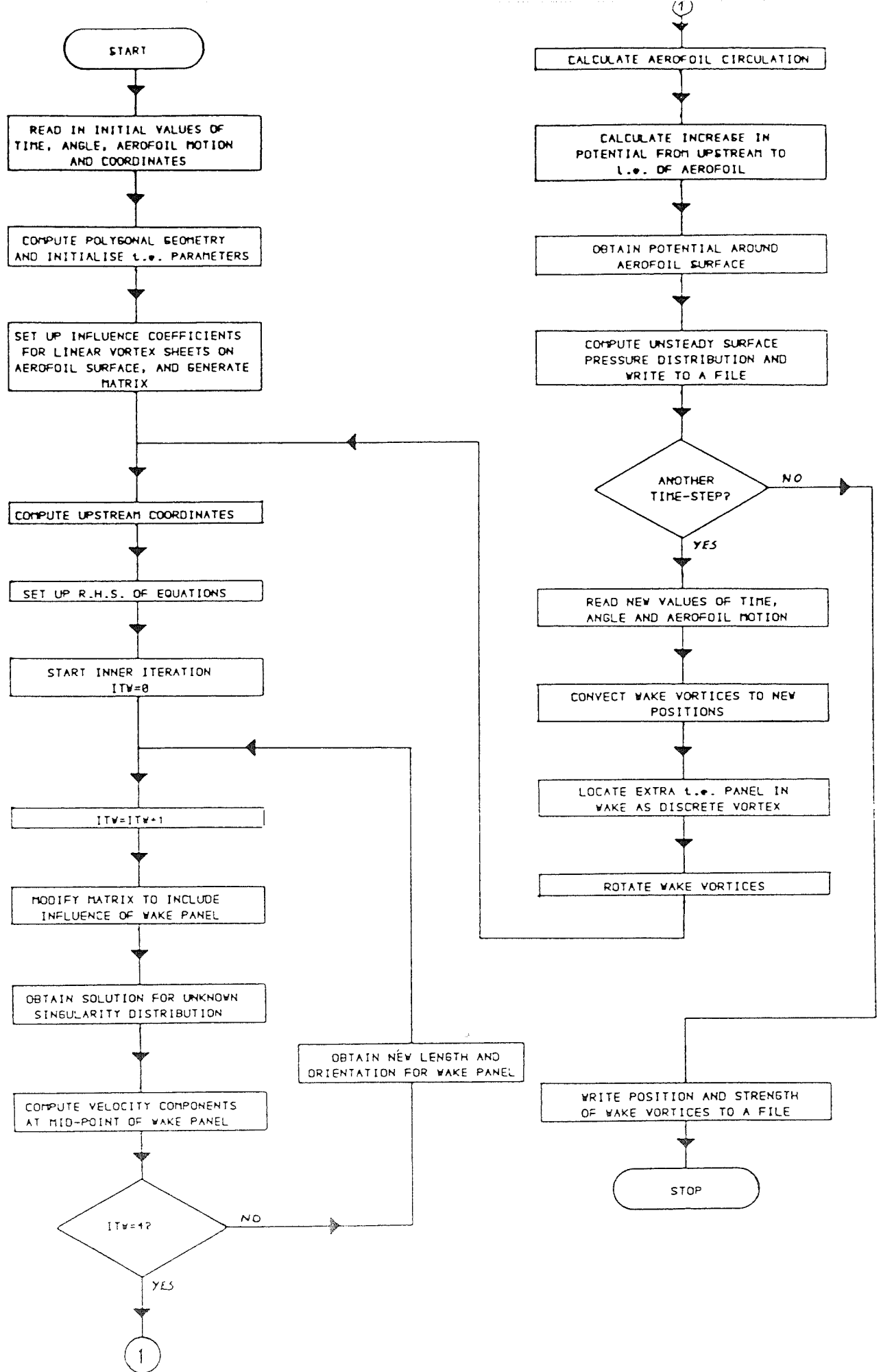
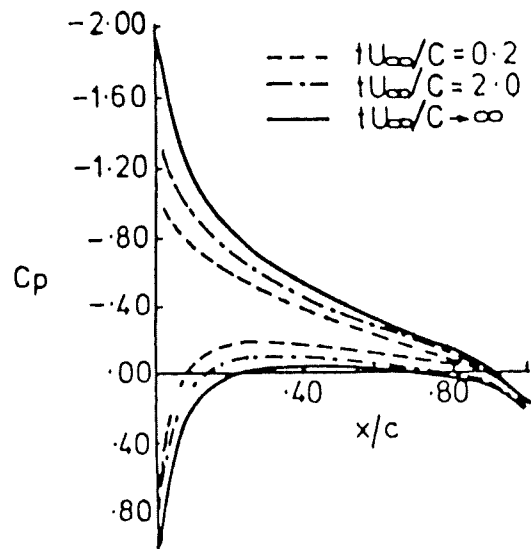
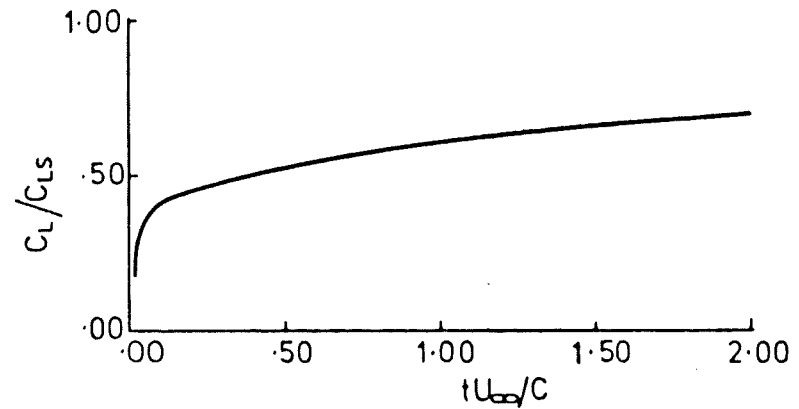


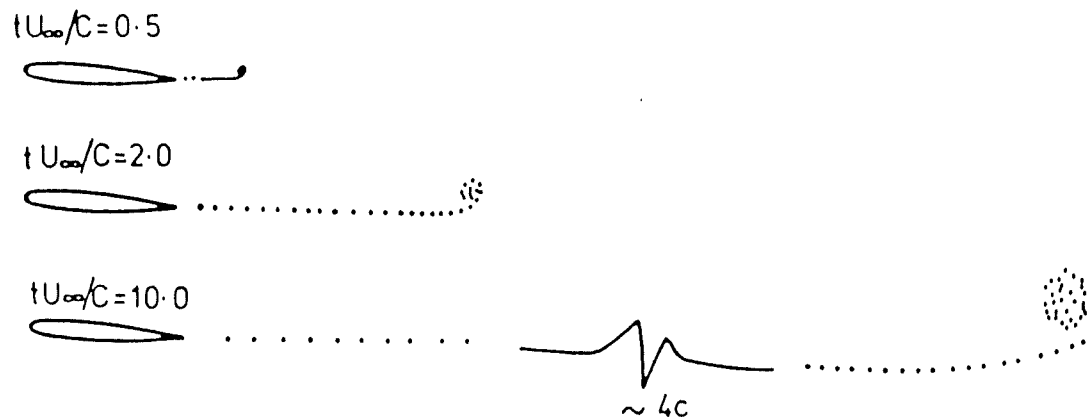
FIG 4.4 FLOW CHART OF NUMERICAL PROCEDURE



(a) PRESSURE BUILD UP

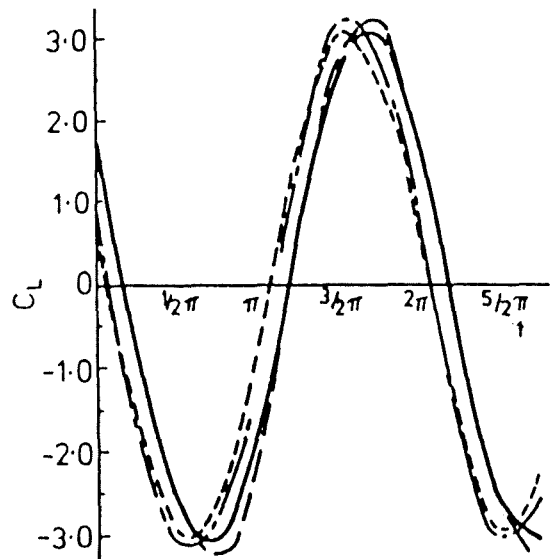


(b) BEHAVIOUR OF TIME DEPENDENT LIFT



(c) WAKE VORTEX CONFIGURATIONS

FIG 4.5 RESULTS OBTAINED FOLLOWING A STEP CHANGE IN INCIDENCE USING THE NACA 0012 AEROFOIL

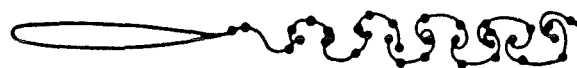


(a) BEHAVIOUR OF TIME DEPENDENT LIFT; $\alpha = 0.573^\circ \sin 20t$ ABOUT l.e.

- PRESENT METHOD
- BASU AND HANCOCK (1978b)
- BASU AND HANCOCK (1978a)
- LINEARISED THEORY



$\alpha = 0.573^\circ \sin 20t$ ABOUT LEADING EDGE OF NACA 0012 AEROFOIL.



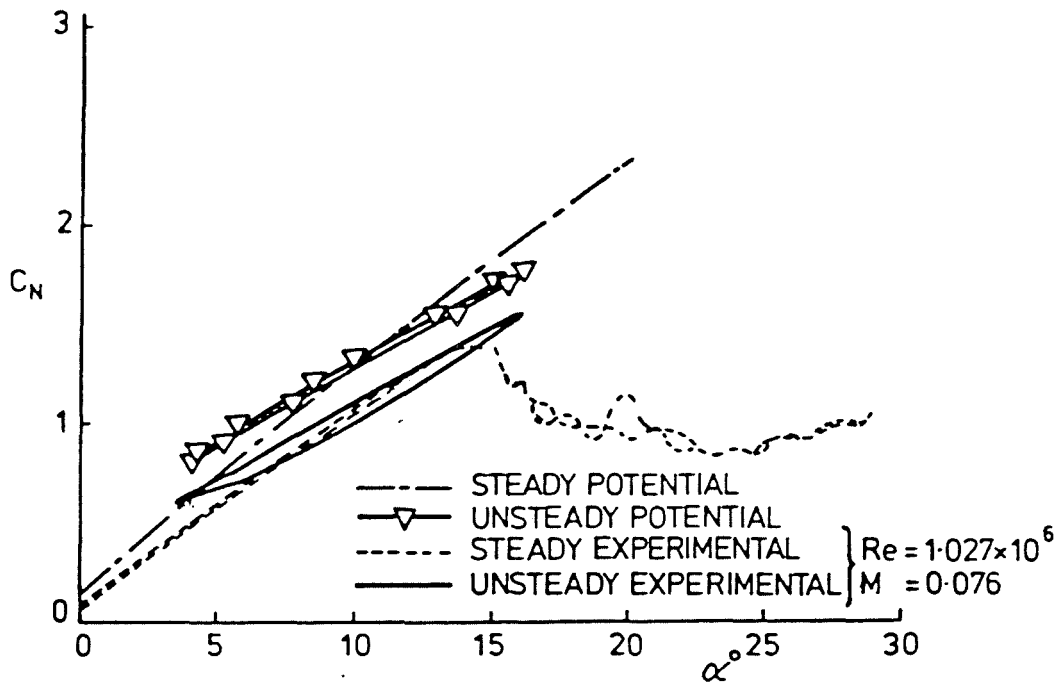
$\alpha = 0.573^\circ \sin 20t$ ABOUT LEADING EDGE OF 8.4% SYMMETRICAL VON MISES AEROFOIL (BASU AND HANCOCK, 1978b)



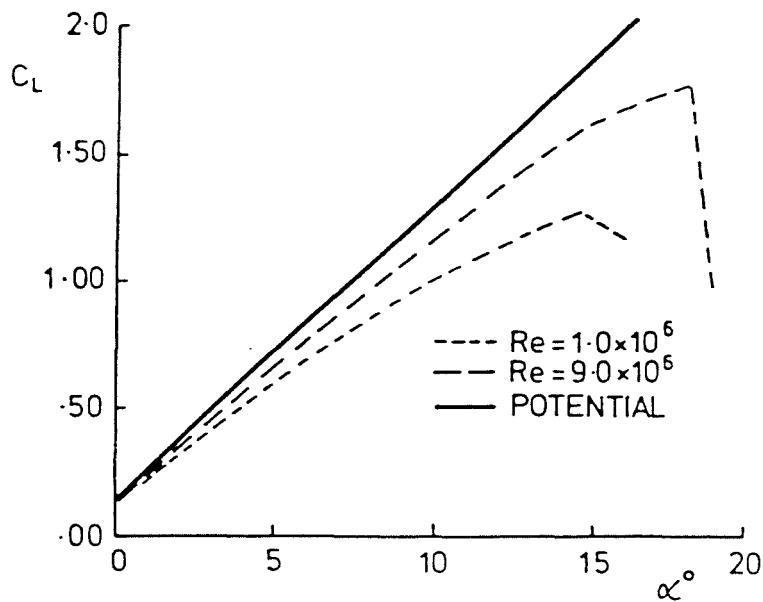
$\alpha = 0.3105 \cos 17t$ FOR NACA 0015 AEROFOIL (GIESING, 1968)

(b) WAKE VORTEX CONFIGURATIONS.

FIG 4.6 RESULTS OBTAINED FROM HIGH FREQUENCY CALCULATIONS



(a) NORMAL LIFT CHARACTERISTICS FOR OSCILLATION ABOUT THE $\frac{1}{4}c$ OF THE NACA 23012 AEROFOIL; $k = 0.2$, $\alpha = 10^\circ + 6^\circ \sin \Omega t$



(b) VARIATION OF C_L vs α WITH REYNOLDS NUMBER FOR THE NACA 23012 AEROFOIL.

FIG 4.7 COMPARISON OF RESULTS OBTAINED FROM A LOW FREQUENCY SUB-STALL TEST ON THE NACA 23012 AEROFOIL

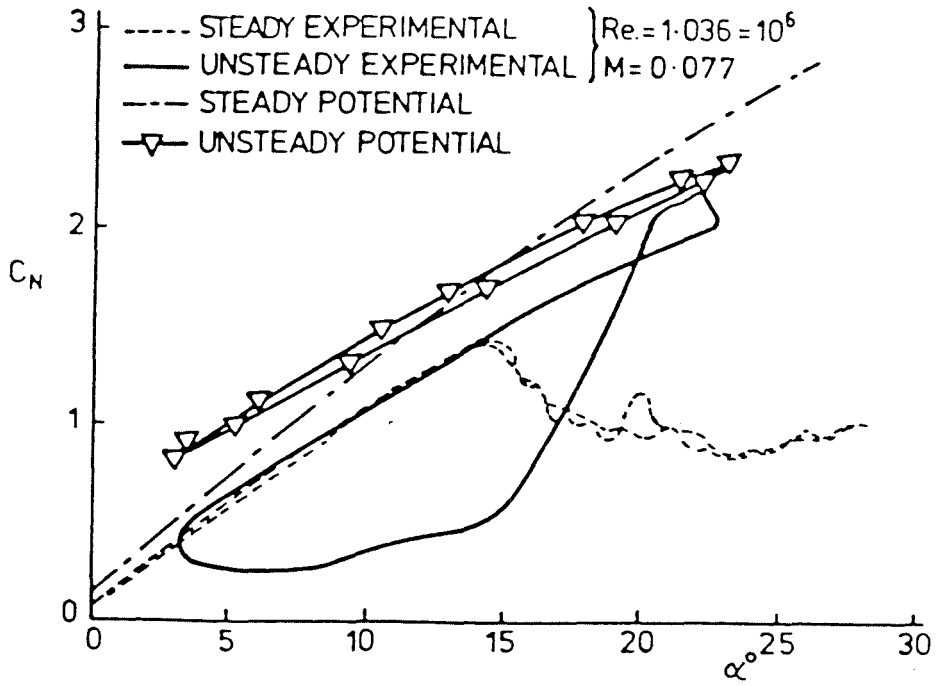


FIG 4.8 COMPARISON OF NORMAL LIFT ON THE NACA 23012 AEROFOIL WHEN OPERATING IN THE STALL REGIME: $k=0.2, \alpha = 13^\circ + 10^\circ \sin(\Omega t)$

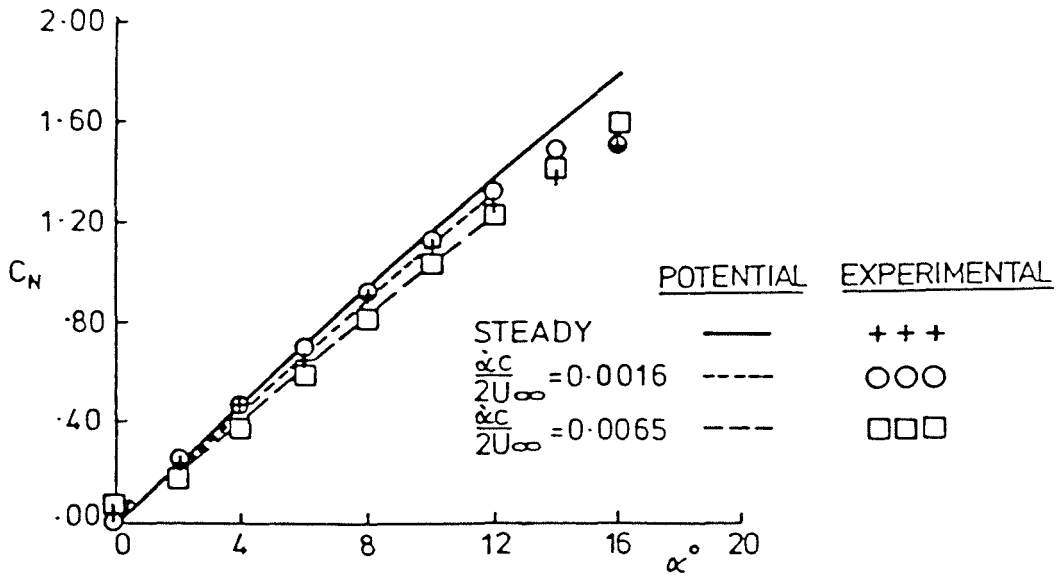


FIG 4.9 RESULTING NORMAL LIFT WHEN RAMP MOTIONS ARE APPLIED TO THE NACA 0012 AEROFOIL (FOR EXPERIMENTS: $Re=2.6 \times 10^6, M=0.3$)

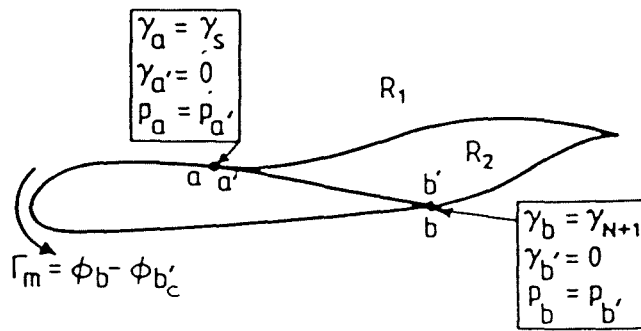


FIG 5.2 INVISCID FORMULATION

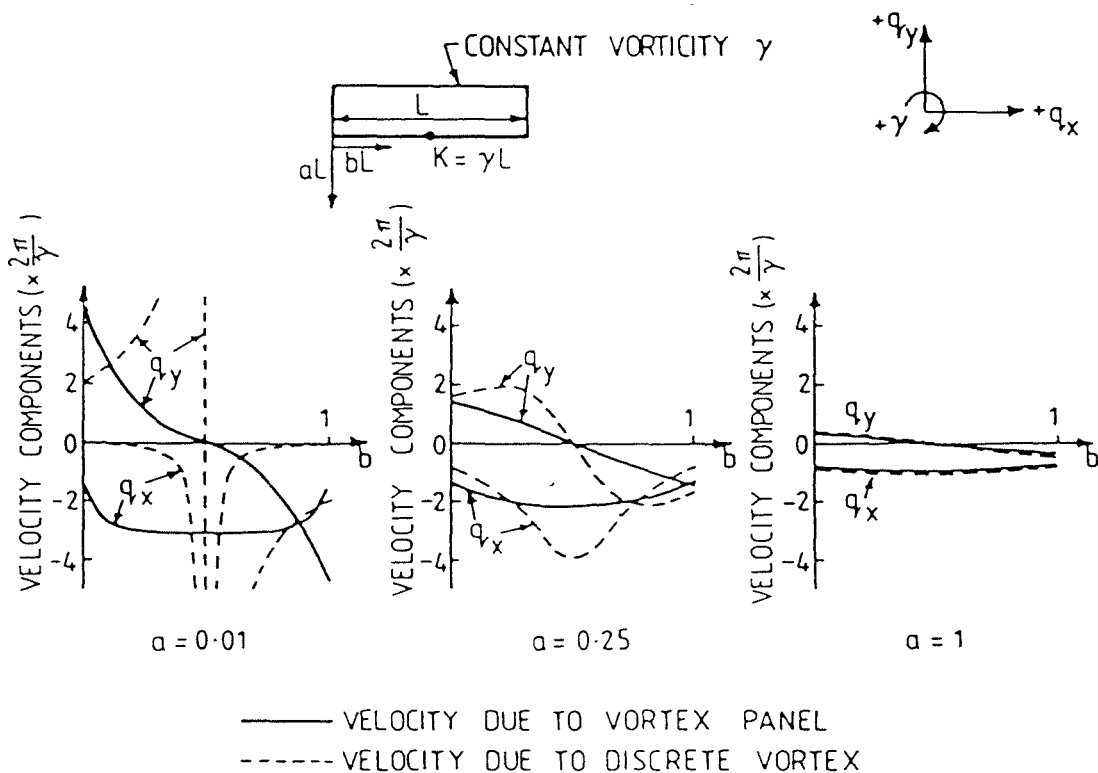


FIG 5.3 COMPARISON BETWEEN THE LOCAL VELOCITY FIELDS INDUCED BY A VORTEX PANEL AND AN EQUIVALENT DISCRETE VORTEX

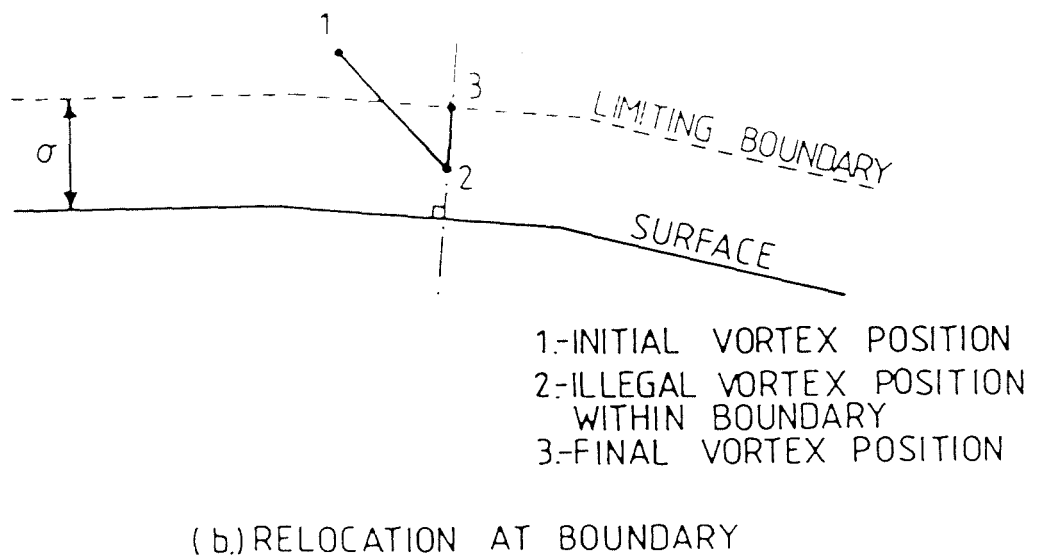
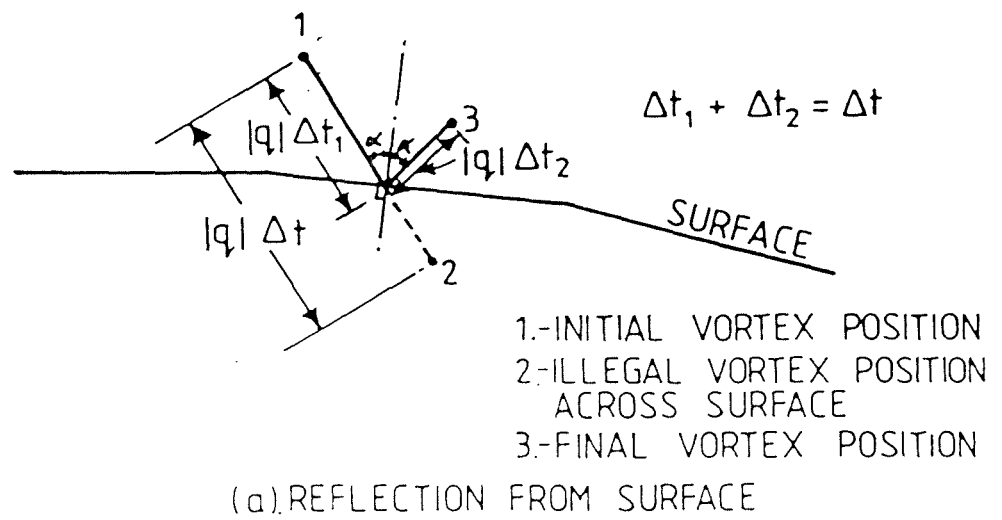


FIG 5.4 RESTRICTIONS ON VORTEX MOTION

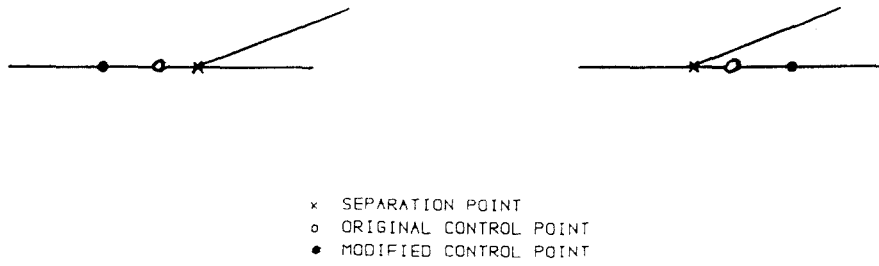


FIG 5.5 TWO CONFIGURATIONS OF SEPARATION PANEL GEOMETRY

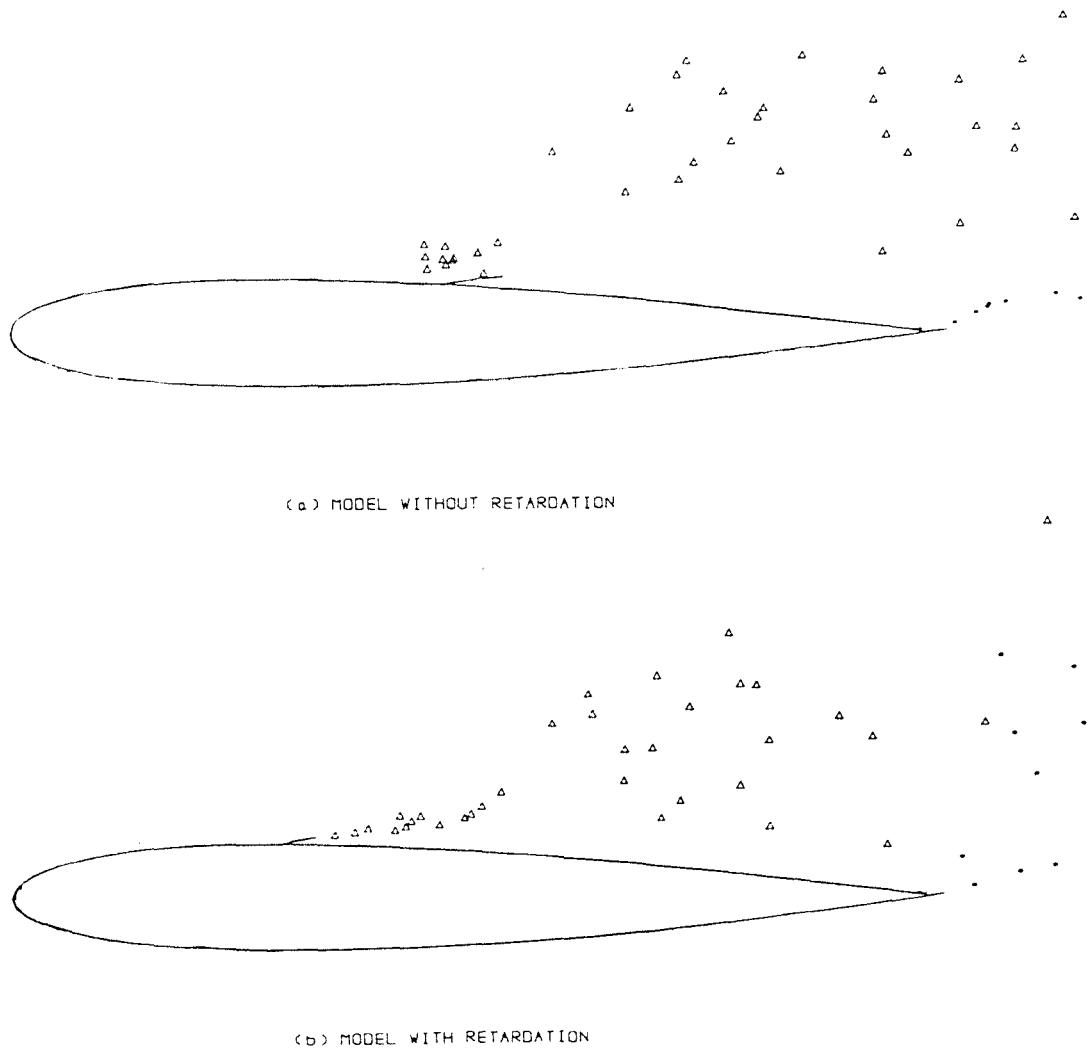


FIG 5.6 EFFECT OF SEPARATION POINT RETARDATION DURING REATTACHMENT

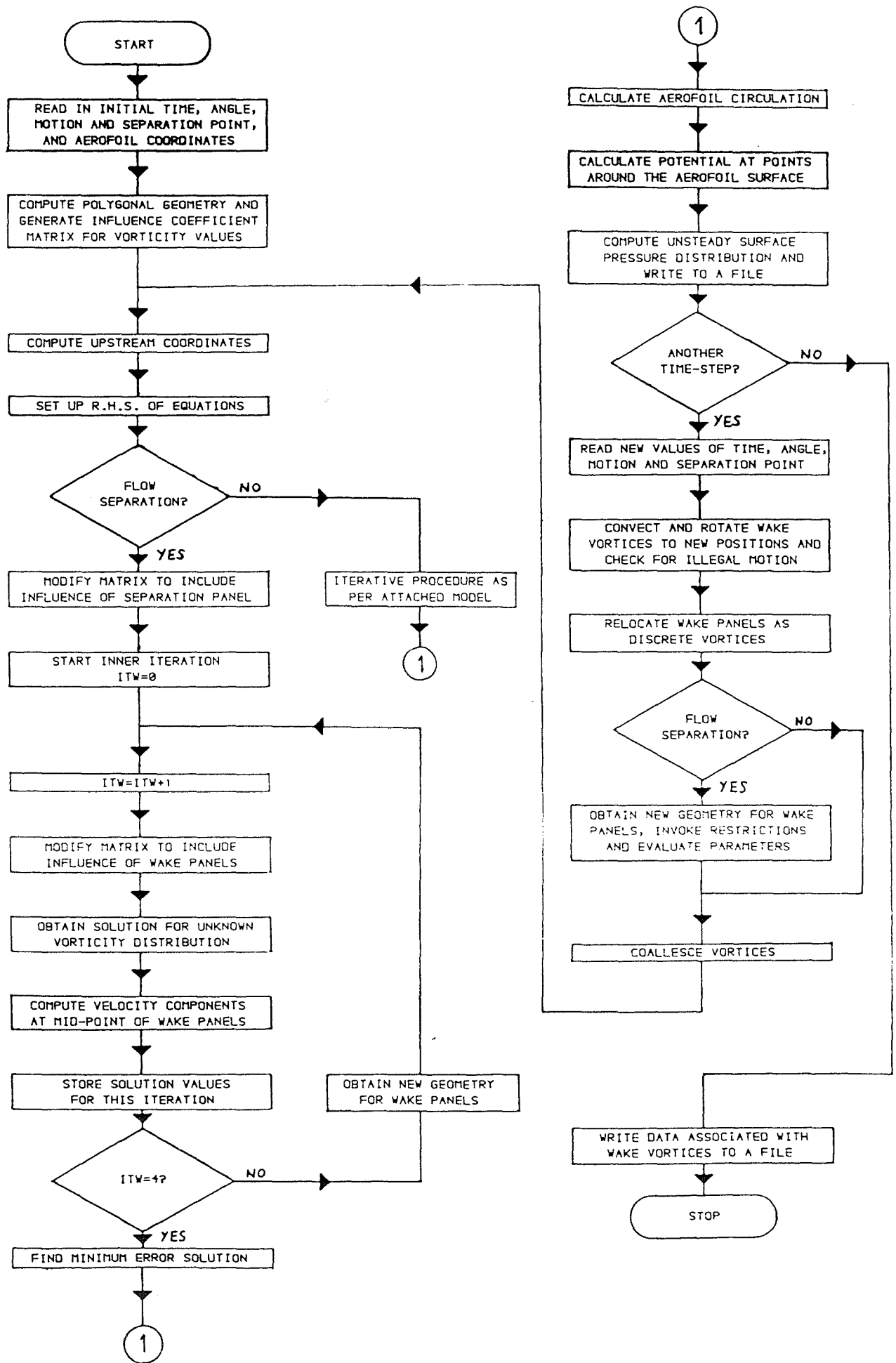


FIG 5.7 FLOW CHART OF THE MODEL WITH MOVING SEPARATION

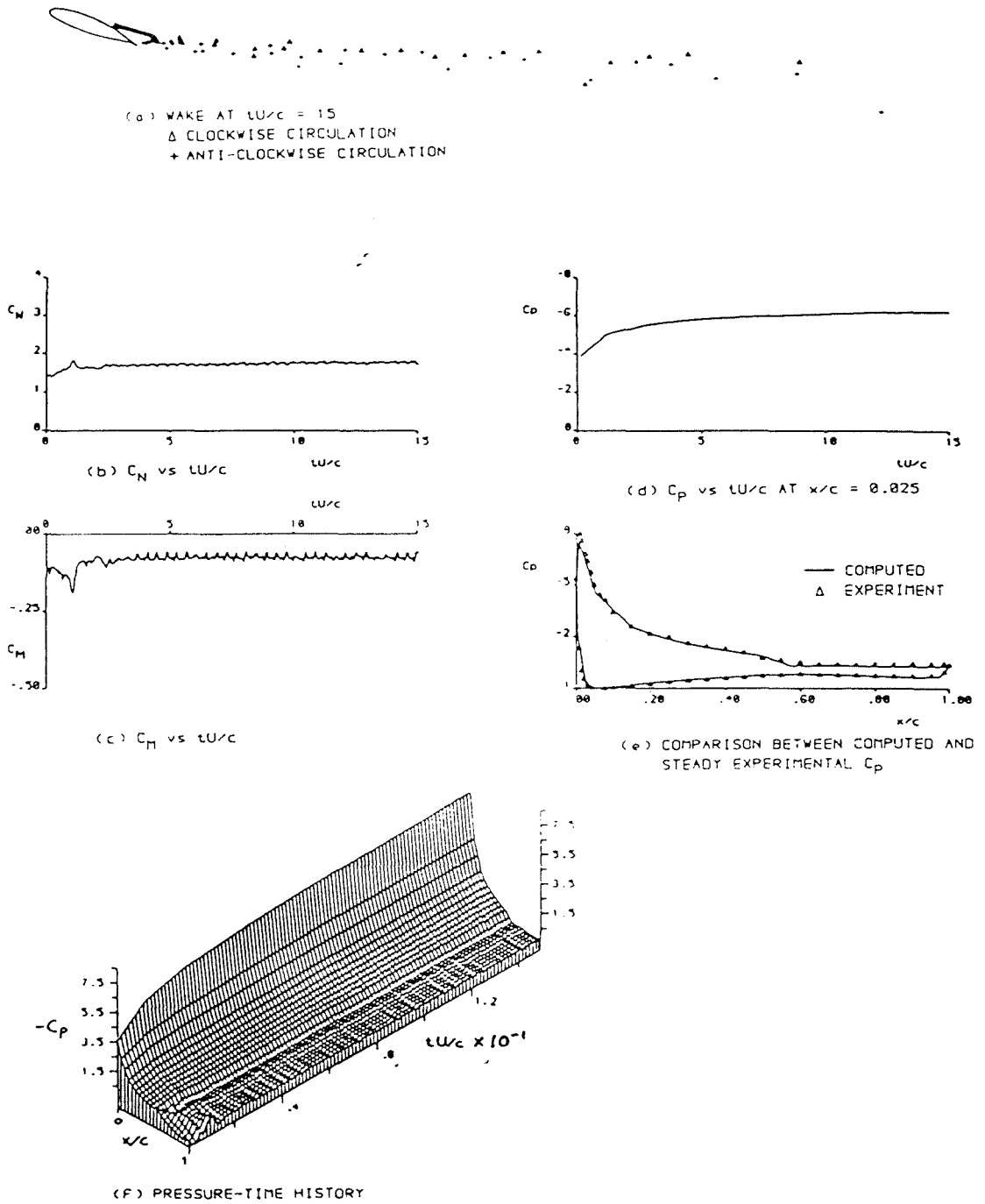
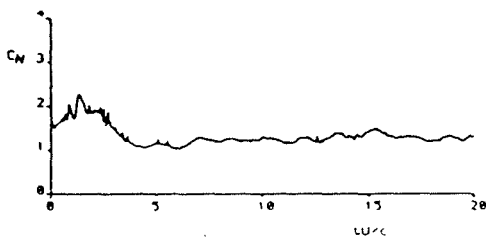


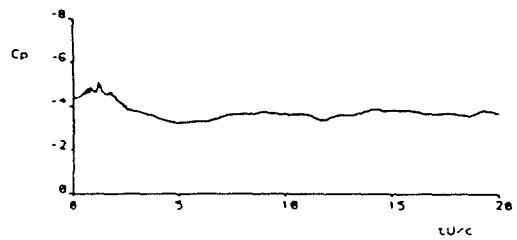
FIG 5.8 RESULTS OBTAINED FOLLOWING A STEP CHANGE IN INCIDENCE FROM 0-18.25 DEG. USING THE NASA GA(W)-1 AEROFOIL



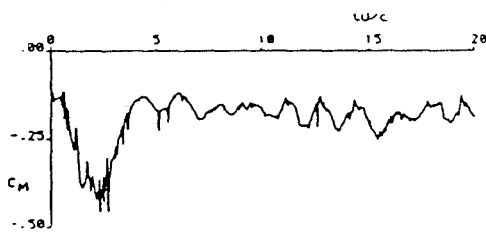
(a) WAKE AT $tU/c = 20$
 Δ CLOCKWISE CIRCULATION
 $+$ ANTI-CLOCKWISE CIRCULATION



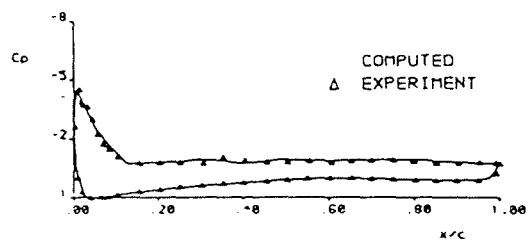
(b) C_N vs tU/c



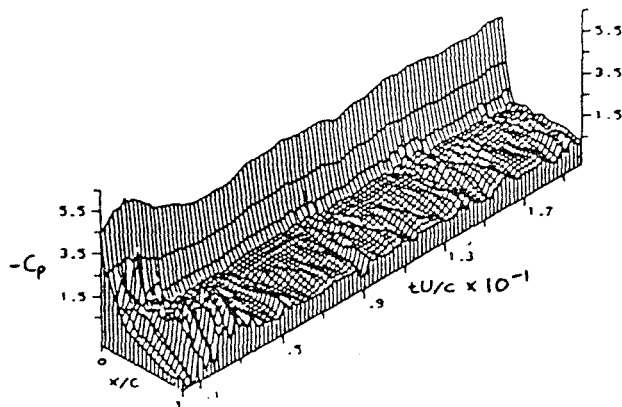
(d) C_p vs tU/c AT $x/c = 0.225$



(c) C_M vs tU/c



(e) COMPARISON BETWEEN COMPUTED AND STEADY EXPERIMENTAL C_p



(f) PRESSURE-TIME HISTORY

FIG 5.9 RESULTS OBTAINED FOLLOWING A STEP CHANGE IN INCIDENCE FROM $0-21.14$ DEG. USING THE NASA GA(W)-1 AEROFOIL



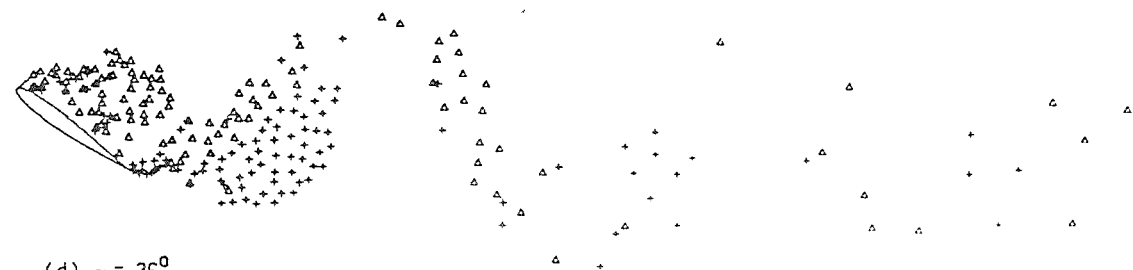
(a) $\alpha = 9^\circ$



(b) $\alpha = 18^\circ$



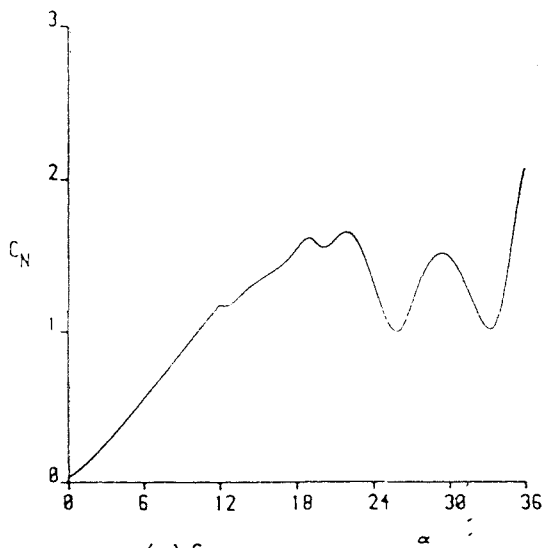
(c) $\alpha = 28^\circ$



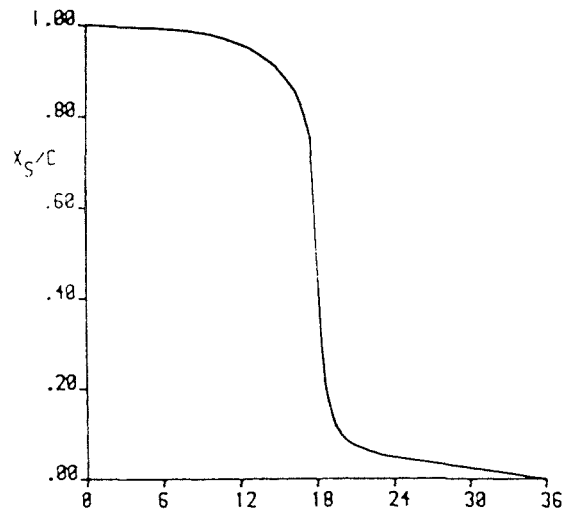
(d) $\alpha = 36^\circ$

Δ CLOCKWISE CIRCULATION
 $+$ ANTI-CLOCKWISE CIRCULATION

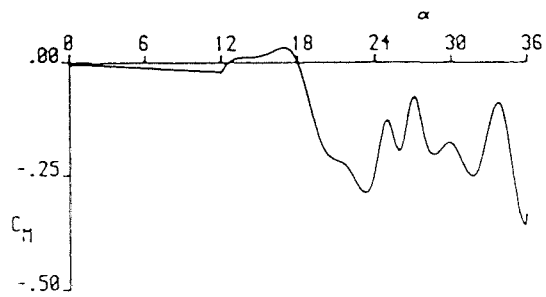
FIG 5.10 WAKE PRODUCED BY THE NACA 0012 AEROFOIL DURING A RAMP FROM 0-36 DEG.: $\frac{\partial c}{U} = 0.02$



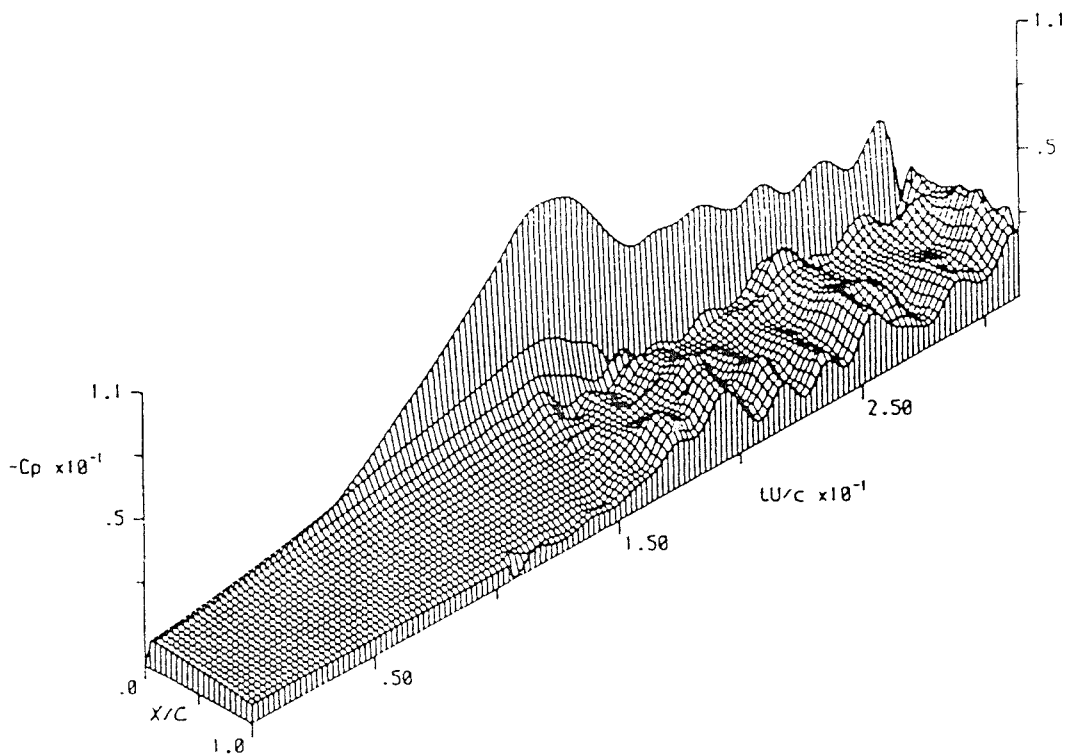
(a) C_N vs α



(c) X_S/C vs α



(b) C_L vs α



(d) PRESSURE-TIME HISTORY

FIG 5.11 RESULTS OBTAINED AFTER A RAMP FROM 0-36 DEG. IS APPLIED TO THE NACA 0012 AEROFOIL: $\dot{\alpha}c/U = 0.02$



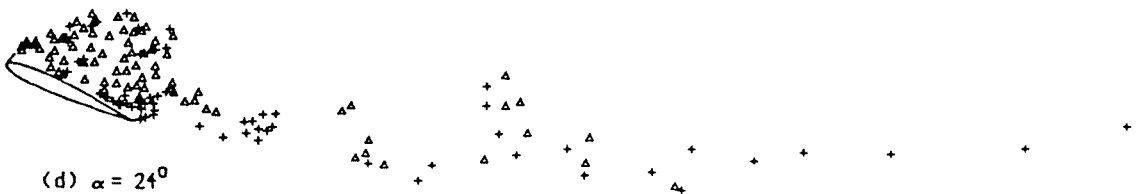
(a) $\alpha = 12^\circ$ †



(b) $\alpha = 17.91^\circ$ †



(c) $\alpha = 18.93^\circ$ †



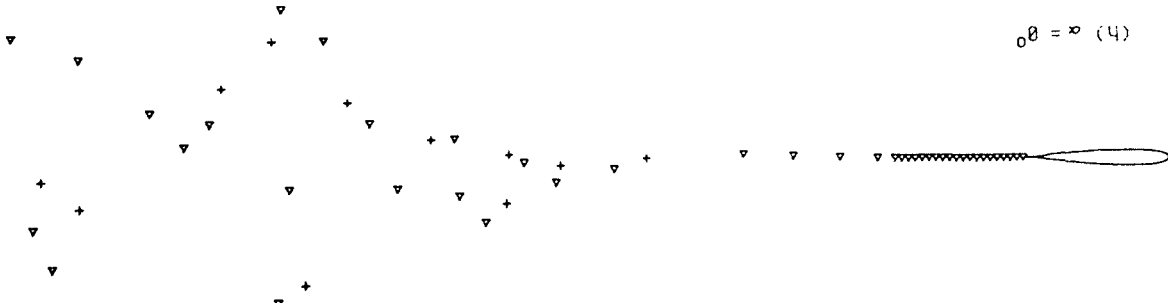
(d) $\alpha = 24^\circ$

FIG 5.12 WAKE PRODUCED BY THE NACA 0012 AEROFOIL DURING SINUSOIDAL MOTIONS: $k=0.125$, $\alpha = 12^\circ + 12^\circ \sin(\omega t)$

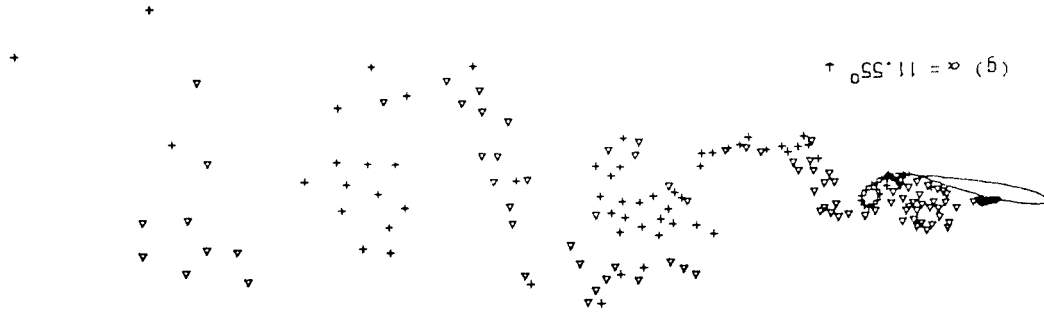
FIG 5.12 (Contd)

△ CLOCKWISE CIRCULATION
+ ANTI-CLOCKWISE CIRCULATION

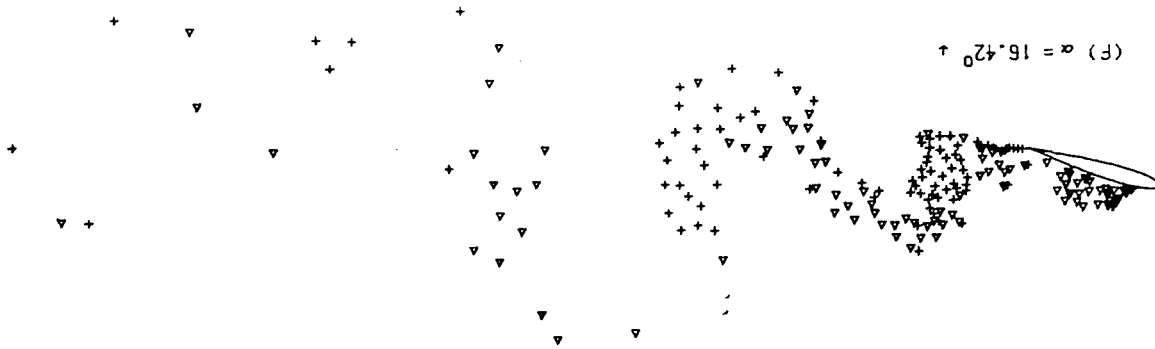
(4) $\alpha = 0^\circ$



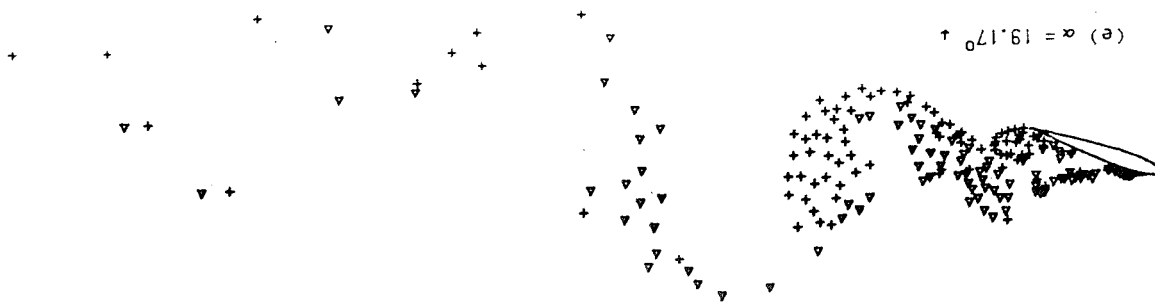
(g) $\alpha = 11.55^\circ$



(f) $\alpha = 16.42^\circ$



(e) $\alpha = 19.17^\circ$



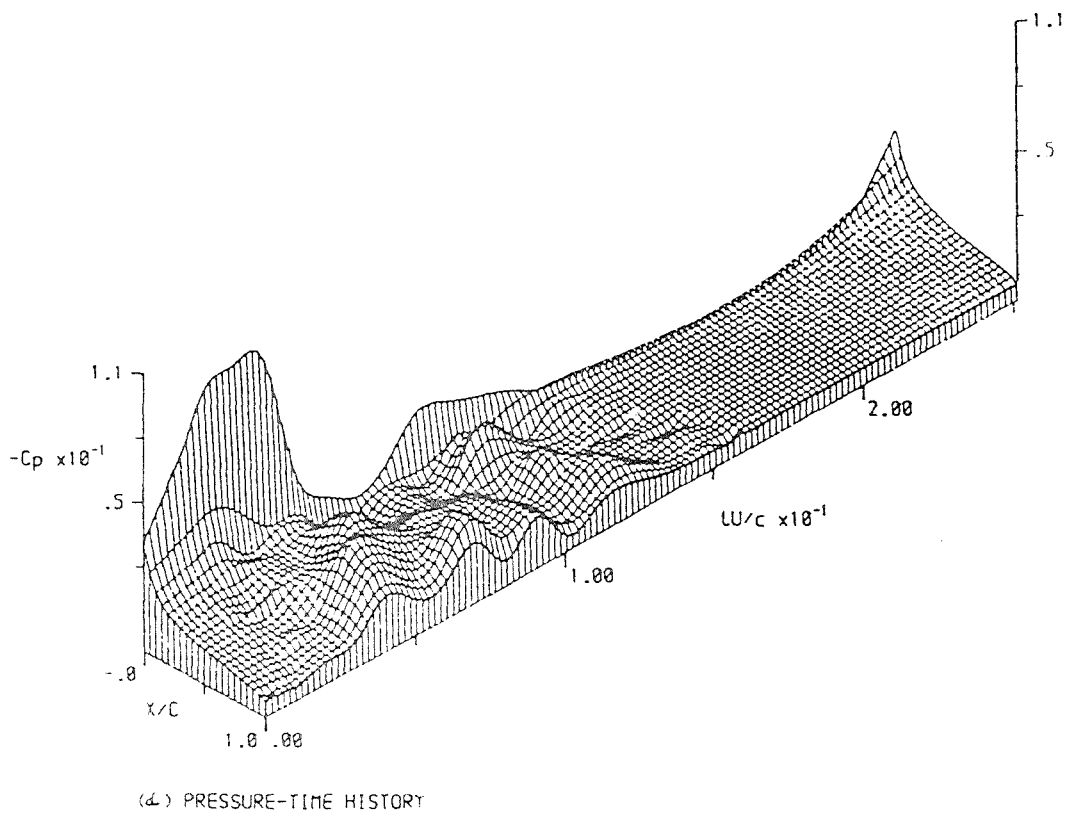
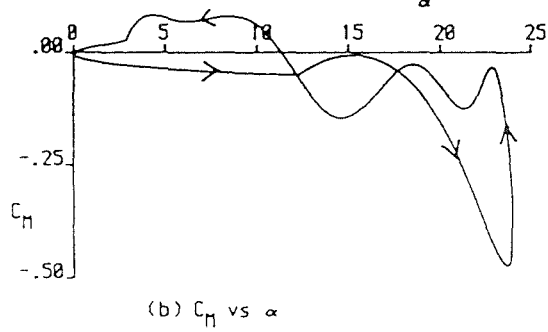
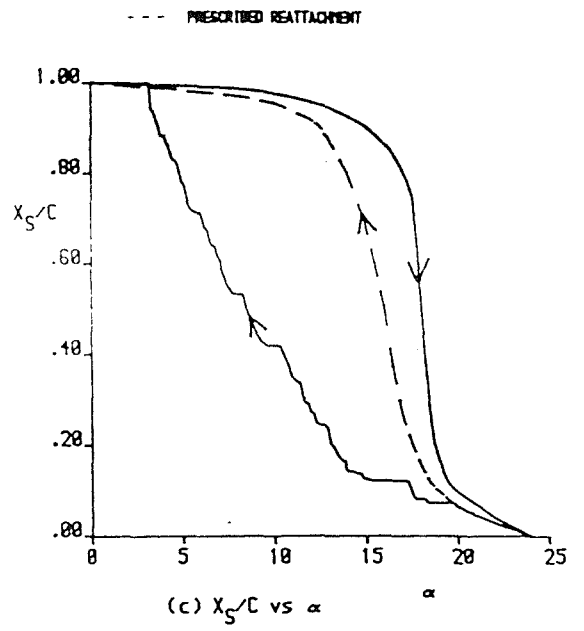
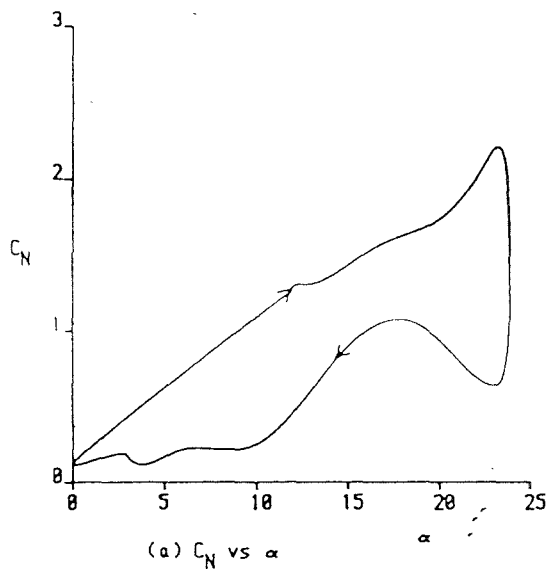


FIG 5.13 RESULTS OBTAINED AFTER SINUSOIDAL MOTIONS ARE APPLIED TO THE NACA 0012 AEROFOIL: $k=0.125$, $\alpha=12^\circ+12^\circ \sin(\omega t)$